

AD-A955 400

Chapter 16
DAMAGE TO MISSILES

DTIC ELECTE
12 MAR 1989
S E D

Missile systems are subject to damage by essentially all of the phenomena described separately in Chapters 2 through 8. Part I. of this manual, i.e., all or part of the system may be damaged by blast and shock (Chapter 2), by thermal radiation (Chapter 3), by X-ray radiation (Chapter 4), by nuclear radiation (Chapter 5) mainly in the form of transient radiation effects on electronics (TREE) phenomena (Chapter 6), or by the electromagnetic pulse (EMP (Chapter 7)). Communications and/or radar subsystems are also subject to degradation of their propagation characteristics as described in Chapter 8.

The damage that might result from several of the phenomena listed above is so dependent on specific system design that general methods for predicting specific missile system response cannot be provided. These phenomena include X-ray radiation, TREE, and EMP. Consequently, general descriptions of the damage mechanisms associated with these phenomena, applicable to missiles as well as other systems, are provided in Sections V, VII, and VIII, respectively, of Chapter 9. Additionally, some ambient nuclear radiation levels for "sure safe" and "sure kill" of missiles are given in Table 14-11, Chapter 14. Chapter 17 discusses the signal degradation of communications and radar systems. No further discussion of the damage or degradation from these phenomena is included herein.

This chapter is divided into two sections. Section I describes blast damage to tactical missiles. Section II describes the response of strategic systems to blast and thermal phenomena. Where appropriate, separate discussions are pro-

vided in Section II for antimissile systems (commonly called ABM) and reentry vehicles (RV's).

SECTION I
BLAST DAMAGE TO
TACTICAL MISSILE SYSTEMS

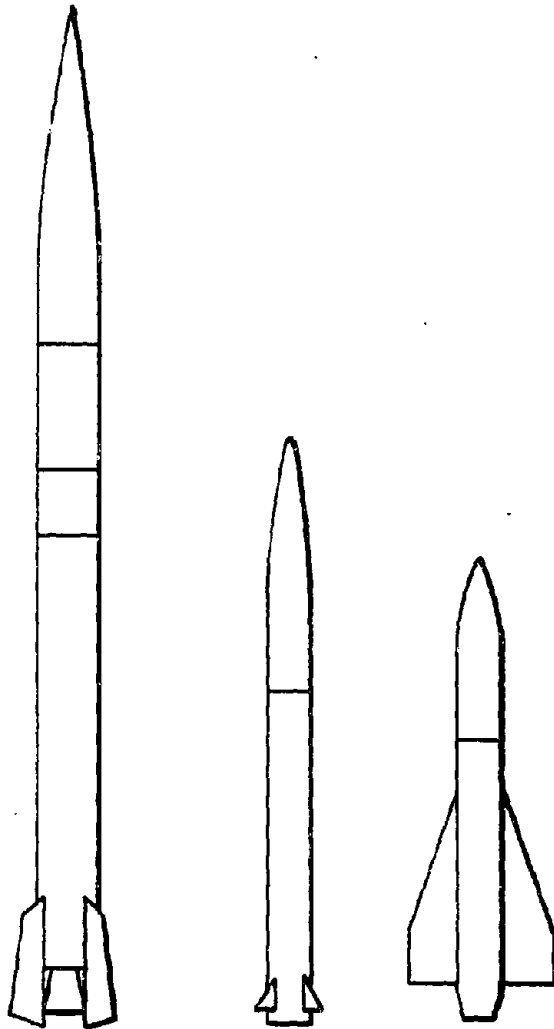
The effects of air blast on three specific sample systems, the SERGEANT, the LANCE, and the HAWK, are described in this section. The vulnerability analysis of these missiles and their support equipment is intended to provide information from which the probable effects of air blast on other tactical missile systems may be estimated. An example of such an estimation for the HONEST JOHN missile is also provided. Outline drawings of the sample systems are shown in Figure 16-1 for comparison purposes.

In the case of each system, it is assumed that the system may be attacked from the time that the missiles are in stockpile until the missile warhead is detonated over the target. During any phase of this stockpile-to-target sequence, the system vulnerability is determined by the most susceptible component that is essential to completion of the mission. The vulnerability of all critical components is tabulated for each system. Vulnerability is expressed in terms of peak overpressure, assuming that the blast wave is from a contact surface burst with a yield between 1 kt and 300 kt. A range of values is given for the overpressure vulnerabilities, e.g., 12 to 19 psi. These numbers mean that either 12 psi from a 300 kt burst or 19 psi from a 1 kt burst is estimated to be sufficient to render the system component incapable of performing its necessary functions to complete the mission. Each vulnera-

DISTRIBUTION STATEMENT A
Approved for public release
Distribution Unlimited

16-1

89 3 02 034



Accession For	
NTIS GRA&I	<input checked="" type="checkbox"/>
DTIC TAB	<input checked="" type="checkbox"/>
Unannounced	<input type="checkbox"/>
Justification	<i>Basic Doc</i>
By	
Distribution/	
Availability Codes	
Dist	Avail and/or Special
A-1	

Missile	SERGEANT	LANCE	HAWK
Length ~ Ft.	34 1/2	20	16
Diameter ~ In.	31	22	14
Weight ~ Lbs.	10,000	3100	1300
Application	Surface to Surface	Surface to Surface	Surface to Air
Range	46 to 137 NM.	5 to 75 NM.	to [redacted] Altitude with Horizontal Range
Warhead Section	1500 Lbs Nuclear	1000 Lbs Nuclear	73 Lbs. H.E.

UNANNOUNCED

AMC
(U-X)(1)
(S)(1)

Figure 16-1. [redacted] Missile Configurations, SERGEANT, LANCE, and HAWK [redacted]



[REDACTED]

bility level is also shown in the form of a number curve, which allows critical values of range and overpressure to be determined as a function of weapon yield.

Many circumstances alter the vulnerability threshold of specific system components. For example, a truck that is carrying a missile to the launch site is less likely to be overturned by a blast wave if it is facing the burst than if it is hit from the side (see Table 14-5, Chapter 14). The velocity and orientation of a missile in flight both are important. If the terrain is conducive to the formation of a precursor, the truck may be subjected to a greatly enhanced dynamic pressure impulse, capable of overturning it much more easily than if it were exposed to the same burst at the same range under near-ideal conditions (paragraph 14-2, Chapter 14). The overpressure and dynamic pressure at the target depend on height of burst as well as distance. In order to reduce vulnerability data to a manageable set of numbers, the following conditions are assumed for the analysis in this section.

- The orientation of the system component with respect to the blast wave is such that the probability of serious damage is a maximum.
- Near-ideal surface conditions exist (no precursor).
- The blast wave is produced by a contact surface burst.

If radically different conditions are expected, appropriate changes in vulnerability levels must be made. In the case of a burst that produces a precursor, the dynamic pressure would be enhanced, and drag sensitive targets, i.e., those susceptible to toppling or overturning, probably would be damaged at an overpressure lower than predicted. Also, an air burst could produce a double shock on a target located in the regular reflection region; again this could lead to significant target damage at an overpressure lower than

predicted. Thus, the numbers given should only be used as guides to the assessment of system blast damage.

Damage to targets that are primarily drag sensitive is determined by the dynamic pressure level. However, for near-ideal surface conditions, there is a known correspondence between peak overpressure and peak dynamic pressure (although the pulse durations can be somewhat different). Therefore, for the purpose of this chapter, all damage levels are expressed as overpressure levels, including the damage levels that apply to drag sensitive targets.

[REDACTED] SERGEANT WEAPON SYSTEM

16-1 Description of the SERGEANT Weapon System

The SERGEANT weapon system is a second generation surface-to-surface missile system capable of being used under all terrain and weather conditions. Major items of the system are:

- *SERGEANT missile M15 and containers.* The SERGEANT missile body consists of four major assemblies: (1) rocket motor M53; (2) guidance section M38; (3) warhead section M65; and (4) control surface assemblies M58. Figure 16-1 shows a drawing of the missile. Figure 16-2 shows the missile parts in containers and ready for transport.
- *Four-wheel, semitrailer mounted guided missile launching station M504.* Figure 16-3 shows this unit in firing position. One component, the launching station firing set, is shown in more detail in Figure 16-4.
- *Four-wheel, 6 ton, low-bed semitrailer M527.*
- *Organizational Maintenance Test Station (OMTS) AN/MSM-35.* This trailer housed

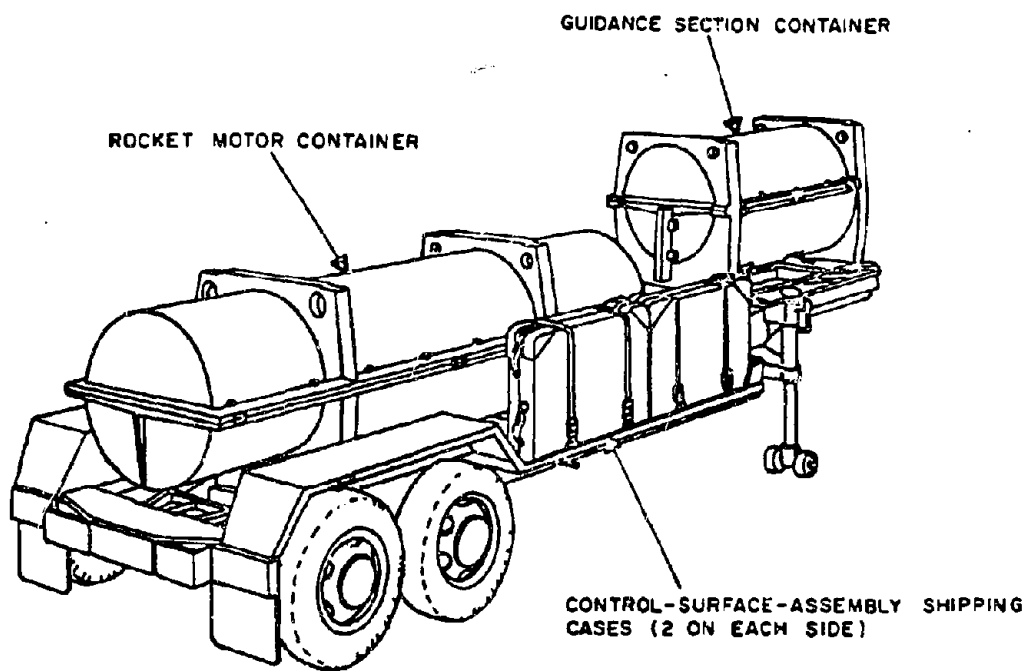


Figure 16-2. SERGEANT System, Semitrailer Transporter with Missile Section Containers

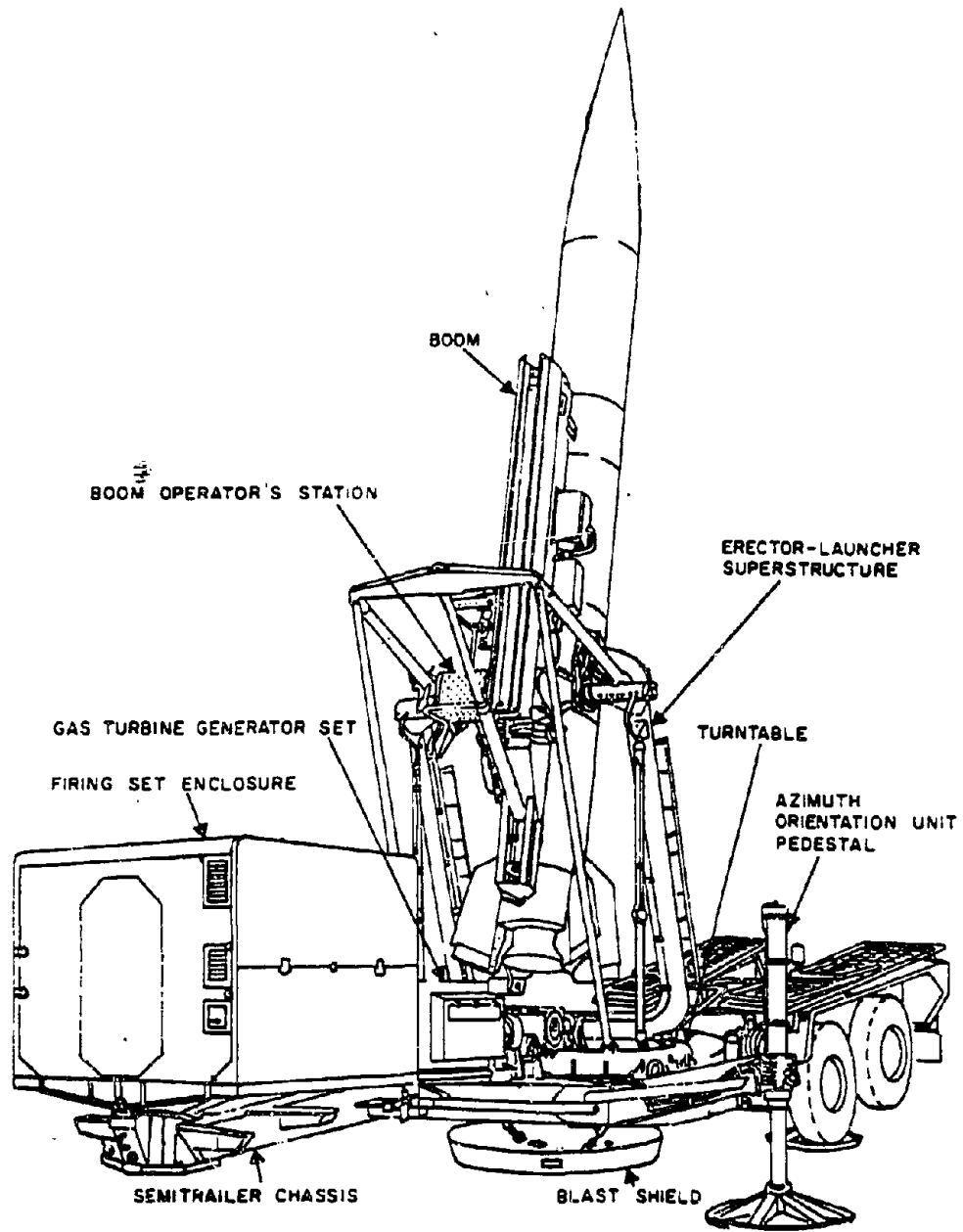


Figure 16-3. SERGEANT System, Launching Station with Missile in Firing Position

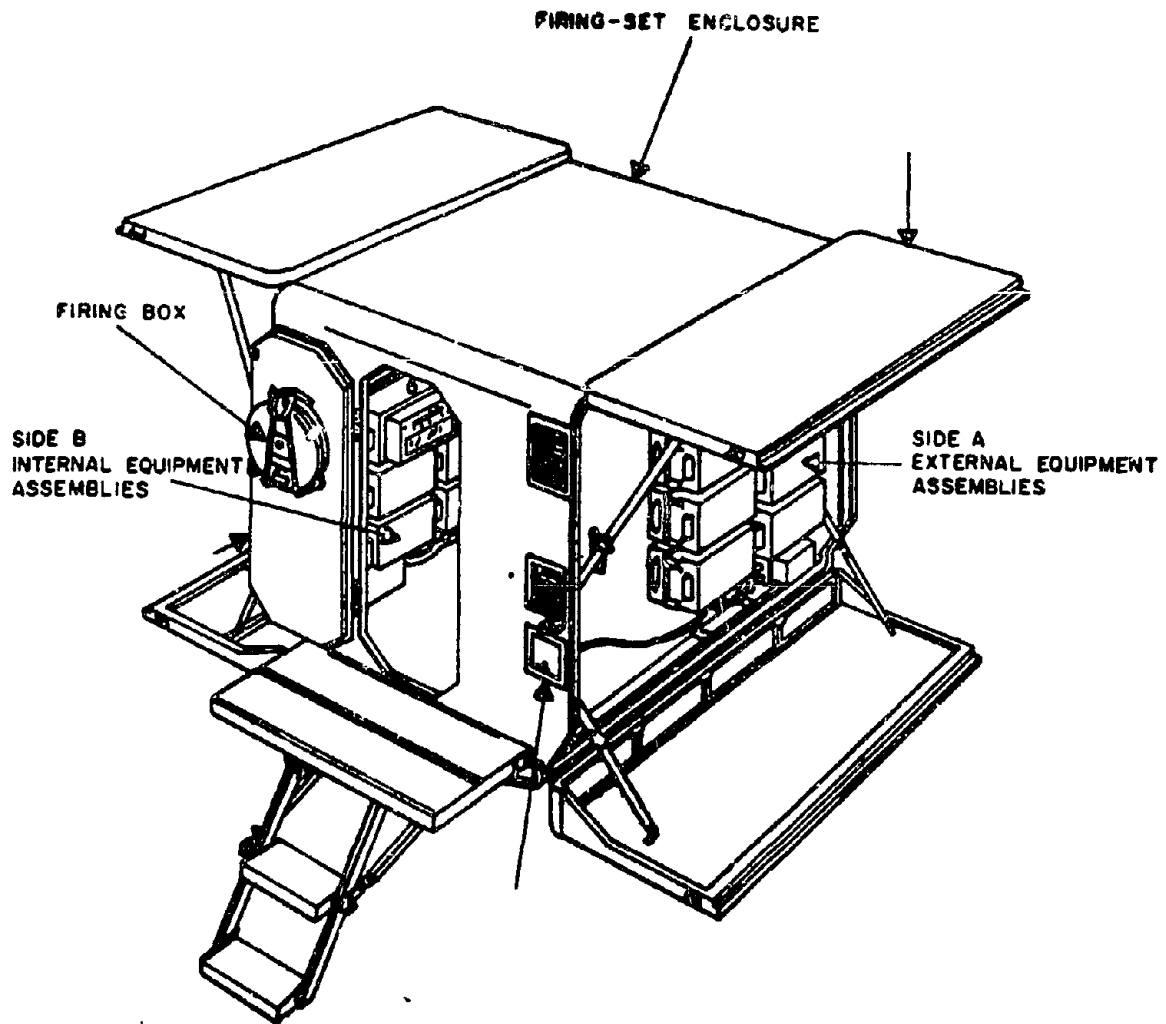


Figure 16-4. SERGEANT System, Launching Station Firing Set

[REDACTED] unit, shown in Figure 16-5, is used for pre-launch testing and replacement of defective assemblies.

- *Field Maintenance Test Station (FMTS) AN/MSM-36.* This unit is similar to the OMTS. It can be used to perform many of the functions of the OMTS, and it is also used in situations that require more extensive testing and repair work than normally is done by the OMTS.
- *Warhead Section Container*
- *Truck, M35*

In addition to the equipment listed above, an M55 cargo truck is used to transport the rocket motor when the M527 is not available.

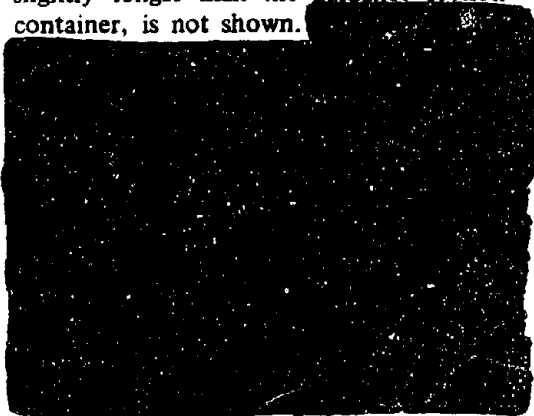
16-2 Vulnerability Levels of the SERGEANT Missile System

[REDACTED] The vulnerability levels of the various components of the SERGEANT missile system are shown in Table 16-1.

[REDACTED] The estimated vulnerability levels of the system in its various operational phases are described below. The most likely damage modes are also described.

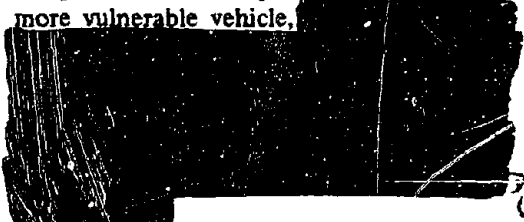
- *Missiles in Containers at Storage Site (SERGEANT).* Figure 16-2 shows the type of containers used to store missile parts. The warhead section container, which is slightly longer than the guidance section container, is not shown.

DNA
(A)(1)



DNA
(A)(1)

- *Missiles in Containers in Transit (SERGEANT).* Since the transport vehicles afford partial protection for the containers, the vulnerability estimates were based on the pressure levels required to overturn the more vulnerable vehicle.



DNA
(A)(1)

- *Equipment and Missile at the Firing Site (SERGEANT).*



DNA
(A)(1)

- *Missile in Flight (SERGEANT).*



DNA
(A)(1)



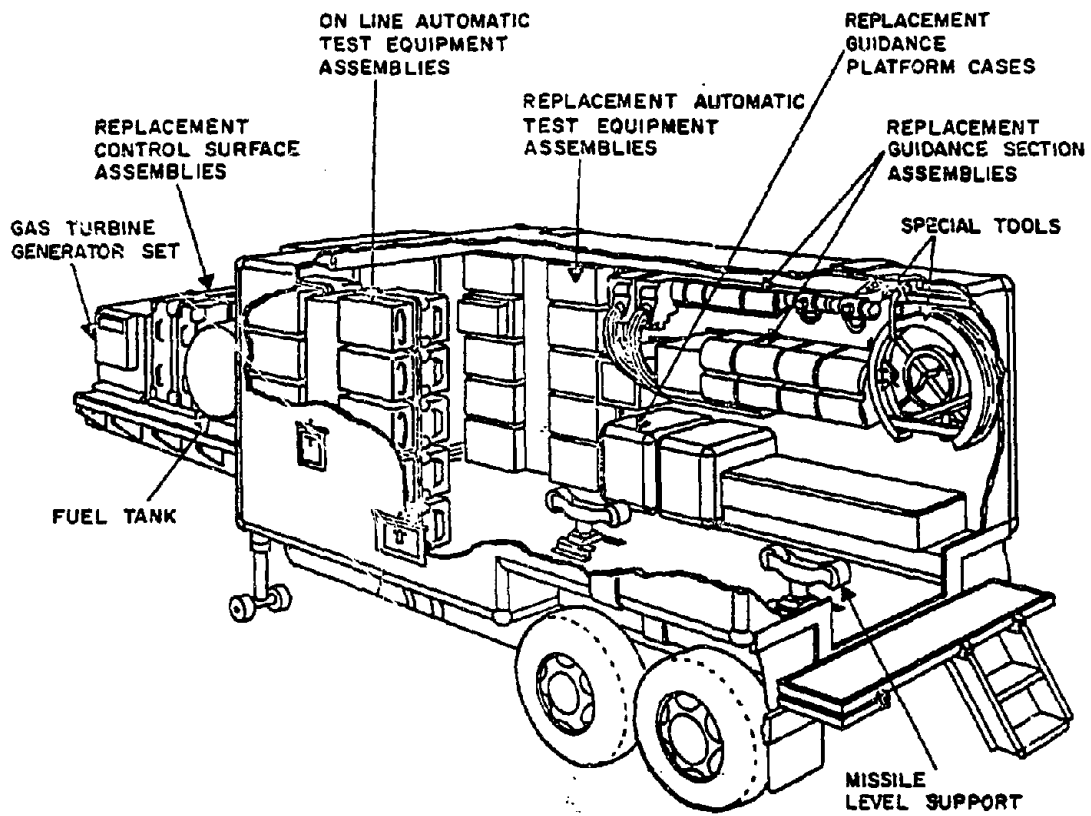


Figure 16-5. SERGEANT System, Organizational Maintenance Test Station (OMTS)

[REDACTED]

Table 16-1. [REDACTED] SERGEANT, Characteristics and Damage Levels for System Components [REDACTED]

USANC
(S)(1)

Deleted

DNA
(S)(3)
(S)(1)

[REDACTED]

[REDACTED]

[REDACTED]

[REDACTED]



The blast vulnerability of the principal components of the SERGEANT missile system can be determined by reference to Table 16-1 and Figure 16-6; the figure provides curves that allow the determination of pressure levels and distances for damage corresponding to various weapon yields. Table 16-2 shows a summary of the blast vulnerability of the susceptible subsystems in the various configurations of the SERGEANT missile system.

USAA CA
(S)(1)

DNA
(S)(3)

16-3 Reliability of SERGEANT Vulnerability Estimates



DNA
(S)(1)

Table 16-2. [REDACTED] Blast Vulnerability Summary, SERGEANT Missile System [REDACTED]

DNA
(S)(1)
+
(A)(3)

USAA CA
(S)(1)

Deleted

[REDACTED]

[REDACTED]

[REDACTED]

20.11
(11) (=)

[REDACTED]

Figure 16-6

[REDACTED]

Figure 16-6. [REDACTED] SERGEANT, Major Item Blast Vulnerability [REDACTED]

[REDACTED]

[REDACTED]

[REDACTED]

DNA
(L)(1)

[REDACTED]

DNA
(L)(3)

The sources of SERGEANT system damage data for the major items considered are:

DNA
(L)(1)

[REDACTED]

LANCE WEAPON SYSTEM

16-4 Description of the LANCE Weapon System

The LANCE is a surface-to-surface missile for general field artillery fire support of Army Divisions. The five major items of the LANCE system are:

- LANCE Missile Body, shown in Figure 16-1.
- Self-propelled Launcher (SPL), shown in Figure 16-7.
- Transporter Loader (TL), shown in Figure 16-7.
- Lightweight Launcher (LWL), shown in Figure 16-7.
- Other Ground Support Equipment, shown in Figure 16-8 (contact Support Test Set is not shown).

[REDACTED]

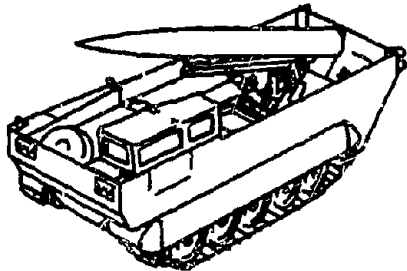
DNA
(L)(1)

16-5 Vulnerability Levels for the LANCE Missile System

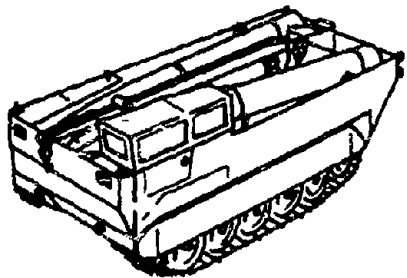
Blast vulnerability levels for the components of the LANCE missile system are shown in Table 16-3. Based on these values, the

[REDACTED]

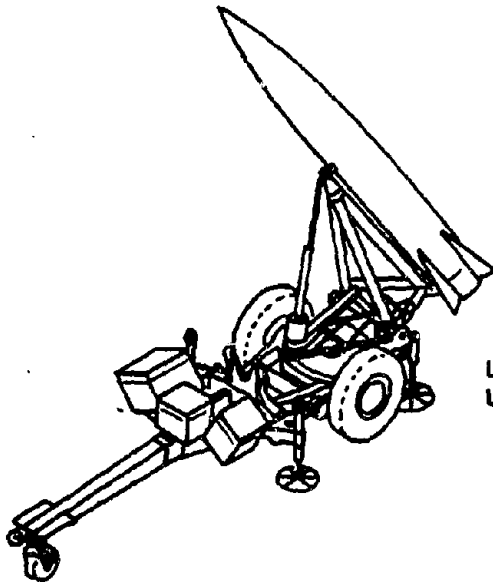
[REDACTED]





SELF-PROPELLED
LAUNCHER



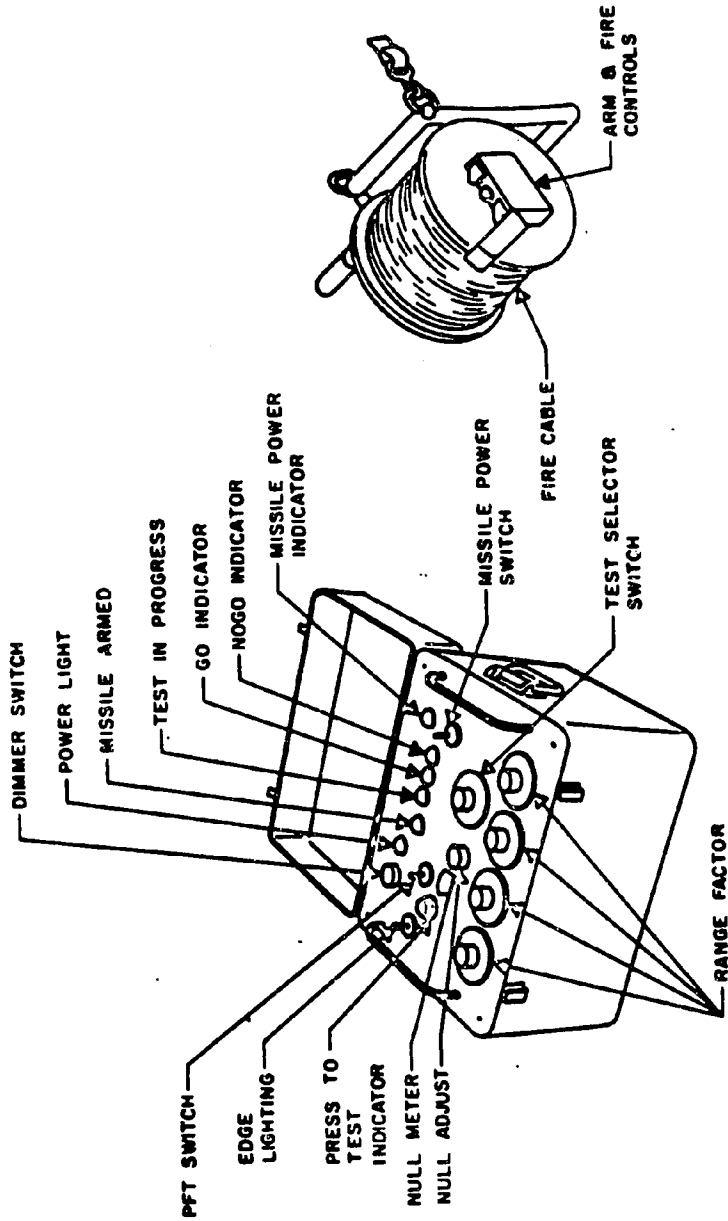
TRANSPORTER
LOADER



LIGHTWEIGHT
LAUNCHER

Figure 16-7.  LANCE System, Primary Units of
the Missile System 





Missile Test Set (MTS) Firing Device (FD)

Figure 16-8. LANCE System, Prefire Tester and Fire Pack

[REDACTED]

Table 16-3. [REDACTED] LANCE, Characteristics and Damage Levels for System Components [REDACTED]

DNA
(L)(1)
+
(L)(3)

USO
/C
(L)(1)

Deleted

[REDACTED]

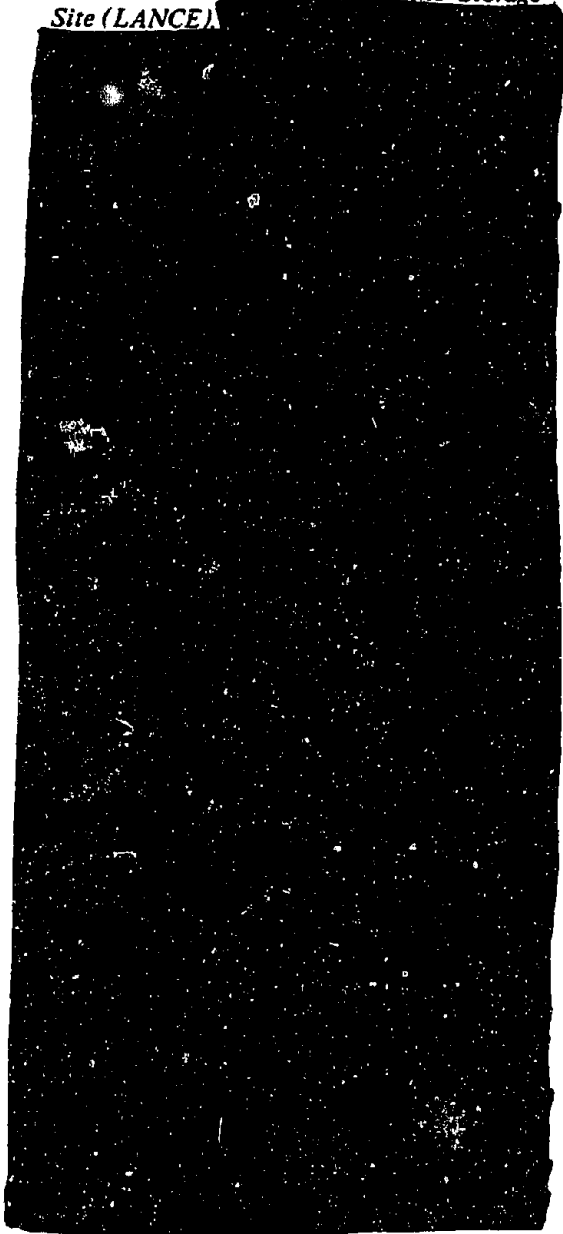
[REDACTED]

[REDACTED]

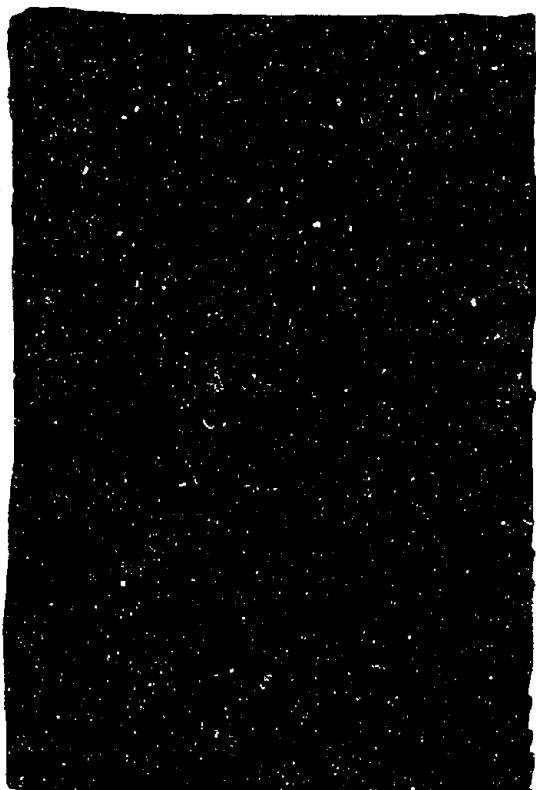
susceptibility levels of the LANCE missile system during its various operational phases are estimated to be as follows:

• *Missile Parts in Containers at the Storage Site (LANCE)*

DNA
(S)(1)



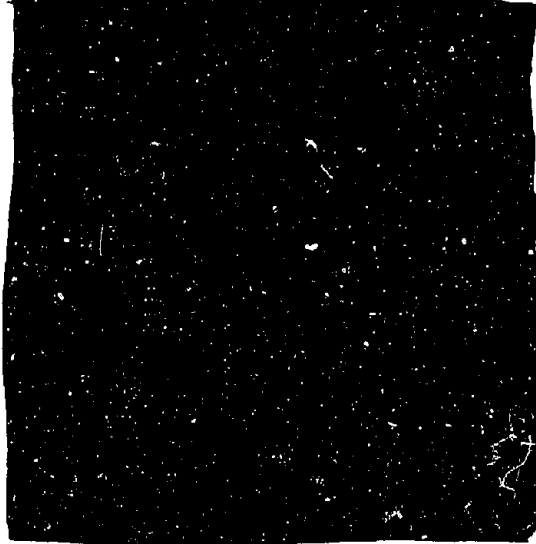
USANCA
(S)(1)



AMC
USCOMCOM
(S)(1)
DNA
(S)(1)

USANCA
(S)(1)

• *Missiles in Containers in Transit (LANCE)*



DNA
(S)(1)
USANCA
(S)(1)

AMC/DA
(S)(1)

DNA
(S)(1)

USANCA
(S)(1)



• *Missile System During Checkout, Prelaunch Phase, and Launching (LANCE).*

DNA
(S)(1)



• *Missile in Flight (LANCE).*

DNA
(S)(3)

AMC/DA
(S)(1)

USANCA
(S)(1)



The blast vulnerability of the principal configurations of the LANCE missile system can

be obtained from Table 16-3 and Figure 16-9; the figure includes curves from which the pressure levels for damage corresponding to various weapon yields and ranges may be obtained. Table 16-4 shows a summary of the blast vulnerability of the susceptible subsystems in the various configurations of the LANCE missile system.

16-6 Reliability of LANCE Vulnerability Estimates

The source of the LANCE system damage data for the major items considered are:



DNA
(S)

AMC/DA
(S)(1)

[REDACTED]

DNA
(A)(3)

Deleted

Figure 18-9. [REDACTED] LANCE, Major Item Blast Vulnerability [REDACTED]

18-18

[REDACTED]

[REDACTED]

[REDACTED]

Table 16-4. [REDACTED] Blast Vulnerability Summary, LANCE Missile System [REDACTED]

DNA
(L)(3)
+
(L)(1)

USADA
(L)(1)

Deleted

AAACIDA
DNA (L)(1)
(L)(1)

[REDACTED]

These data were used for the missile structure vulnerability.

DNA
(L)(1)

[REDACTED]

HAWK WEAPON SYSTEM

16-7 Description of the HAWK Weapon System

The HAWK is a surface-to-air, supersonic air defense system, designed to detect and identify airborne targets by means of radar, and to intercept and destroy those designated as hostile

with homing guidance missiles.

[REDACTED]

DNA
(L)(1)

The major items of the HAWK system are:

- HAWK Missile Body, shown in Figure 16-1.
- Missile Loader, shown in Figure 16-10.
- Missile Launcher, shown in Figure 16-10.
- Assault Fire Command Console (AFCC) or Battery Control Central (BCC), shown in Figure 16-10.
- Radar Units, including
 - (1) Range-only Radar (ROR), shown in Figure 16-11.
 - (2) Pulse Acquisition Radar (PAR), shown in Figure 16-11.
 - (3) CW Acquisition Radar (CWAR), shown in Figure 16-11.

[REDACTED]

[REDACTED]

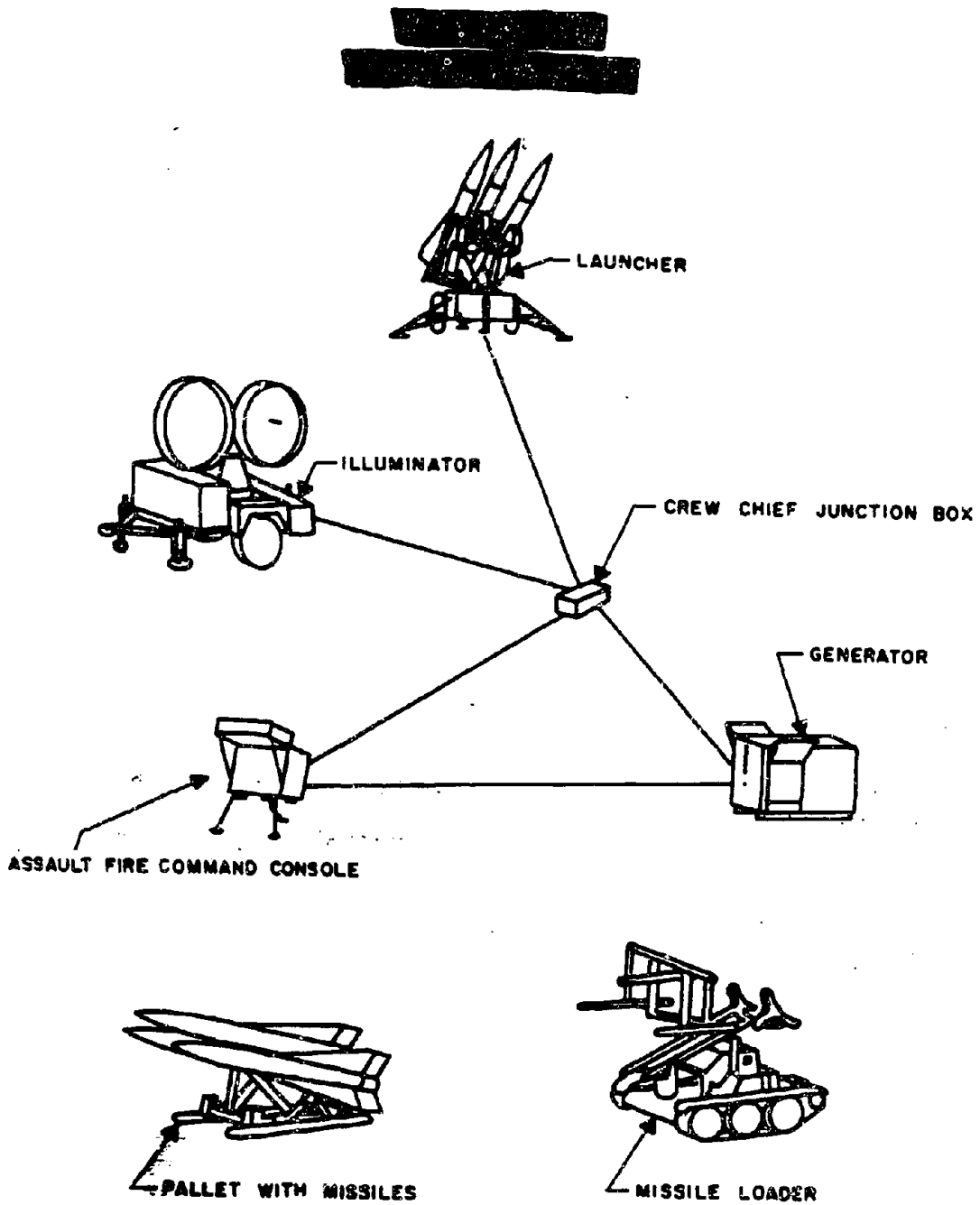


Figure 16-10. HAWK System, Basic Assault Firing Unit

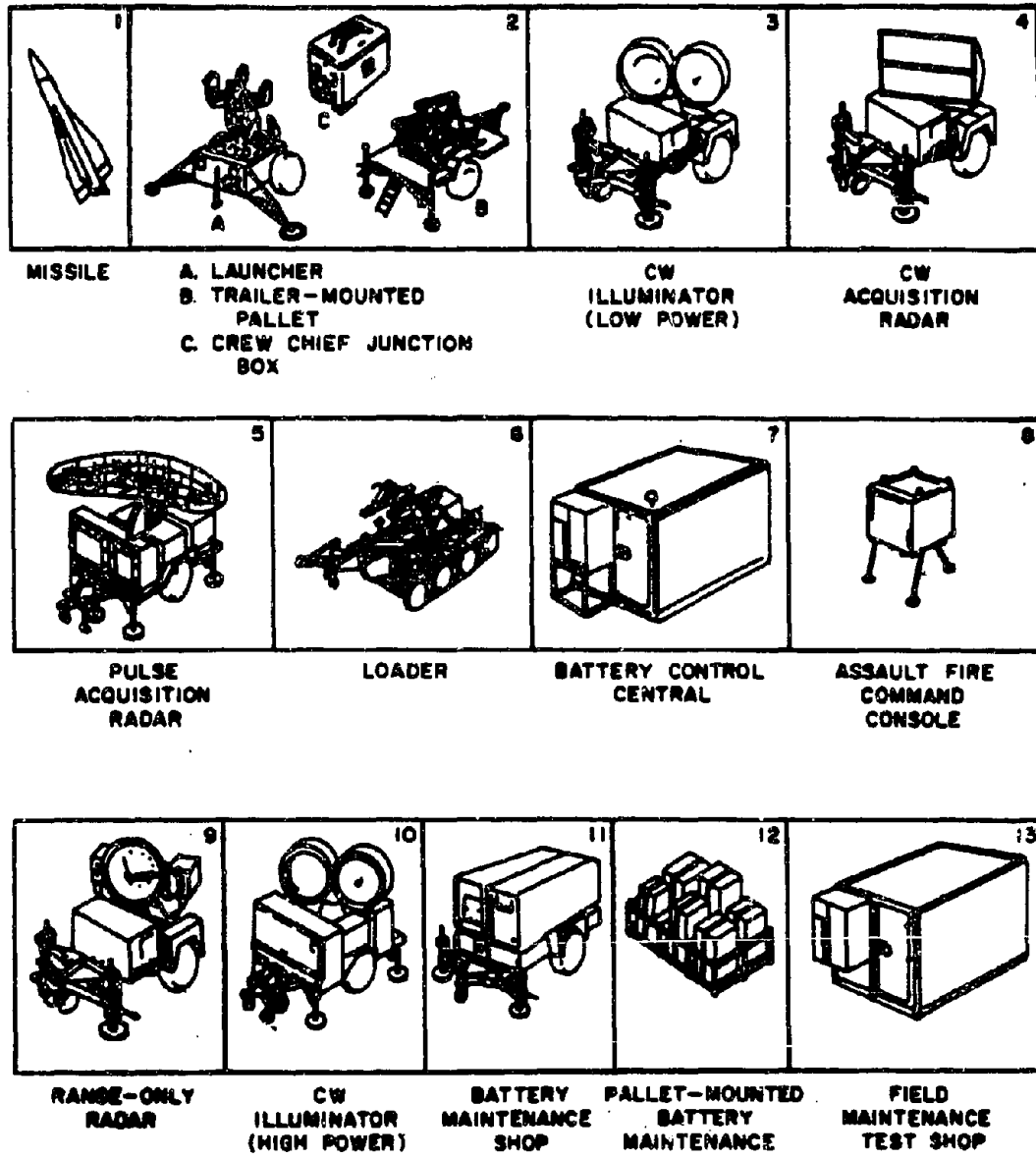


Figure 16-11. HAWK System, Auxiliary Components





Table 16-5.  HAWK, Characteristics and Damage Levels for System Components 

DND
(S)(1)

LISANCA
(S)(1)

Deleted



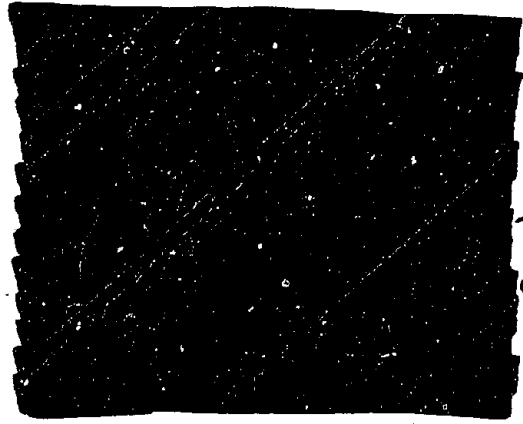


(4) CW Illumination Radar (CWIR), shown in Figure 16-10.

Structurally, the missile body consists of four major sections: the warhead section; guidance components; rocket motor; and surface controls.

16-8 Vulnerability Levels for the HAWK Missile System

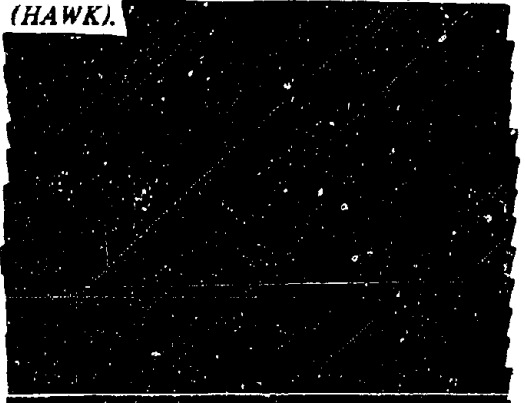
Blast vulnerability levels for the components of the HAWK missile system are shown in Table 16-5. Based on these values, the susceptibility levels of the HAWK missile system during its various operational phases are estimated to be as follows:



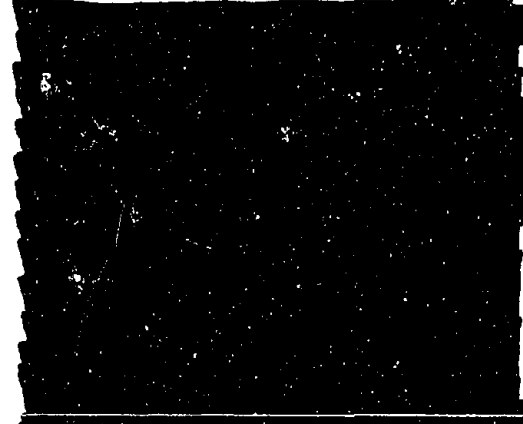
DNA
(S)(1)
NSA/CSS
(S)(1)

- **Missile System During Checkout, Pre-launch, and Launch (HAWK).**

- **Missile Parts in Containers at Storage Site (HAWK).**



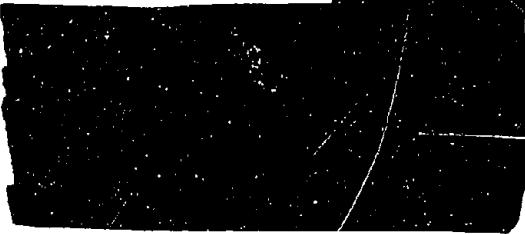
DNA
(S)(1)



DNA
(S)(1)
NSA/CSS
(S)(1)

NSA/CSS
(S)(1)

- **Missiles in Transit (HAWK).**



DNA
(S)(1)



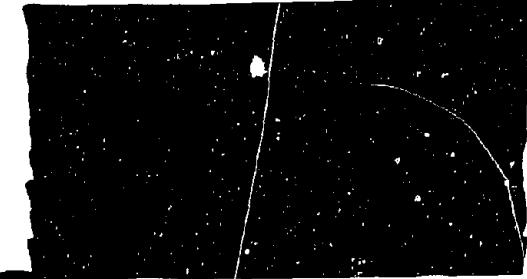
[REDACTED]

DNA
(S)(1)
USANCA
(S)(1)



• *Missile in Flight (HAWK).*

DNA
(S)(1)
USANCA
(S)(1)

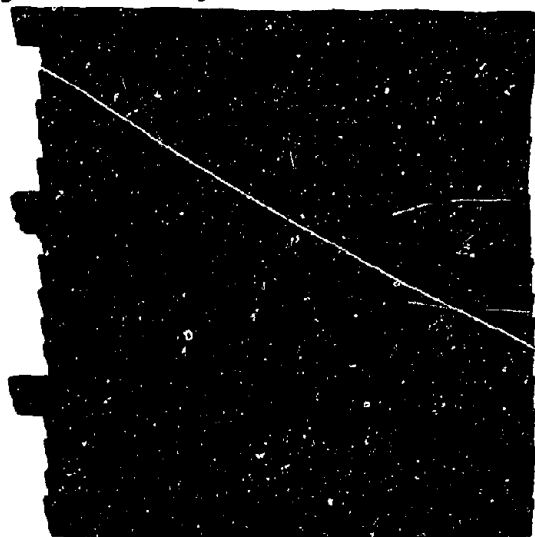


The blast vulnerability of the principal configurations of the HAWK missile system can be obtained from Table 16-5 and Figure 16-12; the figure includes curves from which pressure levels for damage corresponding to various weapon yields and ranges may be obtained. Table 16-6 shows a summary of the blast vulnerability

of the susceptible subsystems in the various configurations of the HAWK missile system.

16-9 Reliability of HAWK Vulnerability Estimates

The sources of the HAWK system damage data for the major items considered are:



DNA
(S)(1)

Table 16-6. Blast Vulnerability Summary, HAWK Missile System

Deleted

DNA
(S)(1)
USANCA
(S)(1)

[REDACTED]



DNA
K-XI

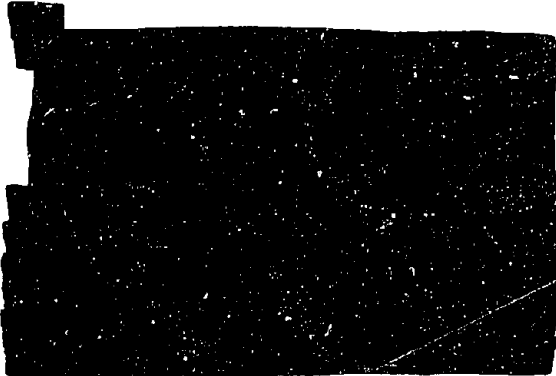
LISANCE
(G)(1)

Deleted

Figure 16-12.  HAWK, Major Item Blast Vulnerability 



DNA
(6X1)



SAMPLE PROBLEM: AIR BLAST DAMAGE TO A TACTICAL MISSILE SYSTEM

The material presented above concerning the SERGEANT, LANCE, and HAWK weapon systems is used to estimate the blast vulnerability of the HONEST JOHN weapon system as an illustration of the methods by which the vulnerability data may be applied.

16-10 Description of the HONEST JOHN System

The HONEST JOHN is a 762 mm, surface-to-surface, field artillery rocket designed to deliver warheads, weighing between 1,000

and 1,500 pounds, at horizontal ranges up to about 26 miles. It uses solid propellant, and it follows a ballistic trajectory after firing (no guidance).

The HONEST JOHN system is mobile by both ground and air transport. The principal units of the system are the following:

- *Complete rocket.* The rocket includes a warhead section, motor assembly, and fins, for which containers are provided (see Figure 16-13).
- *Launcher, truck-or trailer-mounted.* The launcher includes the launching beam assembly, elevating and traverse mechanisms, and electrical controls (see Figures 16-14 and 16-15).
- *Other ground support equipment.* A wrecker, transporter trailer, generator, motor and warhead cradles, and handling-beam make up the ground support equipment (see Figure 16-16).

Table 16-7 lists the weight and size of the various HONEST JOHN components. The principal operational phases can be listed as follows:

- Storage at Storage Site,

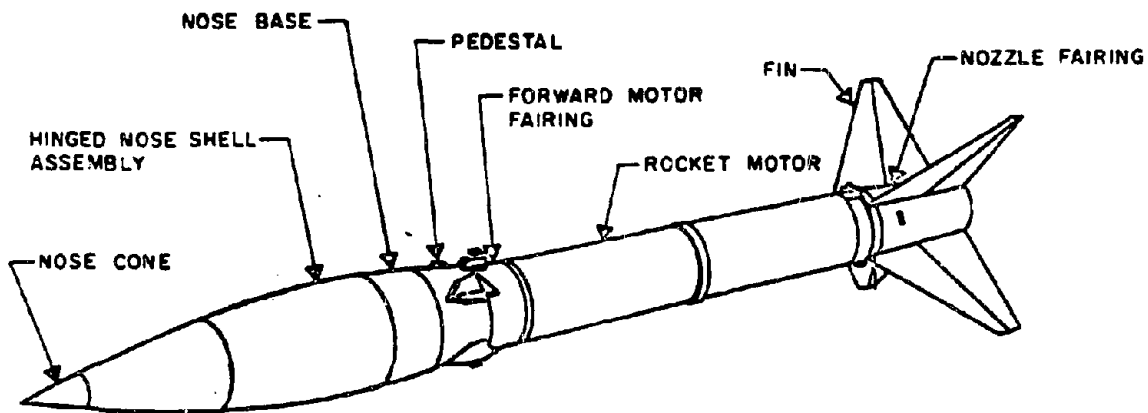


Figure 16-13. HONEST JOHN, Major Components of Rocket

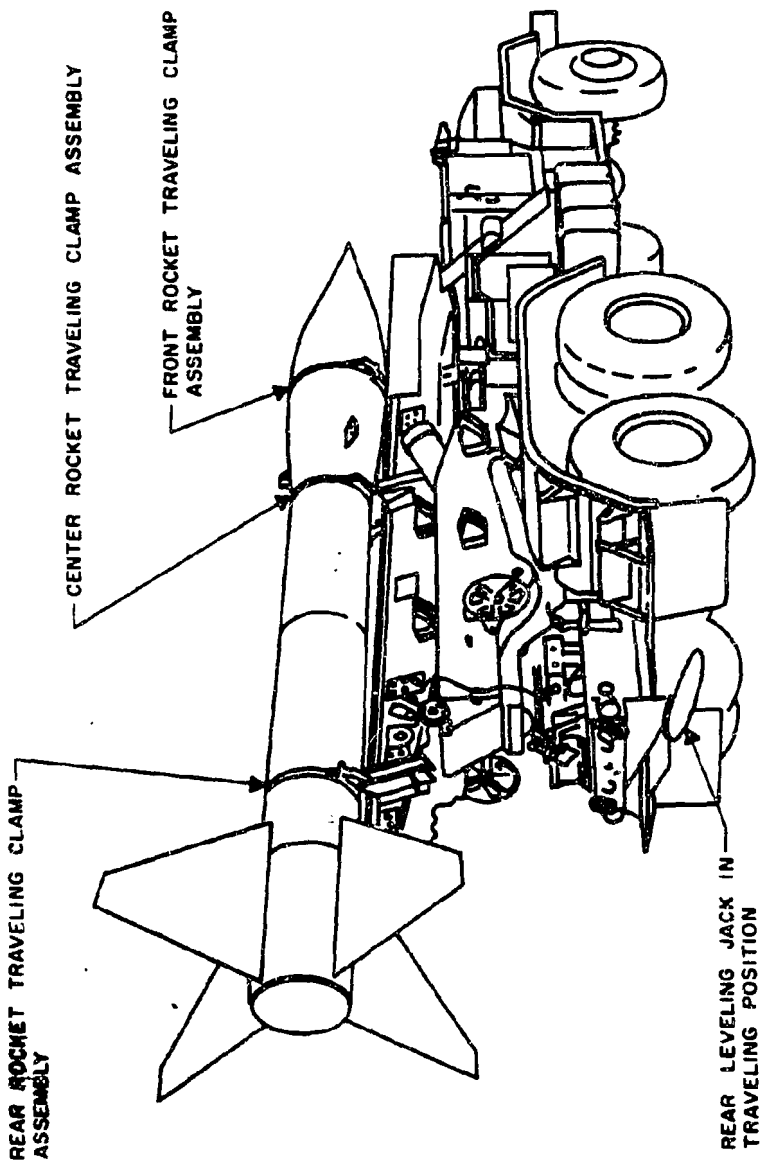


Figure 16-14. HONEST JOHN, Truck-Mounted Rocket Launcher in Traveling Position

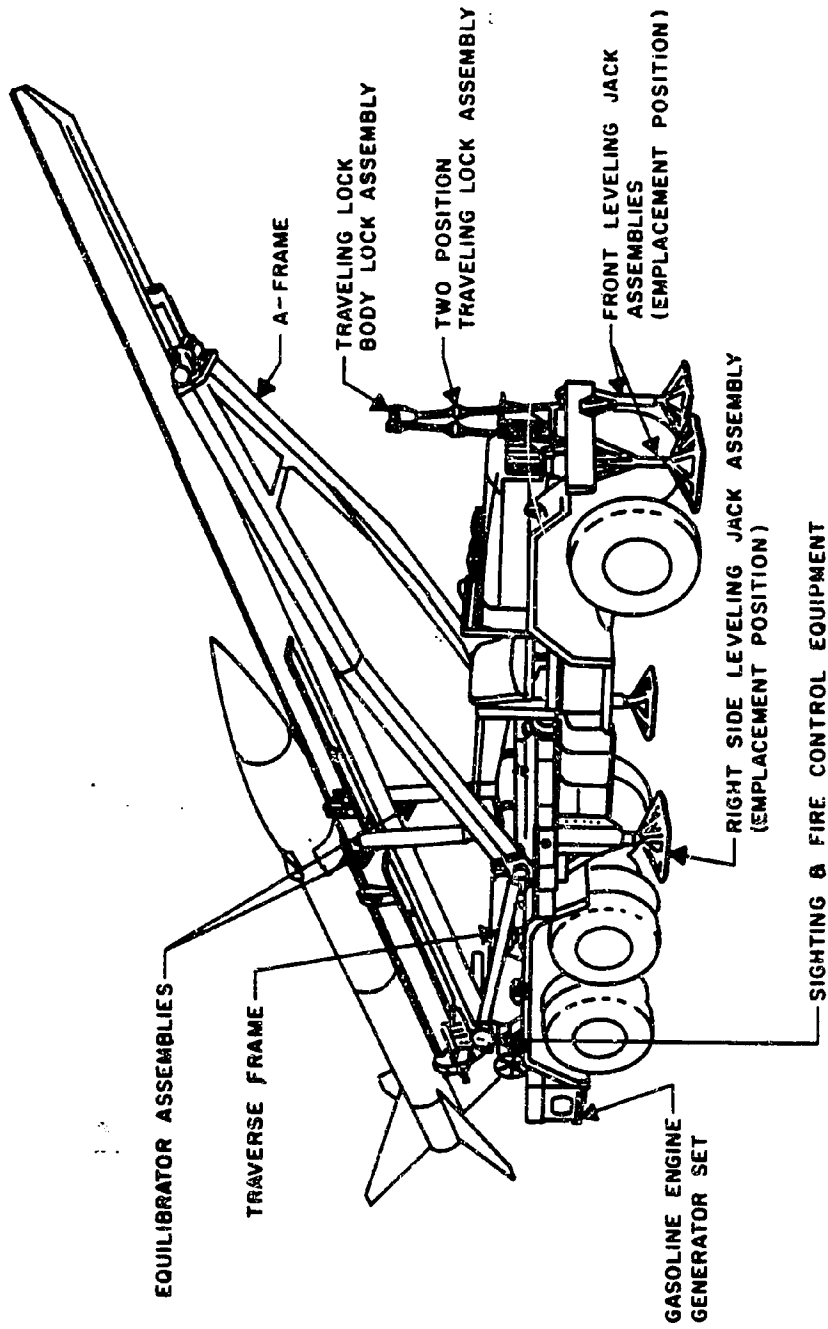
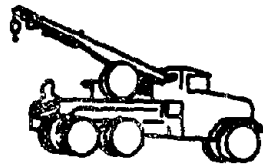
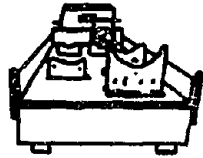


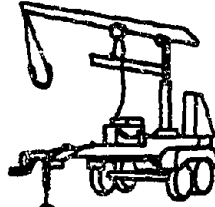
Figure 16-15. HONEST JOHN Rocket Launcher in Firing Position



WRECKER
M62 OR M543



HEATING
& TIE-DOWN UNIT
XM78E1



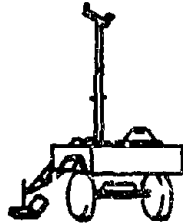
HANDLING UNIT
M405E1



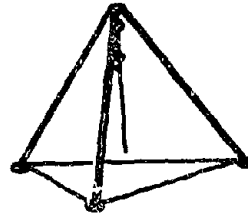
TRANSPORTER TRAILER
M329A1



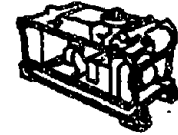
TRANSPORT CART
ASSEMBLY
XM465



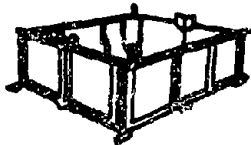
WIND MEASURING
SET



HOISTING UNIT TRIPOD
XM26



GENERATOR SET
M25C



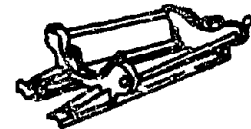
EQUIPMENT DELIVERY
BASKET M2



ELECTRIC BLANKET
M2E2



ROCKET MOTOR CRADLE
M5



WARHEAD CRADLE
M4



HANDLING BEAM
XM4E2



WARHEAD HANDLING SLING
M6

Figure 16-16.  HONEST JOHN, Auxiliary Equipment 

[REDACTED]

Table 16-7. Missile System Components - HONEST JOHN

Item	Refer to Figure	Dimensions (in.) (Weight (lbs))	Remarks
1. Missile Components (in containers)			
(a) Warhead sections	-	144 x 50 x 45 (2,500)	Plywood containers
(b) Guidance sections	None	-	
(c) Rocket motor sections } (d) Fins }	-	235 x 44 x 38 (3,500)	Plywood containers
2. Missile Body (assembled)			
(a) Ready for launch	13	327 x 28 (3,750)	
(b) In-flight (near target)	13	327 x 28 (2,000)	Propellant burned
3. Transport Equipment			
(a) Semitrailers	16	315 x 97 x 48 (3,500)	w/o missile
(b) Trucks (M543 or M62)	16	310 x 97 x 103 (34,000)	
4. Launch Equipment			
(a) Lightweight launchers	-	346 x 83 x 61 (4,375)	w/o missile
(b) Self-propelled launchers	14, 15	508 x 121 x 151 (42,000)	w/o missile
(c) Loaders (handling unit on M62 truck)	16	310 x 97 x 210 (40,000)	w/o missile
5. Auxiliary Ground Equipment			
(a) Firing unit assembly	-	36 x 24 x 24 (300)	
(b) Sighting equipment	-	36 x 20 (175)	
(c) Generator set	16	60 x 30 x 30 (1,800)	On truck chassis

[REDACTED]

[REDACTED]

- Battalion Area Test and Repair,
- Transportation to Firing Site,
- Emplacement and Prefire Preparations,
- Flight.

[REDACTED]

DNA
(S)

16-11 Vulnerability Levels for HONEST JOHN Missile System

[REDACTED] Blast vulnerability levels for the principal system configurations of the HONEST JOHN missile system are given in Table 16-8.

[REDACTED]

DNA
(S)

USAC
(S)

- Missiles in Transit to Firing Site (HONEST JOHN).

[REDACTED]

DNA
(S)

- Missiles in Containers at Storage Site (HONEST JOHN).

[REDACTED]

DNA
(S)

Table 16-8. [REDACTED] Summary - HONEST JOHN [REDACTED]

USAC
(S)

DNA
(S)
+
(S)

Deleted

[REDACTED]

[REDACTED]

DNA
(S)(1)
USANCA
(S)(1)

• *Missile System During Checkout and Launch Operations (HONEST JOHN).*

DNA
(S)(1)
USANCA
(S)(1)

• *Missile in Flight (HONEST JOHN).*

DNA
(S)(3)
+(S)(1)

The blast vulnerability of the principal configurations of the sample missile system (HONEST JOHN) are described in Table 16-8 and Figure 16-17; the figure includes curves that allow the determination of pressure levels for damage corresponding to other weapon yields.



DATA
KEY

Deleted

Figure 16-17.  HONEST JOHN, Major Item Blast Vulnerability 



[REDACTED]

SECTION II
BLAST AND THERMAL
VULNERABILITY OF IN-FLIGHT
STRATEGIC SYSTEMS

INTRODUCTION

The blast and thermal damage to strategic systems are considered together since blast and thermal effects are closely associated in the physics of a nuclear explosion and also because the damage mechanisms of these two effects tend to interact and, at times, complement each other. It should be noted that this section only treats damage to in-flight aerospace systems; blast and thermal damage to surface and underground installations characteristic of the ground support portions of a strategic system are treated separately in Chapter 11.

Blast effects are important to in-flight strategic systems from sea level to altitudes of approximately 100,000 feet (about 30 kilometers). When a nuclear explosion occurs in this altitude region, the blast wave is formed by conventional hydrodynamic processes as the fireball expands. The details of these processes depend on the yield of the weapon, the altitude of burst, and the weapon design (see Chapter 2). The latter consideration (weapon design) is becoming increasingly important as warheads are tailored to [REDACTED] or to enhance specific elements of the output. The mechanisms of blast wave formation are reasonably well understood from a theoretical viewpoint for nuclear bursts up to altitudes as high as 50 kilometers but experimental verification is lacking (see paragraphs 2-42 through 2-44).

(U) Blast is important to in-flight strategic systems operating below about 100,000 feet, in terms of the following effects:

- Overpressure (static or dynamic) crushing or bending of the primary structure.

- Gust (or deceleration) loading on primary and/or secondary (internal) structures.
- Trajectory deviation (CEP degradation).
- Alteration of aerodynamic stability.

The thermal radiation (excluding X-ray effects*) associated with a nuclear burst must be considered from two main aspects:

- "Early" time thermal radiation emitted from a distant source that is incident on the missile surface; this radiation comes from the fireball and from the high-pressure shock front.
- Missile "fly-through" of the fireball region at "later" times, with the associated thermal radiation imposed on the body surface while it is inside the fireball region.

In addition to considering the effects of blast and thermal radiation on in-flight strategic systems separately, the possible coupling of these two effects in producing damage to the system should be considered. The magnitude of possible coupling effects probably will depend on the details of the system design; general statements are not valid.

The two major strategic systems of concern are defensive antimissile missiles (AMM), more commonly known as ABM, and offensive reentry vehicles (RV). Both systems respond to exposures to the environment produced by nuclear explosions in similar manners, despite significant differences in their configurations (Figure 16-18). The degree to which any system will respond depends on the flight characteristics of the specific vehicle involved, but, in general, there is considerable overlap between RV's and ABM's with respect to their velocity at different altitudes within the atmosphere. A comparison of operational regimes is shown in Figure 16-19.

* See Section V, Chapter 9 for a discussion of X-ray effects on aerospace vehicles.

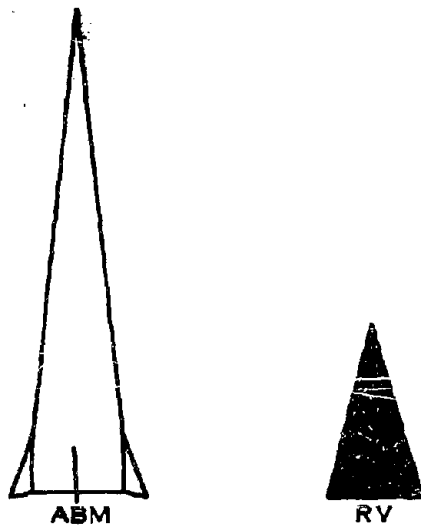


Figure 16-18. ABM and RV Configuration Comparison

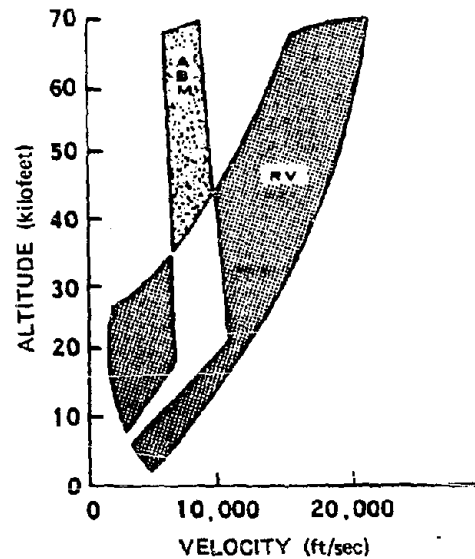


Figure 16-19. ABM and RV Operating Envelope Comparison

The first two categories of blast effects listed above, static and dynamic overpressure crushing (or bending) and gust (acceleration) loading can damage the system physically, i.e., the blast wave from a nuclear explosion at altitudes up to 100,000 feet can cause permanent structural deformation to reentry vehicles, interceptor missiles, boosters, and aircraft. As the structure crosses the shock front, it is suddenly immersed in a "new," transient pressure field, hence, the term "pressure crushing." There is, of course, a complicated shock interaction when the bow shock surrounding a supersonic vehicle intersects the shock front of the blast wave. This interaction results in a high pressure transient ("shock-on-shock" load) that decays quickly to a quasi-steady loading behind the front. The duration of this transient or "spike" can be quite short (tens of microseconds) compared to the response time of the vehicle. At the same time, the vehicle structure is suddenly subjected

to a gust loading or an additional aerodynamic loading that results from the particle velocity and the over-density behind the shock front that causes a jump in the dynamic pressure, which causes an abrupt deceleration of the whole vehicle body.

The extent of physical damage or structural response from either pressure crushing or gust loading depends on the distance from the target to the burst point, the orientation of the blast wave, the strength and duration of the blast wave, and the preblast flight loads imposed on the vehicle. These last loads depend on the speed, trajectory, and physical design characteristics of the vehicle. For an incoming reentry vehicle, the altitude of maximum deceleration from atmospheric drag depends on the ballistic coefficient, β . The ballistic coefficient is defined as $\beta = W/C_d A$, where W is the vehicle mass, C_d is the drag coefficient, and A is the body reference area. As the ballistic coefficient is increased, the

altitude at which the vehicle experiences maximum deceleration is decreased. The high performance, thin, cone-shaped vehicles have very high ballistic coefficients. Figure 16-20 shows the various response regimes for an interceptor missile including structural, e.g., shell buckling and beam bending, rigid body, and thermal response.

Rigid body response describes the gross whole body motion of an in-flight strategic vehicle that results from passing through the blast sphere and the fireball interior. It includes trajectory deviation (CEP degradation), aerodynamic stability changes, and the drag forces exerted on the overall vehicle; it should be noted that the deceleration forces imposed on the whole body also are transmitted, in a complex manner, to the internal components of the missile system. Trajectory deviation occurs when the blast wave deflects or displaces an in-flight vehicle from its preassigned (or benign environ-

ment) trajectory. Since this trajectory alteration results from the direction of the blast winds behind the shock front, this type of rigid body response depends on the relative geometry of the target and the explosion. If the system misses the target by an unacceptably wide margin, it will not be effective.

Passing through the hot fireball results in a thermal load on the system in addition to the thermal loads caused by the benign reentry heating or the supersonic flight of an ABM. Consequently, the impact of the total environment of a high altitude nuclear burst must be examined. Figure 16-21 shows the nuclear encounter sequence for RV and ABM systems. The loading and response of the vehicle at each point from 1 through 6 is a function of the local environment, the physical characteristics of the vehicle, and its flight profile.

After the vehicle enters the blast sphere, it may traverse a region of density lower than

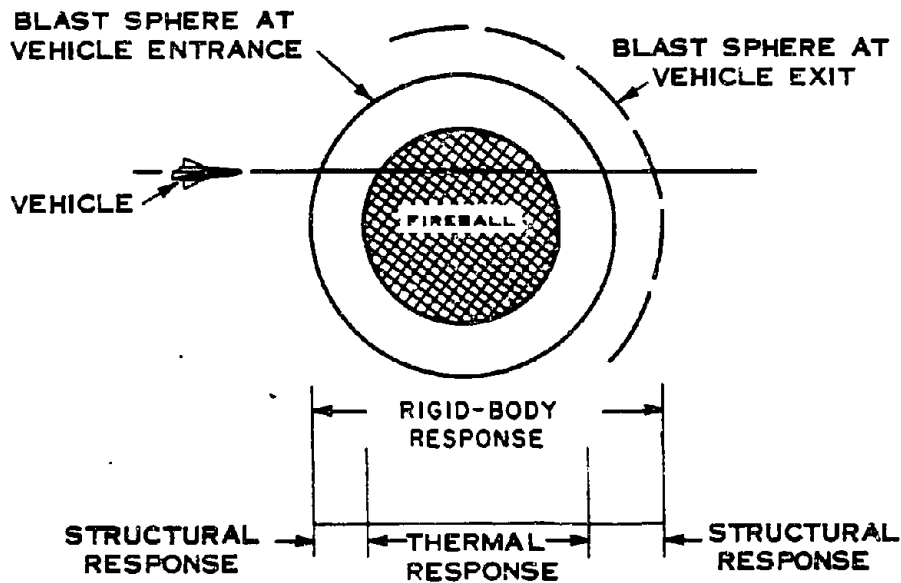


Figure 16-20. Response Regimes for Interceptor Missile

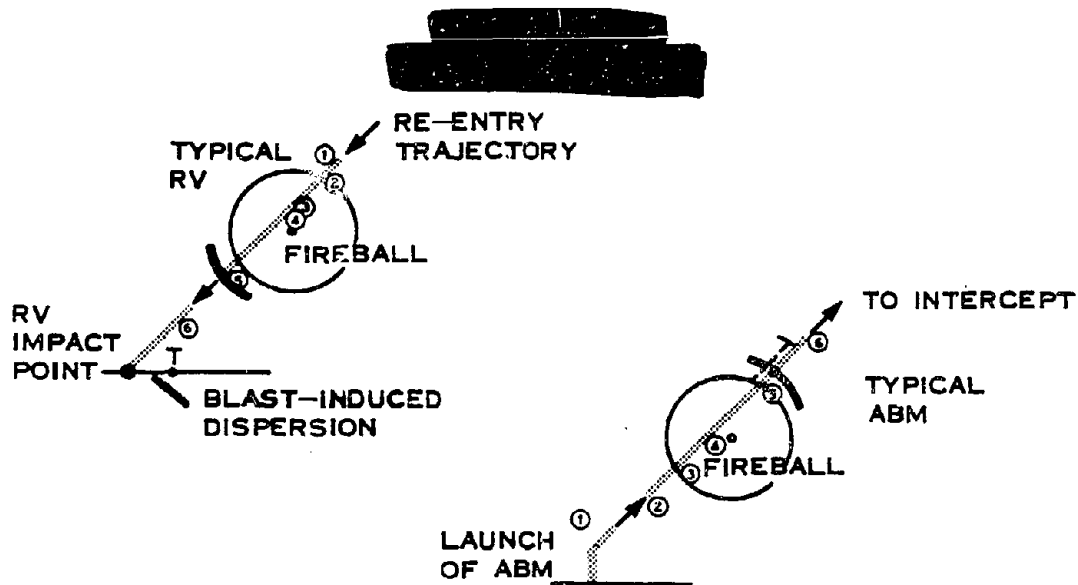


Figure 16-21. Nuclear Encounter and Event Sequence for RV and ABM

ambient before it exits the blast sphere. This may affect its flight stability, depending on the design characteristics, i.e., static margin and rate of damping. Under some conditions, a reentry vehicle on a ballistic trajectory may tumble in this region and/or subsequently emerge from the blast sphere with a large flight angle of attack, which may cause severe structural loading and may result in serious damage. Even if tumbling does not occur, exit loads imposed on a vehicle at a large angle of attack sometimes could be greater than initial entrance loads. Also, since the RV may exit the blast sphere at a large angle of attack, loss of accuracy and increased dispersion are likely. This is particularly true for advanced systems that use slender body configurations whose drag coefficients are very sensitive to changes in angle of attack.

Maneuvering reentry vehicles are being considered with a view toward avoiding a nuclear encounter or reducing the exposure time by altering the usual ballistic trajectory on reentry. However, while the maneuverability of

the reentry vehicle could increase its survivability, it could, under some circumstances, also increase its vulnerability to blast. The maneuvering vehicle would experience more severe aerodynamic preloads, to which the air blast induced loads would be added.

These maneuver load effects also can be important for ABM systems. Since ABM's are required to maneuver within the atmosphere, control surfaces, which also are susceptible to damage from gust loading, are involved. For many situations, assuming a range of yields and warhead designs, spacing between interceptors is governed by blast fratricide. In a saturation attack, the stepdown firing doctrine for defense tactics depends directly on the hardness of the interceptor to all nuclear effects. Consequently, a complete description of the nuclear environment is necessary to predict the effects of a nuclear burst on in-flight strategic systems. With respect to the blast wave, the parameters of interest include overpressure, particle velocity, density and temperature, as a function of both time and distance.

[REDACTED]

The propagation of the blast wave from the point of burst downward through a non-homogeneous atmosphere must be considered. Atmospheric inhomogeneity is not a serious problem for small yields at moderate heights, although it does distort the blast sphere somewhat. Blast wave inhomogeneity becomes more severe as the altitude of burst is raised above about 100,000 feet; however, it is significant that at these higher altitudes, blast begins to be less severe as a damage mechanism than other competing effects.

16-12 Sources of Data [REDACTED]

The blast effects on early RV's were expressed in terms of rigid body gust loading or "g" levels of deceleration. When these g loads were added to the normal "peaceful" reentry loads and then compared to design safety factors, it was found that the early RV designs were relatively soft and had large radii of blast vulnerability that outreached over nuclear effects. At these "vulnerable" ranges, overpressure levels were so low that local crushing or beam bending was not a problem.

As better theoretical models of the nuclear environment have been developed, blast loading and structural response calculations have become more sophisticated. Progress has been made, from the early engineering analysis of simple spring-mass models subjected to idealized loading, to more complex computer codes that handle rings and shells subjected to loads more representative of the nuclear engagement, including local body pressures. Through the use of 6-degree-of-freedom trajectory codes, the trajectory dispersions induced by the blast wave can be computed and the tumbling within the blast sphere can be predicted using approximate values of environment levels. Theoretical analyses have been developed to treat the shock-on-shock interaction and these analyses have been confirmed at normal incidence by experiments.

Test techniques have been developed to determine properties of materials at high strain rates.

Early programs to determine blast and thermal vulnerability of in-flight strategic vehicles include HARTS, SPINE, and ABM Vulnerability and Hardening. These research programs were closely coordinated with the research requirements of systems designers. This coordination is shown by the following list of the various configurations of research vehicles that have been studied and their counterparts in terms of military systems.

<u>Program</u>	<u>Research Vehicle</u>	<u>System Application</u>
Air Force	HARTS A	Mark 12 (RV)
Air Force	HARTS B	Mark 11A (RV)
Army	AIRS I	SPRINT (ABM)
Army	AIRS II	SPARTAN (ABM)

This correlation permits use of physical data and the aerodynamic coefficients obtained during the development of the specific systems.

16-13 Limitations in Application of the Data [REDACTED]

Since vulnerability (or damage) assessment of an in-flight strategic vehicle is such a strong function of the detailed characteristics of the specific vehicle, it is virtually impossible to devise a general method of vulnerability determination that could be applied to any vehicle. Some of the parameters that enter the problem are the details of the design of the primary structure of the vehicle (including all materials used, internal supports, field joint fixtures, etc.), the design features of the internal components and how they are supported on the primary structure, the detailed aerodynamic characteristics of the body and how it may fly (including the possible requirements for maneuvers). Therefore, it is obvious that an accurate definition of

the blast and thermal vulnerability of a particular in-flight strategic vehicle requires a great deal of analysis and the use of specialized computational models as well as experiments. Such analyses are beyond the scope of this manual.

The following discussion will attempt to explain, in general terms, the technical aspects of the problem that appear to have the most important influence on the determination of nuclear weapon blast and thermal damage to in-flight strategic vehicles. The technical discussion will be presented under two main sections, one devoted to RV bodies and the other to ABM vehicles; some of the material appearing under the RV section will be applicable to the ABM and, where this is the case, it will be noted.

BLAST LOADING ON REENTRY (RV) SYSTEMS

The general approach used herein to describe the important factors related to the determination of blast and thermal vulnerability of reentry vehicles was generated primarily under the Hardening Technology Study (HARTS). The HARTS vehicles that were studied are shown in Figure 16-22. Configuration A is a blunted cone and Configuration B is a sphere-cone-cylinder-flare. The dimensions and the ballistic coefficients are shown in the figure. Table 16-9 lists the range of parameters that were used in the HARTS studies. The term "hardness level" will be explained below.

16-14 Environment Scaling

The nomenclature used to describe RV/blast intercept conditions is shown schematically in Figure 16-23. The conditions pictured correspond to those where the RV does not traverse the center of the burst fireball ($\varphi \neq 0^\circ$). As described in Chapter 2, blast scaling has been used extensively to predict air blast environments. Since RV intercept loads and traversal phenomena depend on the blast parameters, it is

Table 16-9. Range of Basic Parameters for HARTS II

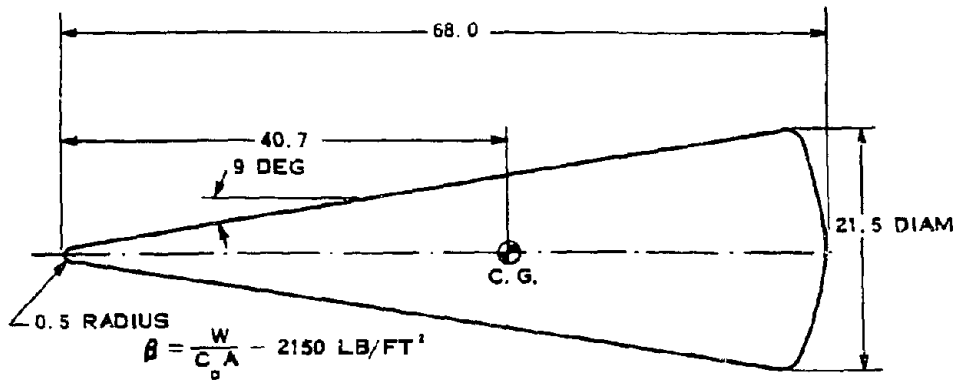
Blast yield	30, 200, and 440 kt - blast environment from Hillendahl FIREBALL code
Intercept altitude	30,000 to 100,000 ft
Intercept angle (φ)	0 to 90 deg
Trajectory	Minimum energy tra- jectories for 2,000, 5,500, and 7,000 nm ranges
Hardness levels (axial acceleration for head-on intercept)	200 to 1,000 g
Configurations (see Figure 16-22)	A: $\beta = 2,150 \text{ lb/ft}^2$ B: $\beta = 680 \text{ lb/ft}^2$

possible to scale RV intercept loads and traversal phenomena in a manner similar to the blast parameters.

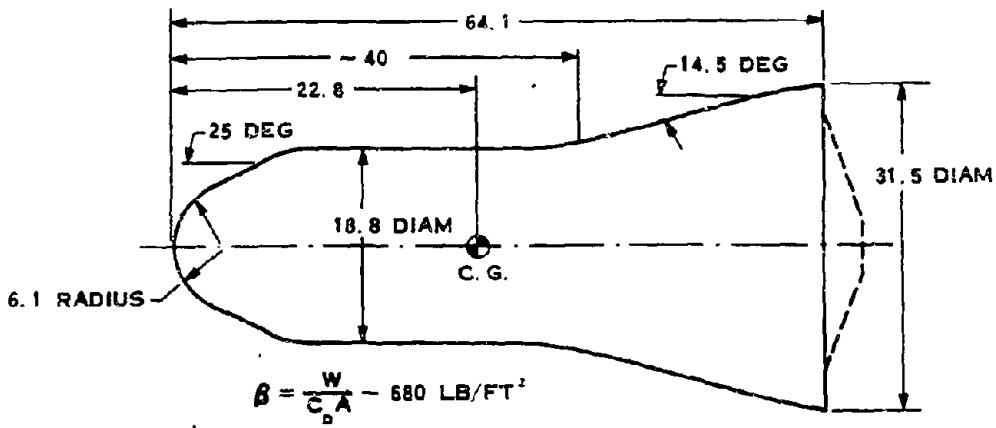
Figure 16-23 indicates that there are two important radii. First, the distance between the burst center and the vehicle at the time of detonation, denoted by RD, is significant for the comparison of *prompt* effects (e.g., neutrons, X-rays, etc.) as well as blast effects. Consideration of these RD values for various vehicle paths and orientations results in vulnerability envelopes referred to as *burst time* envelopes. Second, the distance between the burst center and the vehicle when the blast wave intercepts the vehicle, denoted by RB, results in envelopes referred to as *intercept time* envelopes. The reference time for which the envelope is constructed must be specified for each envelope.

"Hardness Level" is a useful parameter to hold constant when studying blast phenomena. Hardness level is defined as that *axial* load

NOTE: ALL DIMENSIONS
IN INCHES



CONFIGURATION A



CONFIGURATION B

Figure 16-22. HARTS Configuration

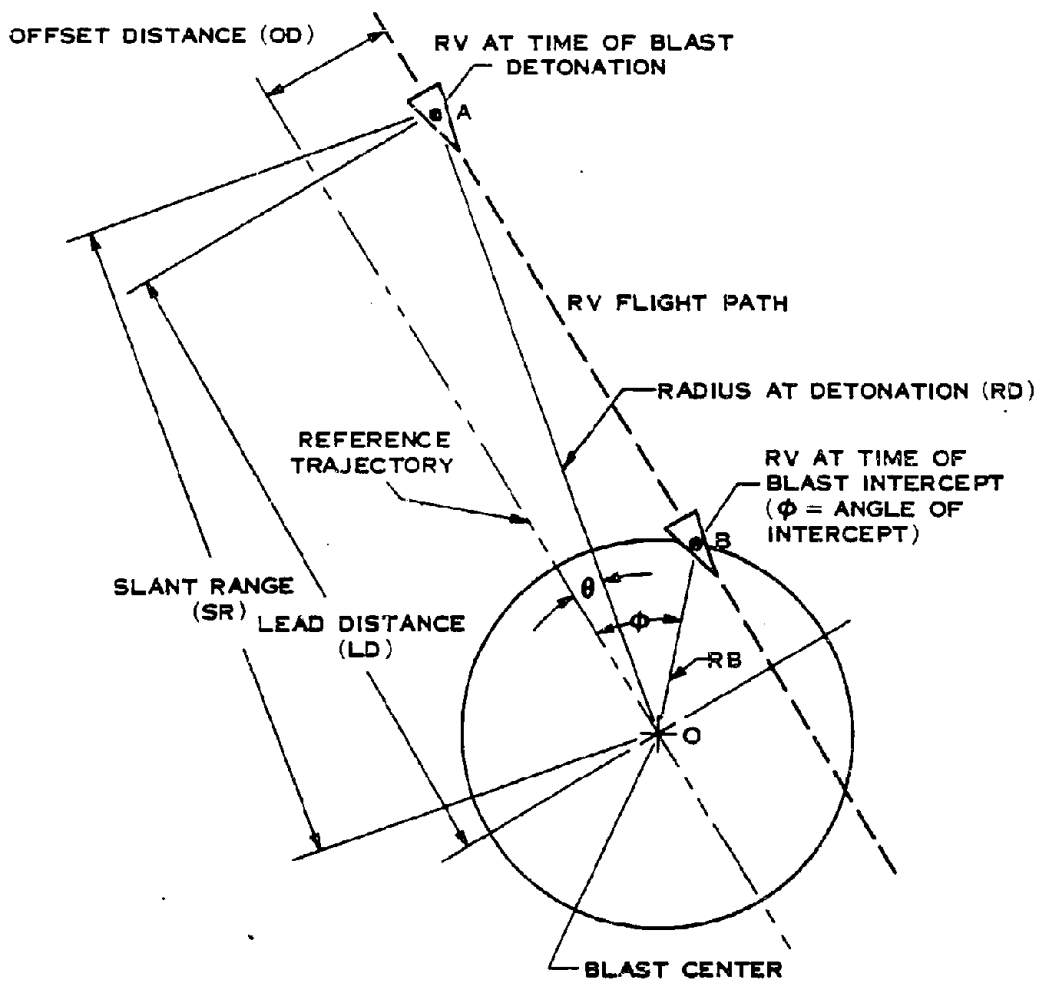


Figure 16-23. Blast Intercept Conditions Nomenclature

acceleration experienced by a vehicle intercepting a blast wave head on ($\varphi = 0^\circ$) at zero angle-of-attack ($\alpha = 0$). For a given yield, burst altitude, and configuration combination, the specification of a blast intercept hardness level determines the blast wave radius. This in turn determines the blast front environment. Blast scaling laws indicate that these blast front conditions are identical to those at a different yield and radius where the new radius is equal to the old radius multiplied by the cube root of the ratio of the yields. For example:

$$RB_2 = RB_1 (W_2/W_1)^{1/3} \text{ (ft),}$$

where RB_2 and RB_1 are the blast intercept radii for yields of W_2 and W_1 , respectively, and in general,

$$RS = RB/W^{1/3} \text{ (ft/kt}^{1/3}\text{),}$$

where RS is known as the scaled intercept radius. Values of scale radius, RS , at constant hardness level for varying altitude are shown in Figure 16-24. A similar presentation of scale time of blast intercept can be made, since time and radius are proportional. Thus, in general,

$$\tau_1 = t_1 W^{1/3} \text{ (sec/kt}^{1/3}\text{),}$$

where t_1 is the time after burst to intercept and τ_1 is the scaled time. Values of scaled time, τ_1 , for

constant hardness levels for varying altitude are shown in Figure 16-25.

The hardness level, position-time relationships are defined in a manner that data for any yield can be derived over the given range of hardness levels and burst altitudes. System analysis parameters such as slant range SR , lead distance LD , and offset distance OD , from the burst at time of explosion also can be derived simply. For a given hardness level and burst altitude one RS and τ_1 combination exists. For specified yield,

$$RB = RS W^{1/3} \text{ (ft)}$$

$$t_1 = \tau_1 W^{1/3} \text{ (sec).}$$

Referring to Figure 16-23, the following spacing relationships are apparent.

$$OD = RB \sin \varphi,$$

$$LD \approx RB \cos \varphi + V t_1,$$

$$SR = (LD^2 + OD^2)^{1/2},$$

where V is the RV velocity, and the other symbols are defined in Figure 16-23.

Determination of lead distance is illustrated in Problem 16-1. The variation of hardness level with altitude and slant range is shown in Figure 16-26

DATA
(1)-(3)

[REDACTED]

Problem 16-1. Calculation of Hardness Level

Figures 16-24 and 16-25 show the scaled blast radius and scaled time of blast intercept, respectively, for a Configuration A vehicle on a 5,500 nautical mile flight path as a function of burst altitude for various hardness levels. Various system parameters may be determined from Figures 16-24 and 16-25 as discussed in paragraph 16-14.

Example

Given: A HARTS Configuration A vehicle (Figure 16-22) is on a 5,500 nm trajectory. The RV hardness level is 500 g.

Find: The slant range at which the RV would experience a head on ($\varphi = 0^\circ$) load equal to its hardness level if it were exposed to the blast wave

[REDACTED]

[REDACTED]

[REDACTED]

[REDACTED]

[REDACTED]

[REDACTED]

[REDACTED]

[REDACTED]

[REDACTED]

[REDACTED]

[REDACTED]

[REDACTED]

[REDACTED]

[REDACTED]

[REDACTED]

[REDACTED]

[REDACTED]

[REDACTED]

Answer: If the RV is more than [REDACTED] away from the specified explosion at the time of burst, it will not be damaged by blast.

DNA
(1-)(3)

DNA
(1-)(3)

[REDACTED]

[REDACTED]

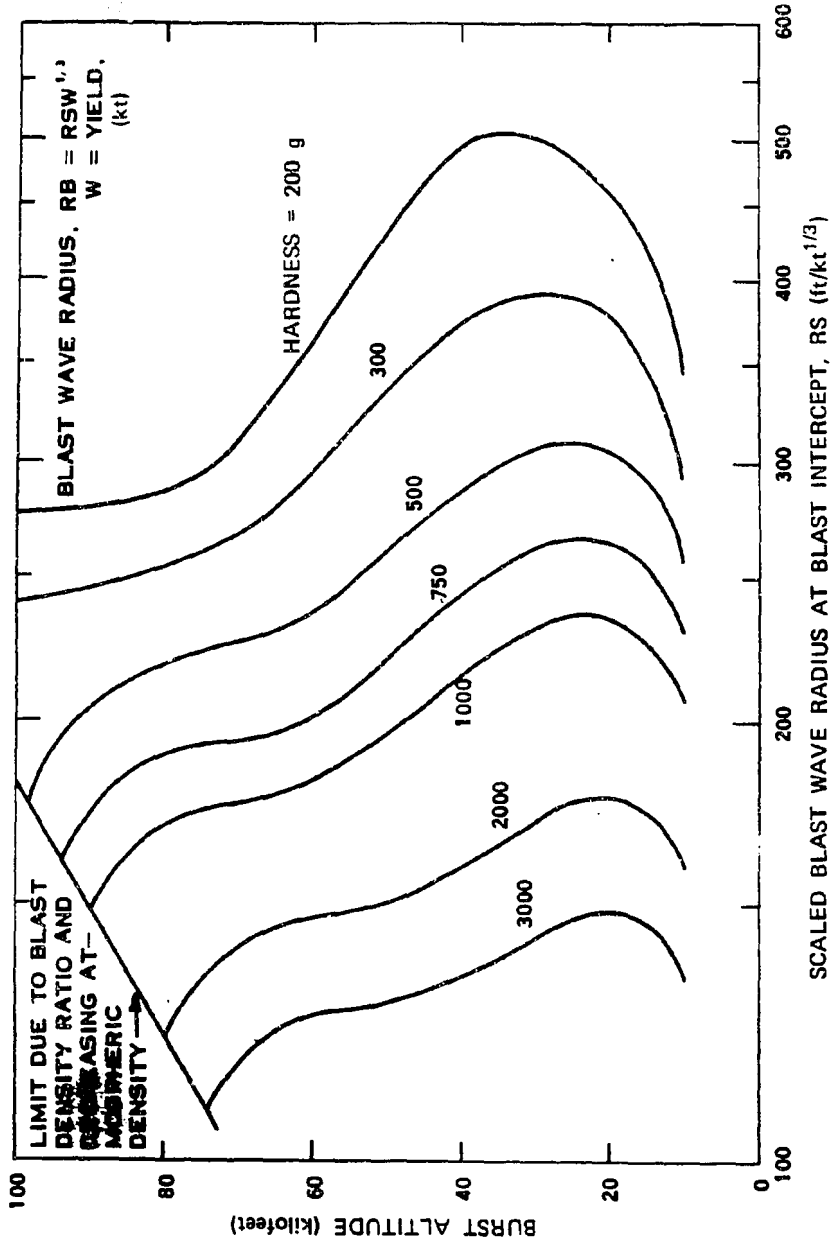


Figure 16-24. Scaled Blast Wave Radius for Constant Hardness Level for Configuration A, 5,500 nm Range

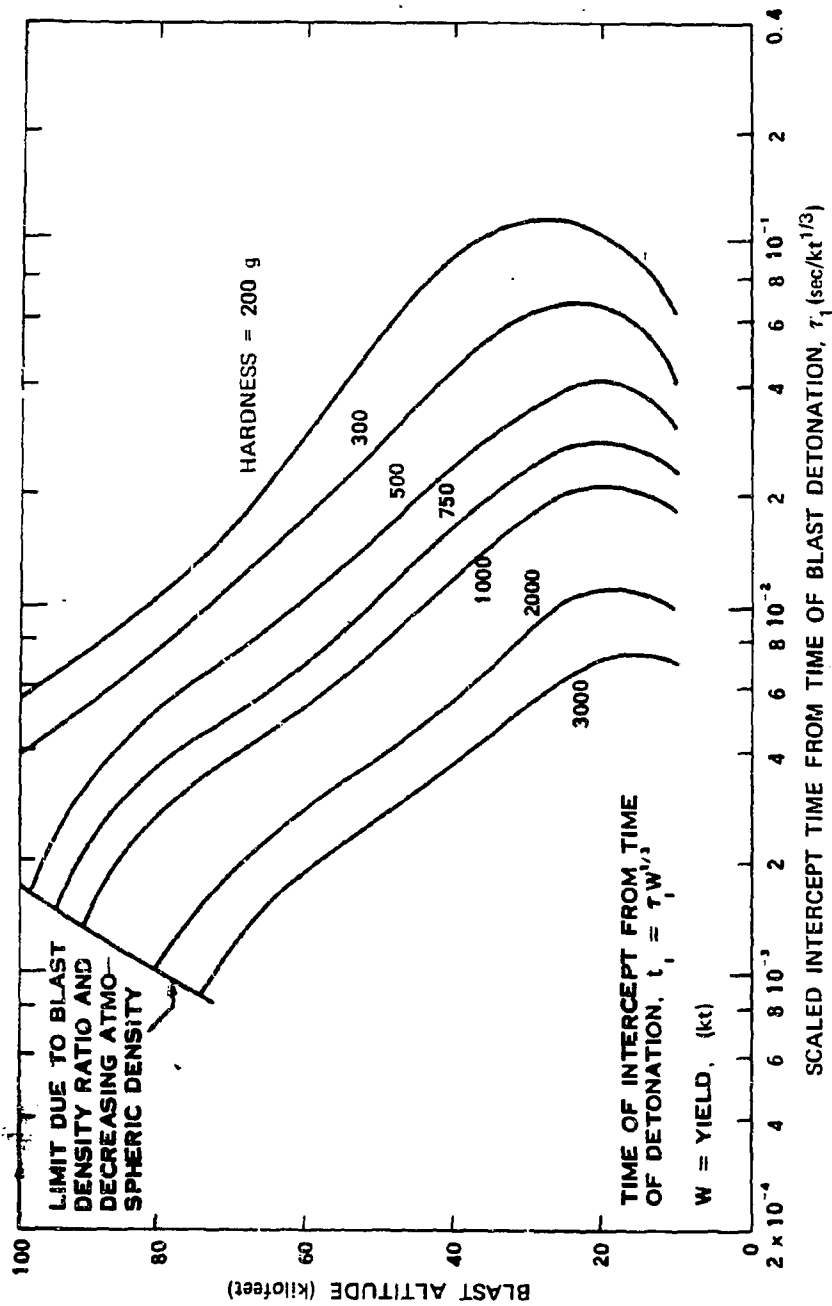
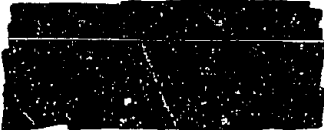


Figure 16-25. Scaled Time of Blast Intercept for Constant Hardness Level for Configuration A, 5,500 nm Range



DNA
(A)(3)



Deleted

Figure 16-26. Variation of Hardness Level with Altitude and Slant Range
for Configuration A



[REDACTED]

16-15 General Intercept Loads and Load Duration

The aerodynamic loading on hypersonic reentry vehicles can be divided into two general categories: steady state loading and transient loading. Steady state loading occurs when the pressure, density, particle velocity, and temperature do not change with time. Transient loading occurs when there is a time change in the environment surrounding the reentry body.

The vehicle experiences a continuing change in environment during normal reentry. However, since this change is relatively slow, steady state drag loading provides a good approximation for normal reentry conditions. For any type of flow over a body, the local pressure at any point on the surface can be found from the relation:

$$P_b = P_f + qc_p,$$

where

P_b = pressure at some point on the body surface,

P_f = free stream ambient pressure,

q = free stream dynamic pressure,

c_p = local pressure coefficient.

Classic Newtonian impact theory provides a simple closed-form solution for the local pressure coefficient, c_p . For steady state, hypersonic flow (above Mach 5) this theory provides adequate loading predictions. For any body of revolution the Newtonian theory predicts:

$$c_p = 2(\cos \alpha \sin \delta - \sin^2 \alpha \cos \delta \sin \beta_r)^2,$$

where

α = angle between the vehicle longitudinal axis and the relative wind vector,

δ = vehicle semivertex angle,

β_r = rotational angle about axis of reentry vehicle.

A vehicle experiences axial and lateral decelerations and local pressure loading during normal reentry. The amount of deceleration and local pressure depends on the vehicle reentry angle, velocity, shape, weight, and altitude. Figures 16-27 through 16-29 show some nominal reentry trajectories. These graphs only include the combinations of reentry velocity and reentry angle that correspond to a ballistic missile having a nominal range of 5,500 nm. The reentry vehicle is characterized by the ballistic coefficient, which is varied over a range of values typical for reentry vehicle designs. Calculations for the parameters (velocity, altitude, and time) of the reentry trajectories were begun at an altitude of 400,000 feet, since this altitude is well above that of appreciable aerodynamic forces for the reentry vehicles considered. The reentry angles measured from the local horizontal at 400,000 feet were chosen arbitrarily as 20 and 30 degrees. The corresponding reentry velocities at 400,000 feet were determined from the basic equation for vacuum ballistic trajectories. The ballistic coefficients vary from 800 to 2,500 lb/ft². Below 100,000 feet the angle of attack is largely damped out, and the lateral force is very small.

The hardness level curves in Figure 16-24 represent one value on the intercept/load matrix of axial rigid body loads, G_A , for zero blast intercept angle ($\varphi = 0^\circ$). It was determined that, at constant hardness level, the blast front environments for varying yields are essentially identical. The last variable to be accounted for in intercept loads is blast intercept angle. At constant hardness level and altitude, the intercept angle is the only factor that can affect intercept loads by changing the angle between the blast wind vector and the vehicle velocity vector, thereby causing a blast induced angle of attack at blast intercept.

(U) Blast yield scaling also can be applied to the scaling of intercept load duration, fireball

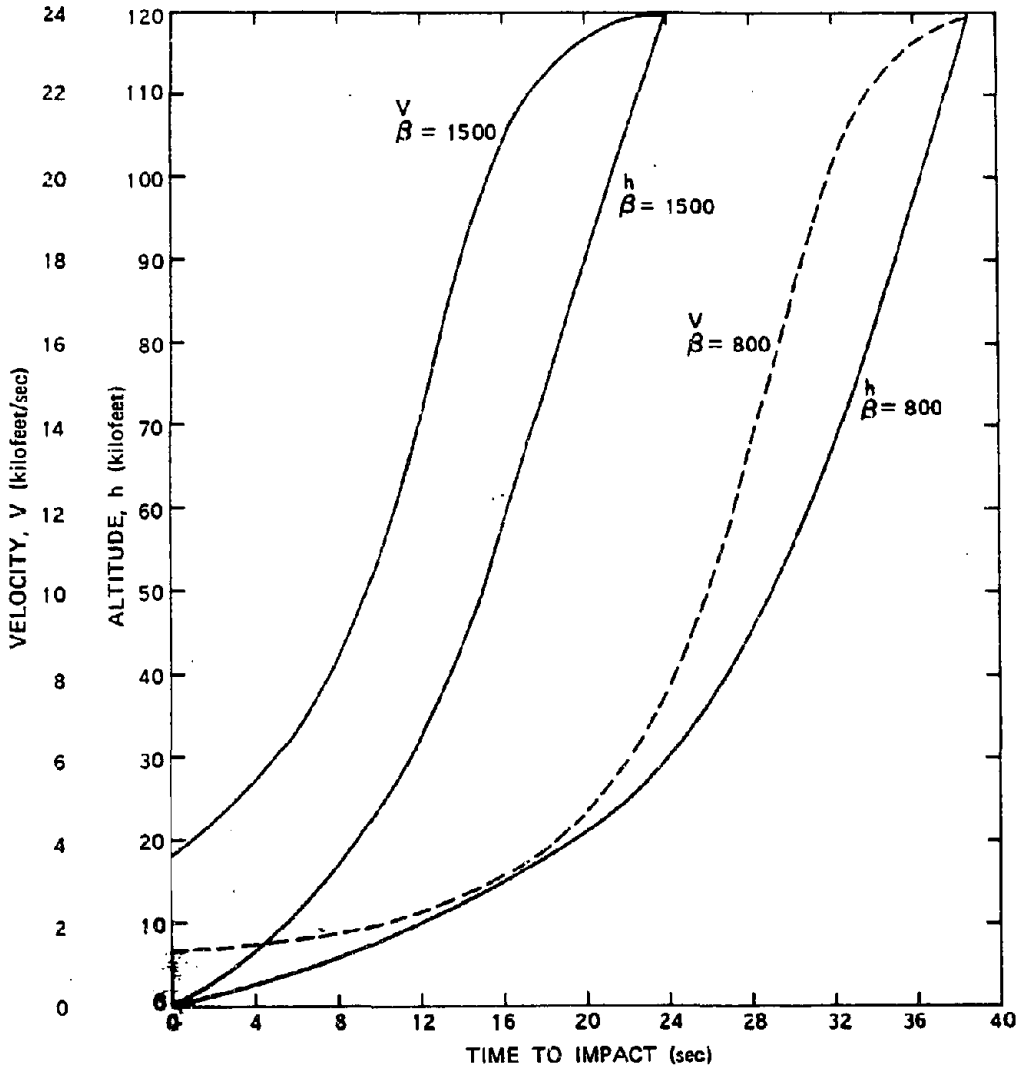


Figure 16-27. Normal Reentry Trajectory; Initial Altitude = 400,000 ft, Initial Velocity (V_i) = 23,900 ft/sec, Initial Flight-Path Angle = 20° , Ballistic Coefficient $\beta = W/C_d A$ lb/ft²

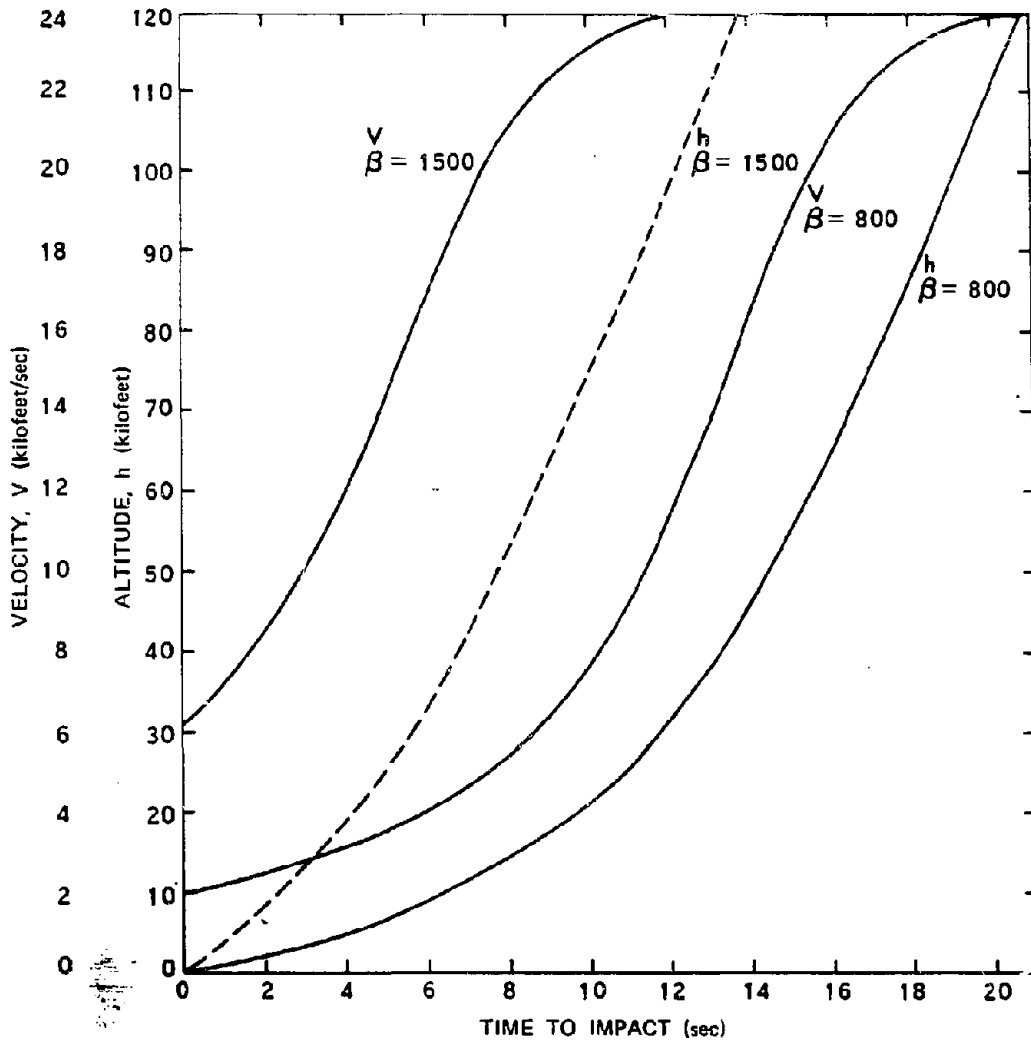


Figure 16-28. Normal Reentry Trajectory; Initial Altitude = 400,000 ft, Initial Velocity (V_i) = 24,000 ft/sec, Initial Flight-Path Angle = 30° , Ballistic Coefficient $\beta = W/C_D A$ lb/ft²

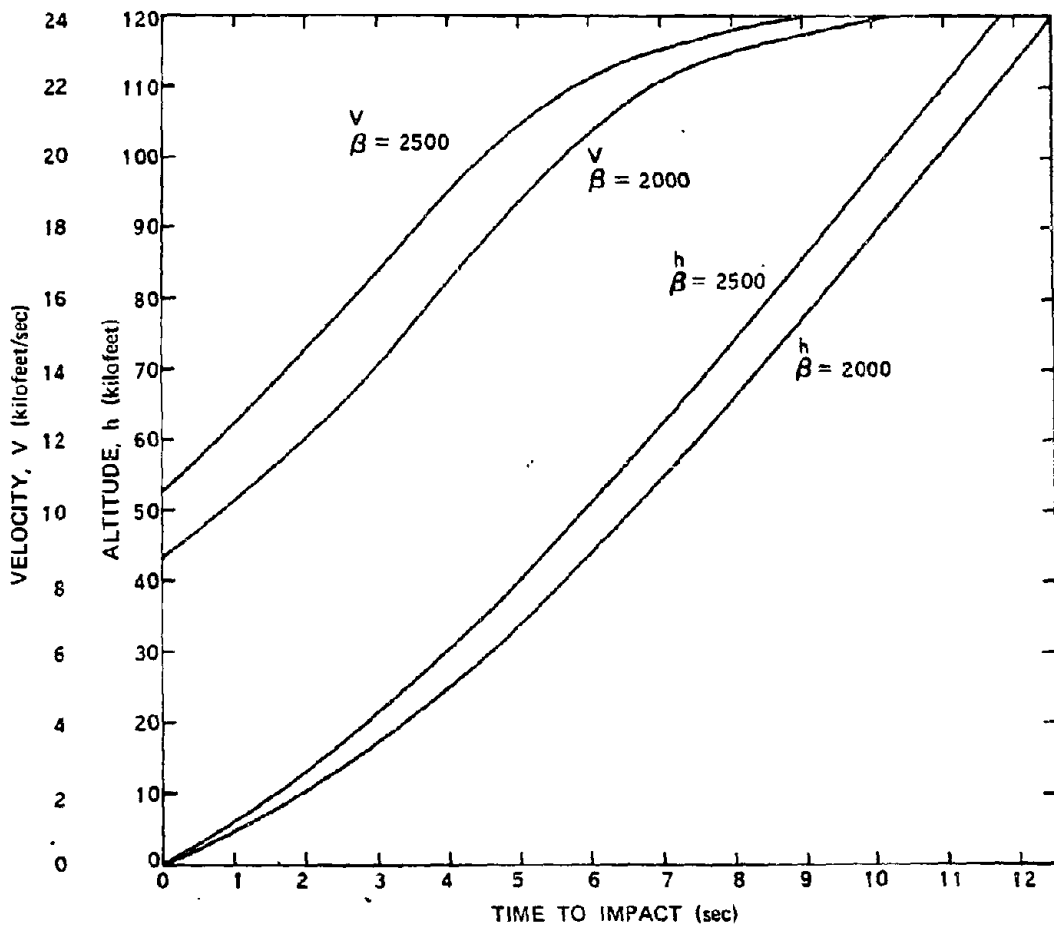


Figure 16-29. Normal Reentry Trajectory; Initial Altitude = 400,000 ft, Initial Velocity (V_0) = 24,000 ft/sec, Initial Flight-Path Angle = 30° , Ballistic Coefficient $\beta = W/C_d A$ lb/ft²

traversal time, and total traversal time. Time and radial distance are scaled with the cube root of the yield. Interior blast phenomena can be assumed to scale with the cube root of the yield to obtain reduced radius or time. At any point in time the blast can be imagined to have a size of unity for 1 kt. The blast size for larger yields is unity times the cube root of yield in kilotons, on a relative basis. Since blast loading duration depends on the blast size, which can be scaled, the loading duration also can be scaled.

16-16 Intercept Load Duration

Intercept loads are a function of hardness level, blast intercept angle, and blast altitude. The duration of the load is necessary to describe the intercept loading phase adequately. Under most conditions, the intercept loading history can be approximated by a triangular shaped pulse, i.e., intercept impulse is essentially one-half the maximum load multiplied by the duration time.

$$I_1 = \frac{G_1 \Delta t_{ILP}}{2} \text{ g-sec.}$$

The intercept load time constant, Δt_{ILP} , is

$$\Delta t_{ILP} = t_1 - t_{10\%} \text{ sec,}$$

where $t_{10\%}$ is the point at which the intercept load decays to 10 percent of its maximum value. The scaled intercept load duration time, τ_{ILP} , is

$$\tau_{ILP} = \frac{\Delta t_{ILP}}{W^{1/3}} \text{ sec/kt}^{1/3}.$$

Scaled intercept load duration times for a hardness level of 500 g are shown in Figure 16-30 for various intercept angles and altitudes. The intercept load duration times and intercept loads provide a usable set of data for estimating

the intercept load impulse. The duration times apply to axial, normal, or total resultant loads. In general,

$$\Delta t_{ILP} = \tau_{ILP} W^{1/3} \text{ sec,}$$

and any load impulse is

$$I_1 = \frac{1}{2} \Delta t_{ILP} G_1 \text{ g-sec}$$

where I_1 and G_1 represent any intercept load impulse and maximum load, respectively.

16-17 Fireball Traversal Time

The time at which the intercept load has decayed to 10 percent of its maximum value (end of the intercept load pulse) corresponds approximately to the time when the vehicle enters the fireball (temperature $\approx 10,000$ to $15,000^\circ\text{R}$). For practical considerations, the end of the intercept load pulse and initial fireball immersion can be considered as the same time. The time of fireball traversal is

$$\Delta t_{FB} = t_{EFB} - t_{10\%} \text{ sec.}$$

where t_{EFB} is the time of exiting the fireball, and the scaled time of fireball traversal is

$$\tau_{FB} = \Delta t_{FB} / W^{1/3} \text{ sec/kt}^{1/3}.$$

Scaled fireball traversal time for a hardness level of 500 g is shown in Figure 16-31 for various intercept angles and altitudes. The time of exiting the fireball, t_{EFB} , is that time during the exit phase when increasing dynamic pressure reaches the ambient level at the blast altitude. This time also is approximately when the temperature level drops below $10,000$ to $15,000^\circ\text{R}$. It should be noted that the point during entry at which the decreasing dynamic pressure reaches

[REDACTED]

ambient level is about the same as the point of 10 percent load.

16-18 Total Traversal Time [REDACTED]

[REDACTED] Total blast traversal time is

$$\Delta t_t = t_E - t_i \text{ sec,}$$

where t_E is the time of exit from the blast wave

shell, and as before, t_i is the time of intercept. The scaled time of blast traversal is

$$\tau_t = \Delta t_t / W^{1/3} \text{ sec/kt}^{1/3}.$$

Scaled total blast traversal time for a hardness level of 500 g is shown in Figure 16-32 for various intercept angles and altitudes.

[REDACTED]

**Problem 16-2. Calculation of Load Characteristics, Fireball
Traversal Time and Total Traversal Time**

[REDACTED] Figures 16-30 through 16-32 provide the information necessary to calculate the load characteristics, the fireball traversal time, and the total blast traversal time for a vehicle similar to Configuration A with a hardness level of 500 g that enters the blast front at various intercept angles.

[REDACTED] *Example* [REDACTED]:

Given: An RV similar in design to HARTS Configuration A (see Figure 16-22) with a hardness level of 500 g that is traveling on a 5,500 nm trajectory.

Find: The intercept load characteristics, and traversal times if the RV is exposed

[REDACTED]

[REDACTED]

[REDACTED]

DNA
HXE

[REDACTED]

[REDACTED]

[REDACTED]

[REDACTED]

[REDACTED]

[REDACTED]

[REDACTED]

[REDACTED]

[REDACTED]

[REDACTED]

DNA
(1-)(3)

[REDACTED]

[REDACTED]

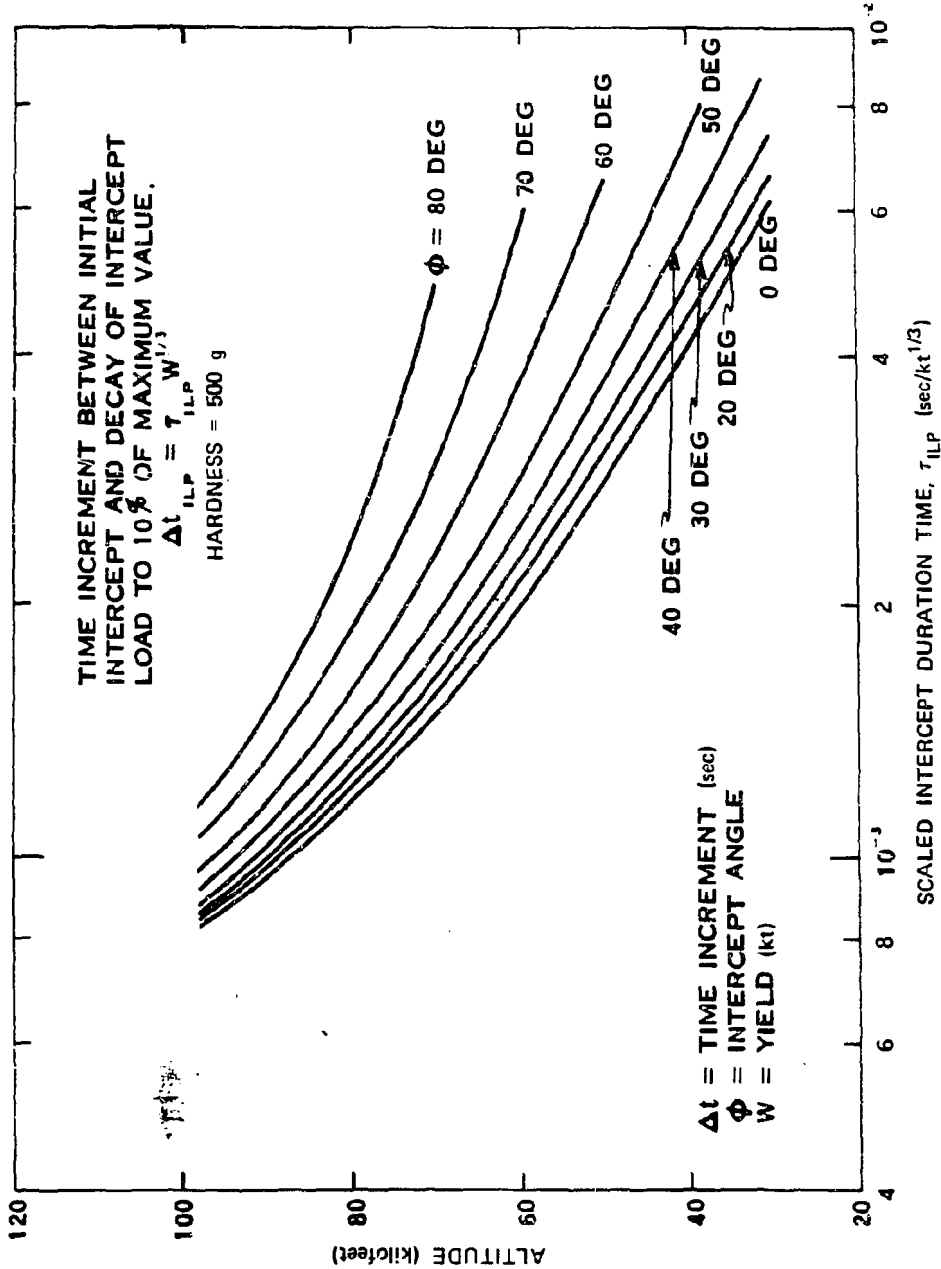


Figure 16-30. Scaled Intercept Load Duration Time, 500 g Hardness, Configuration A

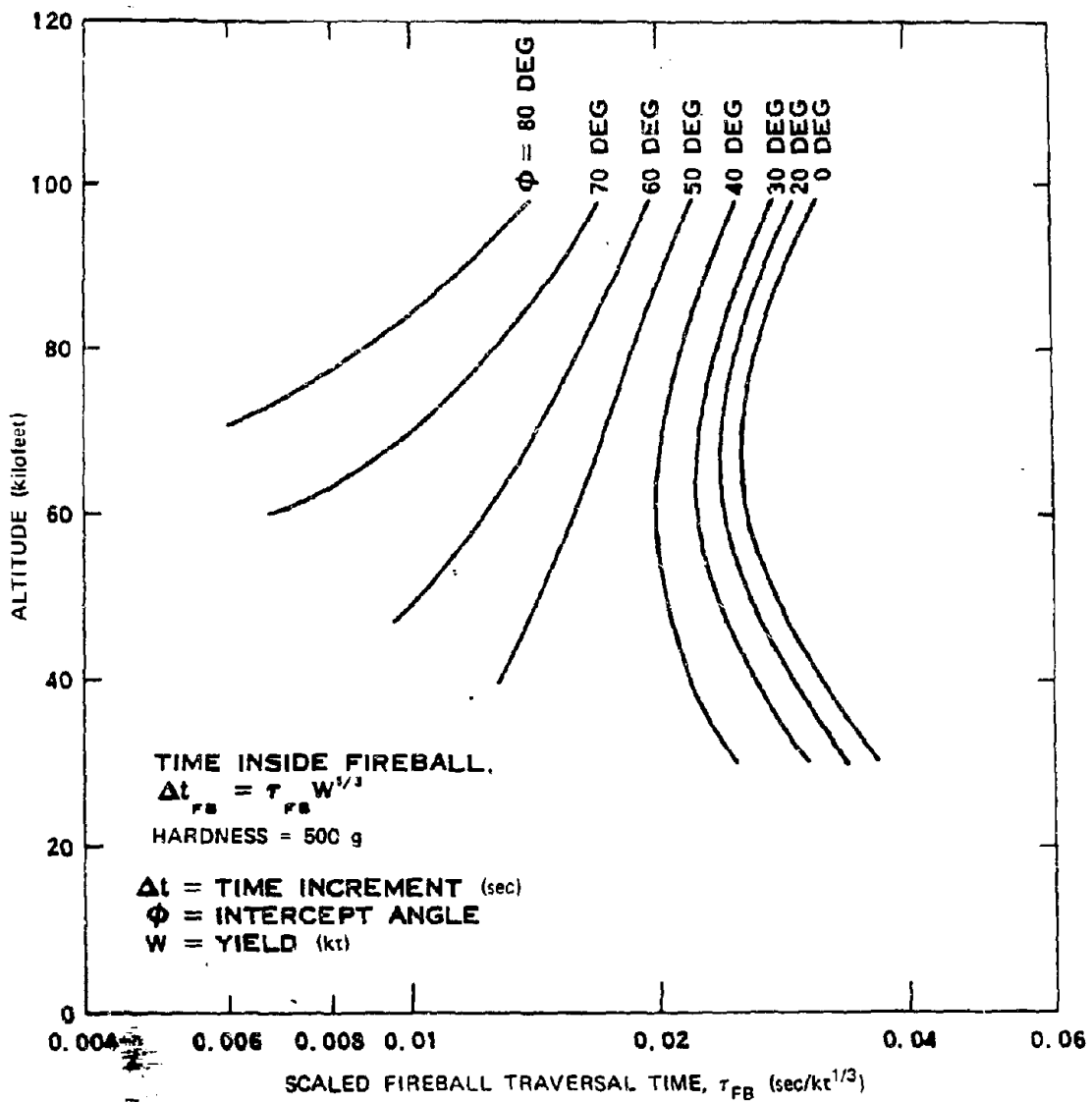


Figure 16-31. Scaled Fireball Traversal Time,
 500 g Hardness, Configuration A

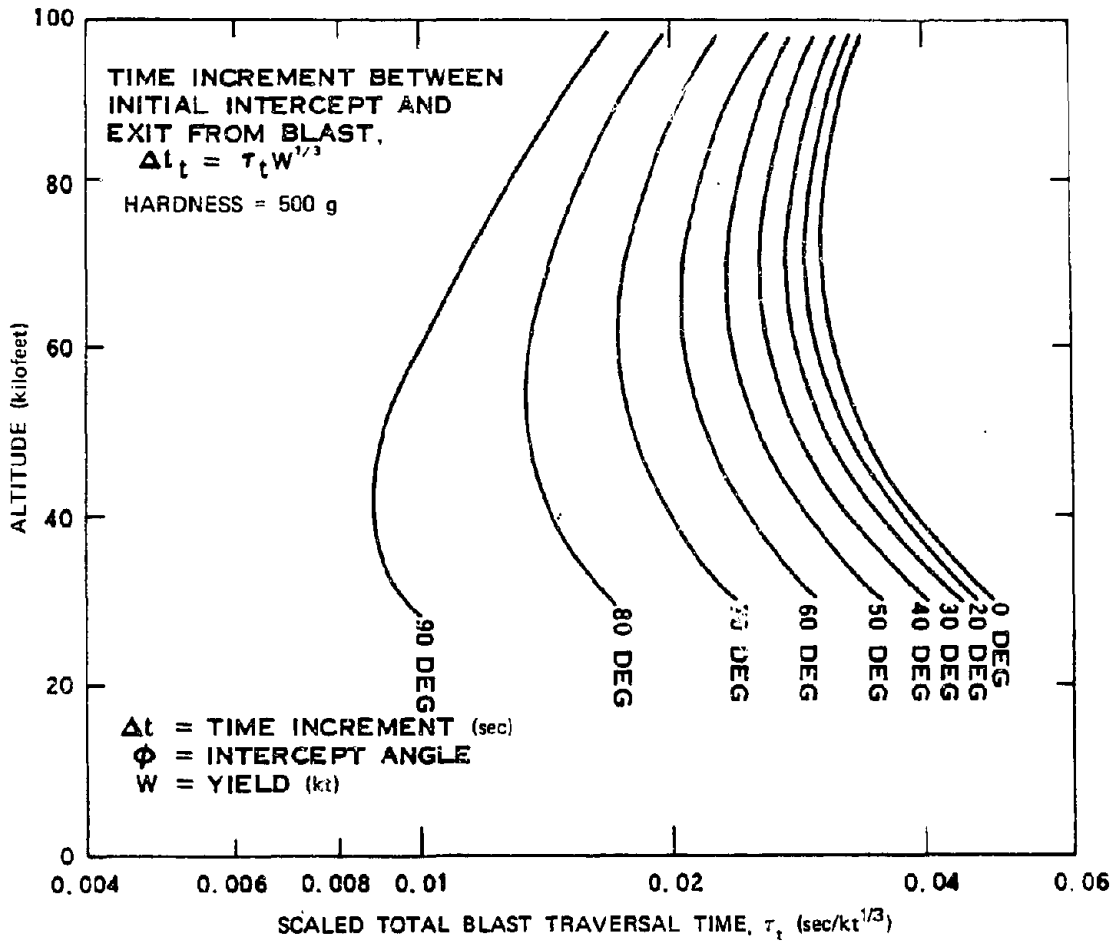


Figure 16-32. Scaled Total Blast Traversal Time,
 500 g Hardness, Configuration A

16-19 Exit Loads

Intercept load, intercept load duration, fireball traversal time, and total traversal time are functions of hardness level, blast intercept angle, and blast altitude (on a scaled basis). Exit loads also depend on blast yield as well as the functions listed above. This precludes any universal scaling of exit loading; however, the following are generally true of exit loading conditions:

- The probability of obtaining higher exit than intercept loads is very low for vehicles similar to Configuration A.
- Exit loads decrease with decreasing intercept hardness level.

16-20 Blast Data Generalization

The data summarized in the preceding paragraphs were generated for Configuration A with a 5,500 nautical mile range minimum energy trajectory. Loading and duration scaling procedures applicable to the blast problem were demonstrated for this case. These specific data are *not* directly applicable to *any* configuration-range combination. However, by some simple relationships and approximations, the data can be applied to different configurations and ranges, or combinations of both, within limits.

Configuration Variations. For other configurations, assume that the velocity, flight path

angle, and intercept conditions at the same blast altitude are identical. With these constraints, the intercept loads become a function of ballistic coefficient and lift characteristics. For axial loads,

$$\frac{G_{AI_1}}{G_{AI_2}} \approx \frac{\beta_2}{\beta_1}$$

and for normal loads,

$$\frac{G_{NI_1}}{G_{NI_2}} \approx \frac{\beta_{\alpha 2}}{\beta_{\alpha 1}}$$

where

$$\beta = \frac{W}{C_D A} \text{ lb/ft}^2$$

$$\beta_{\alpha} = \frac{W}{C_{N\alpha} A} \frac{\text{lb-deg}}{\text{ft}^2}$$

The term β_{α} is defined as the normal force ballistic coefficient.

16-21 Typical RV Aerodynamics

A body that is moving along a reentry trajectory at hypersonic velocities has a flow field associated with it. The flow field is composed of the following main regions or characteristics (see Figure 16-33): stagnation point,

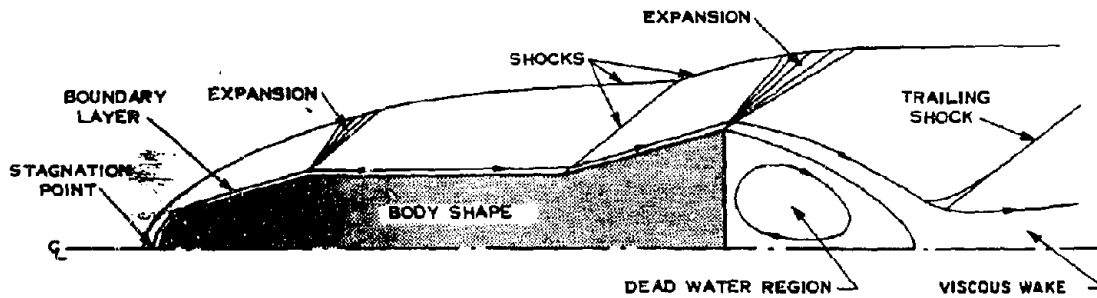


Figure 16-33. Flow Pattern Around an Axisymmetric Blunt-Nosed Body

shock layer, boundary layer, expansion shocks, pressure and density contours, wake, etc. The details of these flow regions are a strong function of the body shape, its velocity, and the properties of the air (i.e., altitude) through which the body is moving. Consequently, the flow field associated with even a single body is constantly changing during the reentry process.

Figure 16-34 shows the pressure distribution (in terms of pressure ratio) over the surface of a body similar to a HARTS Configuration B vehicle as a function of vehicle velocity. The pressure ratio is $(P_b - P)/P$, where P_b is the local pressure at any point along the surface and P is the ambient pressure. The overpressure $(P_b - P_o)$ are shown for sea level conditions (P_o is the ambient pressure at sea level) to provide some idea of the overpressures involved. It is evident that the overpressures near the stagnation region exceed all other pressures by a wide margin for this blunt body. It should be pointed out that these pressures do not take account of boundary layer perturbations, but the calculated pressures are indicative of actual flow field conditions: the overpressures associated with the flow field shock front are slightly higher than pressures on the surface. The curves in Figure 16-34 may be used to interpret the flow fields at altitude. For instance, the ambient pressure at 50 kilofeet is about one-tenth that at sea level. Thus, a vehicle at 50 kilofeet traveling at Mach 10 would have an overpressure on the flare of about 12 psi (i.e., $120/10$) and stagnation value in excess of 150 psi. If the vehicle were traveling at Mach 20, the flare overpressure would be about 41 psi ($410/10$).

Another typical reentry flow field, which gives the pressure ratio distribution over a body similar to the HARTS Configuration A (i.e., cone-sphere shape), is shown in Figure 16-35. Figures 16-34 and 16-35 emphasize the differences caused by body shape. Depending on the bluntness of the nose section, there is a very

small region over which high stagnation pressures exist. The pressures are virtually constant over the conical section. Figure 16-36 also shows sea level overpressure values for reference: the overpressures shown indicate that at altitudes near 50 kilofeet with the body traveling at Mach 20, the overpressure at the surface of the cone section is about 32 psi.

16-22 Initial Interaction of Vehicle Flow-Field and Blast Wave (Shock-Shock)

When the reentry vehicle bow wave and the blast wave contact each other a region of high pressure is generated. This region is characterized by a value of pressure that is larger than the value of pressure associated with either shock wave before the interaction. The HARTS results can be summarized by referring to a representative figure. Figure 16-36 shows the variation of maximum overpressure ratio (shock-shock maximum overpressure divided by quasi-steady maximum overpressure, *after interaction*) and duration with the nose surface angle for a hemispherical nose at typical intercept conditions ($M_\infty = 15$ to 22 and $M_B = 5$ to 8) assuming $\gamma = 1.4$. The general conclusion to be drawn from the upper curve of Figures 16-36 is that the shock-shock interaction peak overpressure will not exceed a factor of two larger than the quasi-steady overpressure (after interaction). Also, the lower curve on Figure 16-36 indicates that the duration of the shock-shock interaction is extremely short; as an example, if $\tau V_v/R$ is 0.2, then $\tau = 1 \mu\text{sec}$ (10^{-6} sec) for $V_v = 20,000$ ft/sec and $R = 0.1$ ft. However, it is evident that for the same nose radius (R), the value of τ increases as the vehicle speed (V_v) decreases.

16-23 Damage Envelopes

The culmination or end result of loading and response calculations is the damage envelope. The damage envelope defines a volume

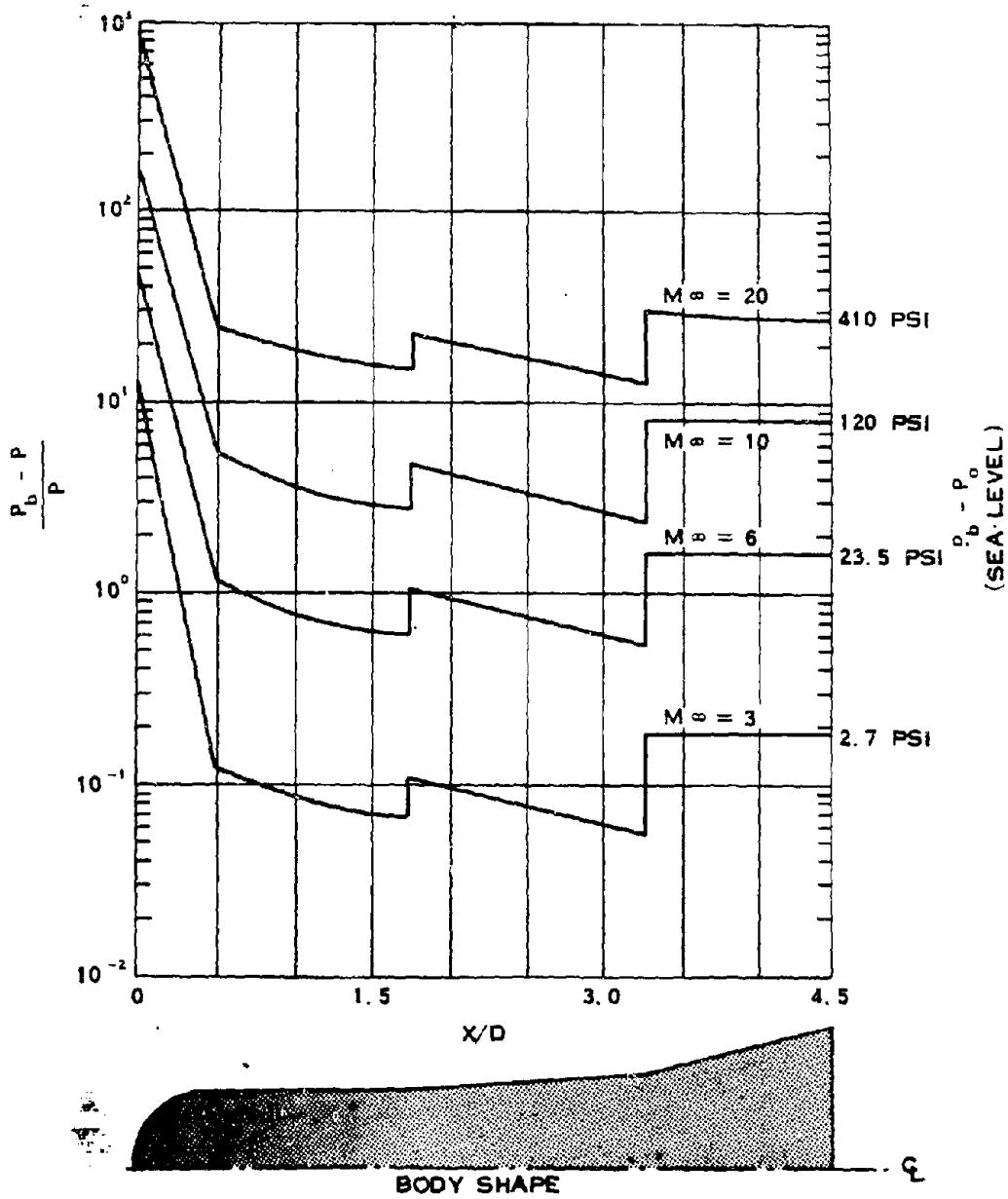


Figure 16-34. Steady State Flow Field Surface Pressures, Sphere-Cone-Flare Body

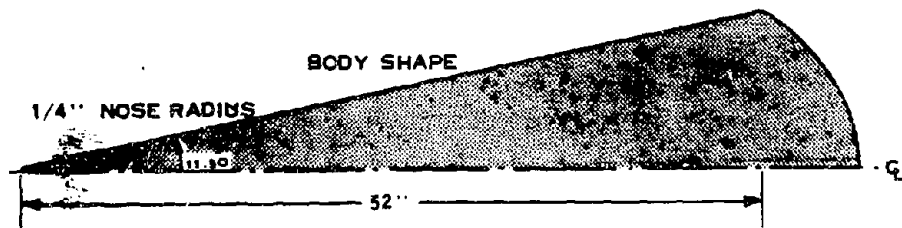
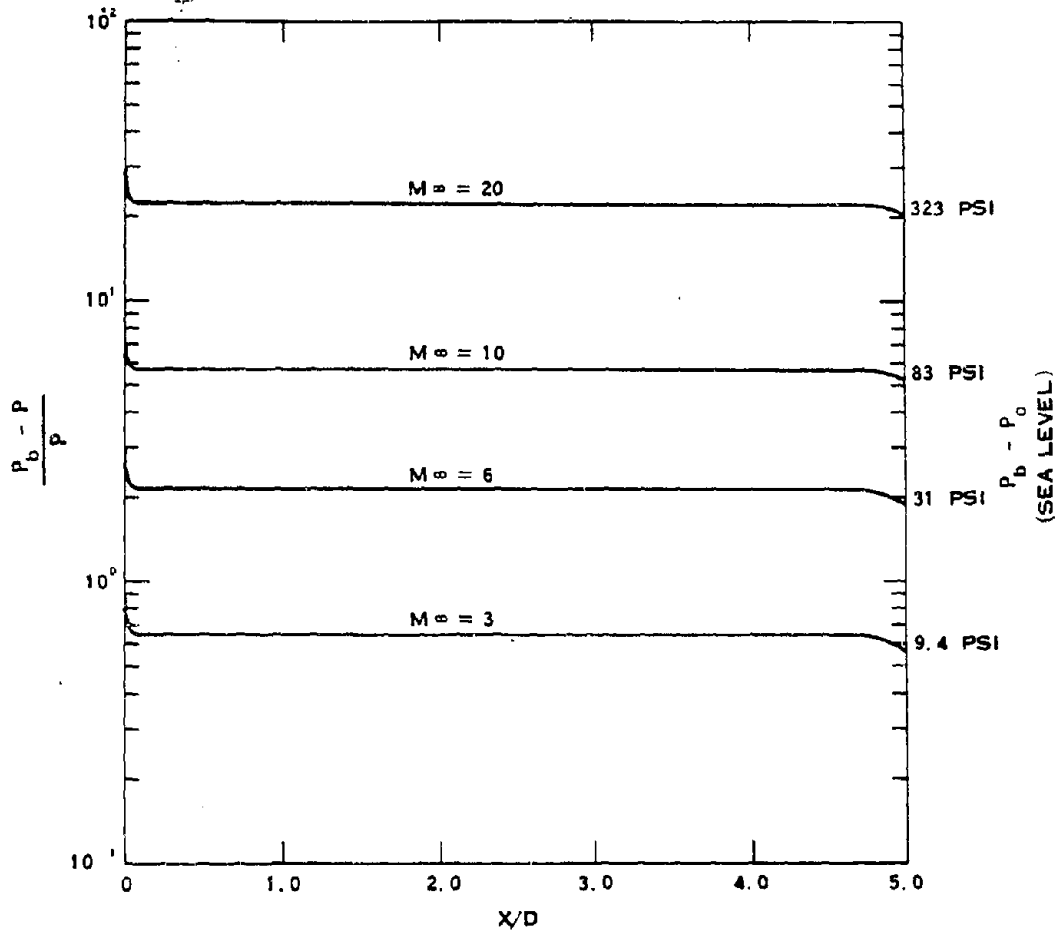


Figure 16-35. Steady State Flow Field Surface Pressures, Cone Sphere Body

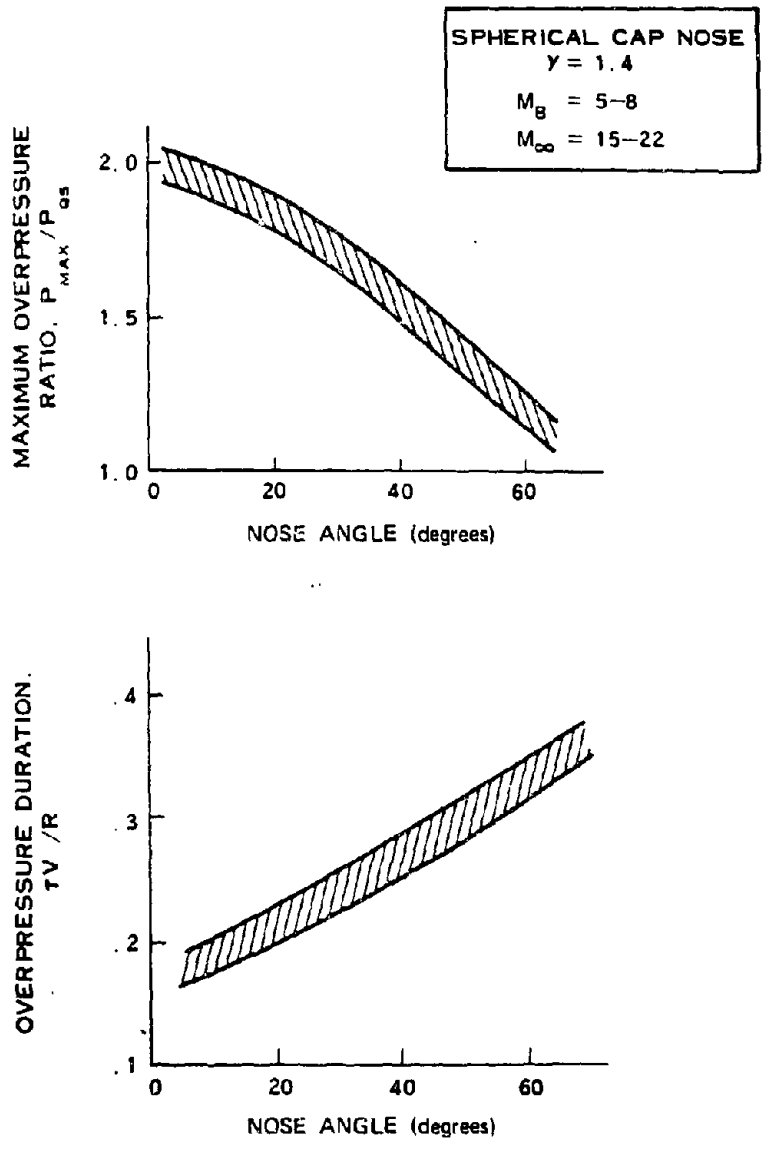


Figure 16-36. Maximum Overpressure and Overpressure Duration for Typical Shock-Shock Interactions

[REDACTED]

within which a burst of specific yield will cause axial or lateral forces greater than those for which the vehicle was designed. This envelope is required as part of the iterative processes in which tradeoffs involving weight penalties, yields, target damage criteria, defense capabilities, dispersion and booster capabilities must be considered. Two basic steps in determining the damage envelopes for an RV are: construction of the Locus of Escape (LOE); and location of points, relative to burst point, where the RV is subjected to forces equal to design loads.

[REDACTED] The nomenclature defined by Figure 16-23 will be used for simplicity and clarity. In this blast-intercept configuration, point A is the position of the RV at time of detonation; B is the point of intercept of the RV and the blast sphere; OD is the distance of closest approach of the RV to the burst center. The distance LD is called the lead distance, and RB is the radius of intercept.

[REDACTED] A reference trajectory is introduced to define a new coordinate system. This trajectory, which is one axis of the new coordinate system, is parallel to the RV trajectory and intersects the burst point (0) (see Figure 16-23). With the center of this coordinate system at 0, the other axis is perpendicular to the reference trajectory. This coordinate system locates the position of the vehicle at the time of detonation relative to the reference trajectory.

[REDACTED] The following procedure is used to construct the locus of escape (LOE). The LOE defines a volume, outside of which the reentry vehicle will not intercept the blast shock wave. Figure 16-37 illustrates a situation from which one point on the LOE is defined. During the time interval $(t_c - t_o)$, the shock front expands to point C. During the time interval $(t_c - t_x)$ the vehicle travels from point X to point C where it intersects the shock front. If $(t_c - t_x) = (t_c - t_o)$, X is a point on the LOE. The distance XC is the lead distance, while OC is the cross range. To

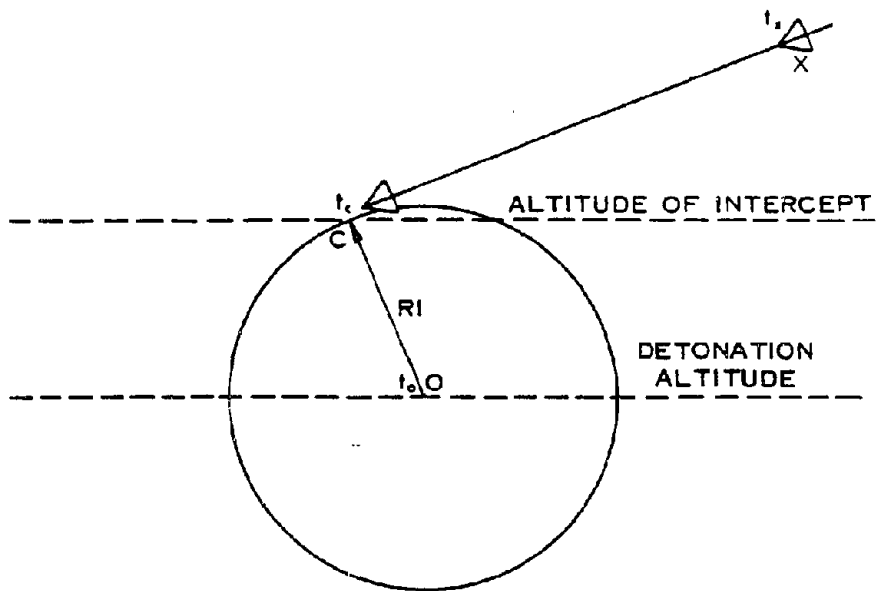
determine another point on the LOE, pick another radius of intercept and find a distance $X'C'$ such that $(t'_c - t'_x) = (t_c - t_o)$. Determination of several points, both above and below the reference trajectory, will define the LOE.

[REDACTED] The next step in defining the damage envelope is to determine locations, with relation to the burst, at which the reentry vehicle would suffer lateral and axial forces equal to the design loads. Sufficient locations must be selected and g loads calculated for each point so that iso-g contours can be constructed. Correlation of design loads with these iso-g contours defines the damage envelope. In this case, a g level is specified as the damage criterion.

(U) Figure 16-38 is a qualitative example that shows the LOE and the lateral and axial iso-g contours. This figure is oriented with respect to a reference trajectory. Figure 16-39 shows the relation between Figure 16-38 and a real situation.

[REDACTED] It must be realized that the g loadings described in the above examples are those experienced by a rigid body vehicle. Since the forces are applied dynamically, dynamic amplification factors must be considered. Displacements that result from dynamic loading can be greater than those that result from static loading. Thus, the effective force experienced by the warhead or other internal components may be more than the rigid body g's.

[REDACTED] It should also be noted that the response of reentry vehicles depends not only on peak values of the force, but also on the rate of application and the rate of decay of the force. Having sustained the peak value of the force, which occurs at the shock front, the reentry vehicle suffers lesser forces and pressures as it penetrates the blast sphere. Complete and accurate definition of the damage envelope must include responses during the entire force-pressure time history. This will be discussed further in connection with the structural response analyses of



t_0 = TIME OF DETONATION

t_c = TIME SHOCK FRONT AND RV ARE AT POINT C

t_2 = TIME RV IS AT POINT X

Figure 16-37. Determination of Locus of Escape

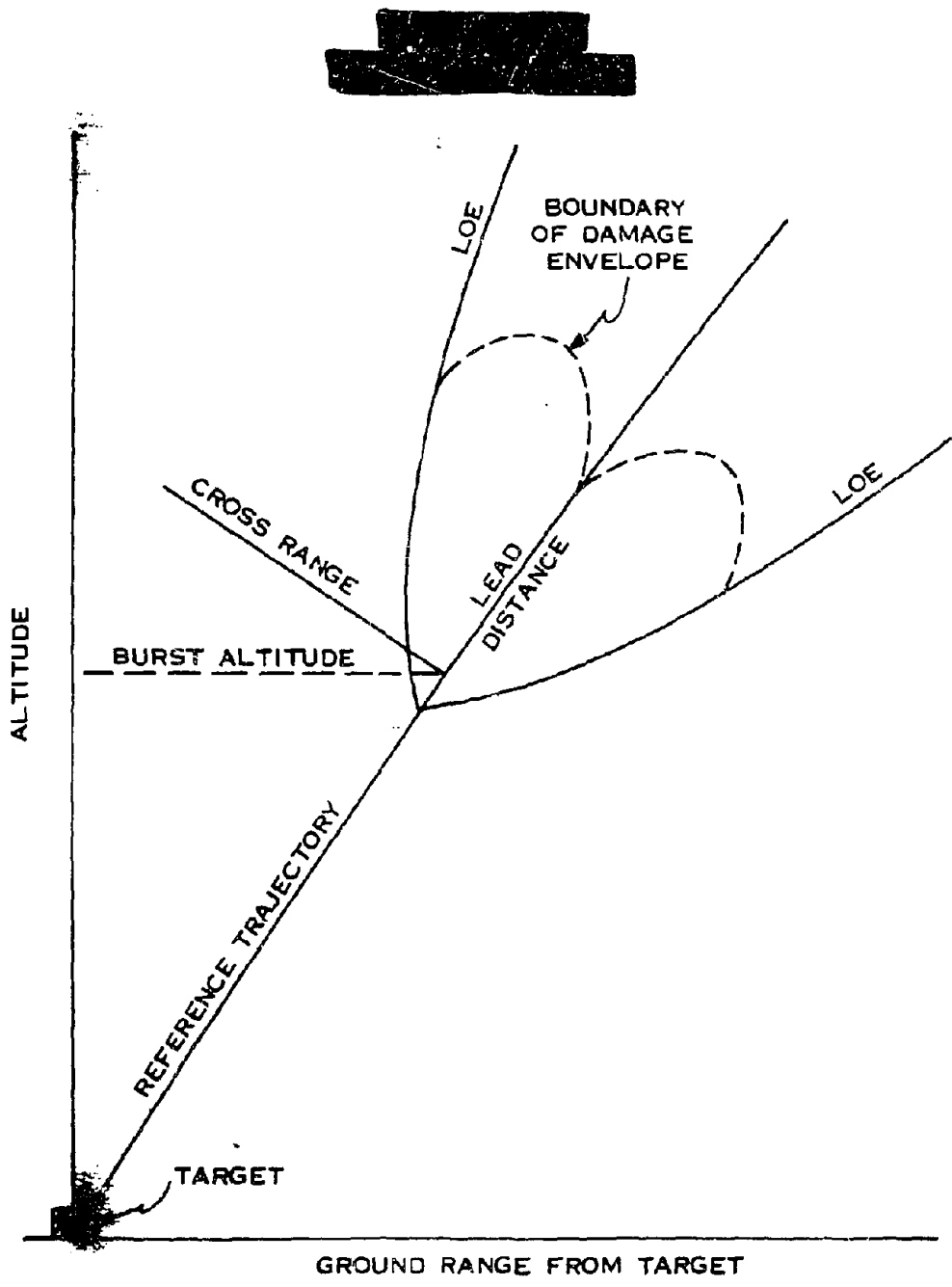


Figure 16-39. [redacted] In-Flight Intercept [redacted]



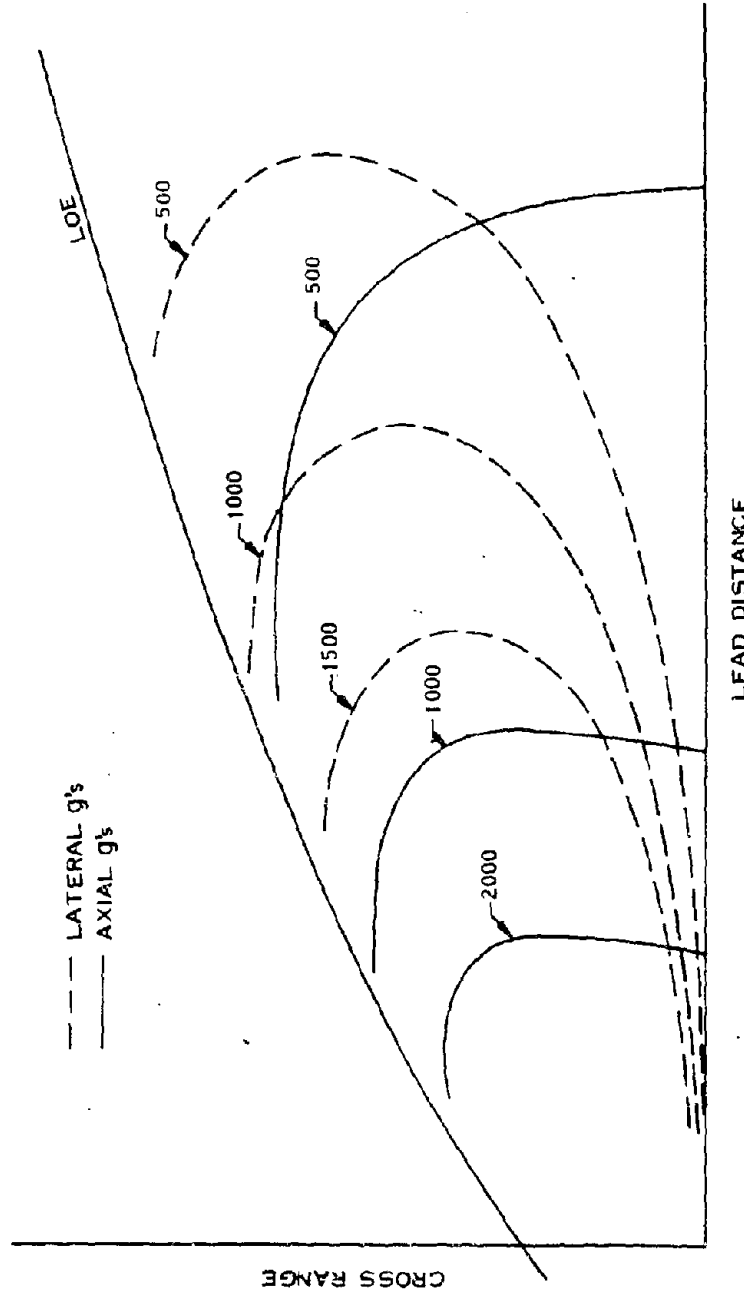


Figure 16-36. Qualitative Iso-g Contours

[REDACTED]

ABM vehicles (paragraph 16-32). It is evident that damage criteria other than rigid body g levels can be specified to define the damage envelope for a vehicle.

RESULTS OF SOME RV BLAST AND THERMAL LOAD AND VULNERABILITY CALCULATIONS

As pointed out in paragraph 16-13, it is impossible to condense the determination of blast and thermal vulnerability into a generalized methodology suitable for hand computation. The computations are associated too intimately with the design details of the particular RV of interest. In order to provide the users of this manual with some understanding of the procedures involved in such computations, some typical calculations are described in the following paragraphs.

16-24 Blast Loads on the RV

Assume that a reentry vehicle is hardened to survive 200 cal/cm² incident X-ray environment. The information desired is whether or not the RV will be vulnerable to blast and/or thermal effects at any point along the trajectory. The sample vehicle is assumed to have the following parameters.

- It is a 6° sphere cone configuration.
- The ballistic coefficient is $\beta = 1,000 \text{ lb/ft}^2$.
- Reentry altitude = 400,000 feet.
- Reentry angle = -35°.
- Reentry velocity = 17,000 ft/sec.

Two questions are examined separately to obtain the desired information.

- What blast load (axial and lateral accelerations) accompanies 200 cal/cm² incident X-ray exposure at the altitudes of interest from the standpoint of blast?
- What are the minimum axial and lateral rigid body accelerations that will allow

blast survival through all altitudes for separation distances equal to the vacuum separation distance for 200 cal/cm² incident X-rays (the minimum separation during exoatmospheric flight)?

Figure 16-40 shows the results of calculation of the axial and lateral rigid body g loads as a function of intercept altitude that would result when the RV is initially separated from [REDACTED] burst so as not to receive more than 200 cal/cm² X-ray energy incident on the vehicle. The vacuum separation distance for this X-ray level is about 11,000 feet (Chapter 4), and if the vehicle maintains that separation between altitudes of 40 and 100 kilofeet it will attain maximum g loads at an altitude of 40 kilofeet. The axial load at this altitude is 230 g's and the lateral load is 280 g's. At intercept altitudes less than 40 kilofeet, the rigid body loads will be less for the same separation distance.

The axial and lateral loads that would be sustained if the separation distance is such that 200 cal/cm² X-ray energy were deposited from [REDACTED] weapon are also shown in Figure 16-40. The approximate distances are shown as a function of intercept altitude in Figure 16-41.

Figure 16-41 shows near maximum separation distance as a function of intercept altitude for the 230 g axial load and the 280 g lateral load. The approximate 200 cal/cm² separation distances also are shown as a function of intercept altitude for the [REDACTED] weapon.

The maximum separation distances for the axial loads were obtained for the near head on interception of the RV by the blast wave. The maximum distances for the lateral loads were obtained from the near side on interception, i.e., 65 to 70° measured from the nose of the vehicle.

The incident blast overpressures required to induce the g loads are shown in Figure 16-42 for the 230 g axial and 280 g lateral loads of

[REDACTED]

Figure 16-41. At 40 kilofeet intercept altitude, a minimum overpressure of 22 psi is required to attain the 230 g axial load. The overpressure required to attain 280 g's laterally is 18.5 psi at 40 kilofeet, and a minimum of 13.5 psi is required above 90 kilofeet altitude.

Figure 16-43 shows the curves of g load as a function of maximum separation distance for a 40 kilofeet altitude intercept by a blast wave from [REDACTED] weapon. It should be noted, from this figure, that extremely large separation distances are indicated if the lateral hardening of an RV is less than 100 g's. For yields less than or greater than [REDACTED] this separation range changes approximately as [REDACTED]. The approximate nature of this ratio results from the change in the velocity of the vehicle between the points of initial separation and interception.

Based on this brief examination of the results of calculation of blast vulnerability, the main conclusion is that rigid body loads of 280 g's axially and 230 g's laterally are compatible with the 200 cal/cm² X-ray hardening of the RV. Moreover, if the RV rigid body response hardness level falls short of these g levels, the blast effects may predominate as a damage mechanism. More specific trajectory/blast cases must be studied to determine the required g loading criteria for balance with a 200 cal/cm² X-ray criterion.

16-25 Thermal Radiation Loads on the RV [REDACTED]

A sample investigation has been made of the free field thermal radiation incident on the same RV described in paragraph 16-24 as it flies through a nuclear burst in the lower atmosphere. The basic trajectory considered in this study had a reentry velocity 17,000 ft/sec and a flight path angle of -35°. In addition, a limited study was performed for a 19,200 ft/sec/-75° trajectory. Thermal radiation heat loads

[REDACTED]

were computed for head on intercepts of [REDACTED] burst at 40-, 60-, 80-, and 100-kilofeet burst altitudes. Burst yields of [REDACTED] and [REDACTED] were also considered at the 60 kilofeet altitude.

The thermal radiation heat flux produced by a nuclear burst can be obtained as a function of distance, direction and time from the radiation/hydrodynamic calculations of Hillendahl that were used to describe the thermal source in Chapter 3 together with the appropriate form factors. These are free field thermal radiation data and do not include any interaction between the vehicle and the radiation field, i.e., the possible attenuation of radiation resulting from an opaque layer of vaporized heat shield material in the flow field surrounding the vehicle was not included (see paragraph 16-31 for a discussion of these "blocking" effects). The total free field heat load to the stagnation point, cone, and base region of the RV was determined by integrating the heat flux as a function of time after detonation, assuming a straight line, constant velocity trajectory in the vicinity of the burst.

The total radiation heat load for this example is shown in Figures 16-44 through 16-46 as a function of the initial slant range of the vehicle, burst altitude, burst yield, and trajectory. For initial slant ranges less than about 3 to 5 kilofeet, the heat load is very large (35,000 Btu/ft²) and is essentially independent of location on the vehicle. For a fixed burst yield and initial slant range, the heat load decreases with increasing altitude; conversely, for a fixed burst altitude and initial slant range, the heat load increases with increasing yield. Finally, a higher velocity trajectory increases the heat load for a fixed yield and altitude.

The thermal data shown in Figures 16-44 through 16-46 could be used in conjunction with the blast data of paragraph 16-24 to determine the total radiation heat loading as a function of blast loading (rigid body axial load

[REDACTED]

DNA
(N=)

Delayed

Figure 16-44. [REDACTED] Thermal Radiation Heat Load on the Cone as
a Function of Initial Slant Range for
Several Burst Altitudes [REDACTED]

16-72

[REDACTED]

[REDACTED]

[REDACTED]

DNA
4(3)

Deleted

Figure 16-45. [REDACTED] Thermal Radiation Heat Load on the Cone as
a Function of Initial Slant Range for
Several Burst Yields [REDACTED]

[REDACTED]

[REDACTED]

[REDACTED]

DNA
(2)(3)

Deleted

Figure 16-46. [REDACTED] Thermal Radiation Heat Load on the Cone as
a Function of Initial Slant Range for
Several Trajectories [REDACTED]

16-74

[REDACTED]

[REDACTED]

[REDACTED]

factors). As a particular example, these data show that, for a 350 kt burst at 40 kilofeet and the 17,000 ft/sec/-35° trajectory, the radiation heat load on the cone associated with a 200 g head on intercept condition is only 530 Btu/ft², whereas for a 300 g intercept condition it is 5,400 Btu/ft². This particular example indicates that a 50 percent increase in blast hardness (as measured by the rigid body g criteria) produces an order of magnitude larger thermal environment.

16-26 Description of a Blast/Thermal Vulnerability Determination

[REDACTED] This paragraph continues the description of the sample computations that were described in paragraphs 16-24 and 16-25. The determination of the sample RV to blast and thermal effects produced by a nuclear weapon burst is described below.

[REDACTED] The blast vulnerability analysis of the RV is made under the following assumptions:

- 6° sphere cone vehicle with a ballistic coefficient of 1,000 lb/ft² (assumed constant for normal reentry).
- Point mass-zero lift trajectories were used in the computations.
- Reentry altitude = 400,000 ft.

[REDACTED] The blast model used in the computations is considered to be an upper bound to a conventional weapon blast output. Modified Sachs' scaling (see paragraph 2-14) was used in conjunction with curve fits to radius-time-overpressure data. The other peak blast parameters, such as density and particle velocity, are Rankine-Hugoniot values consistent with the scaled overpressures. The environment to which the vehicle is exposed in the interior of the shock front was simulated by assuming constant vehicle velocity during fly through and Sach's scaling curve fits to the interior profiles. It should be noted that, in actual practice, vehicle fly through loading calculations are performed

on an electronic computer using the results of detailed radiation/hydrodynamic calculations corresponding to the nuclear device and burst altitude of interest.

[REDACTED] The vehicle reentry conditions used for this calculation are as follows:

- Case 1
 - a. Reentry velocity = 17,000 ft/sec
 - b. Reentry angle = -35°
- Case 2
 - a. Reentry velocity = 19,200 ft/sec
 - b. Reentry angle = -75°

[REDACTED] The temperature of the heat shield can be an important factor in determining the structural response of the RV to blast induced loading because of the possible temperature dependence of some of the structural properties, e.g., elastic modulus and yield stress, at elevated temperatures. For the study discussed here, predictions of the heat shield bulk temperature accounted for ascent heating, normal reentry heating to the burst altitude, and thermal radiation heating from the nuclear burst. The bulk temperature is symbolically related to the heat loads by

$$Q_{\text{ascent}} + Q_{\text{reentry}} + \alpha Q_{\text{radiation}} = \rho t \int_{T_{\text{launch}}}^{T_{\text{bulk}}} C_p dT \text{ (Btu/ft}^2\text{)},$$

where it has been assumed that the temperature is uniform across the thin ablator skin and that heat losses are negligible compared to heat inputs. In general, considerable caution must be exercised in employing the thin skin-bulk temperature method.

[REDACTED] The thermal radiation heat flux produced by the nuclear burst was obtained as described in paragraph 16-25. The thermal radiation heat load incident on the vehicle was deter-

[REDACTED]

[REDACTED]

mined by numerically integrating the flux, as a function of time after detonation, assuming constant vehicle velocity at that altitude and no vehicle spin. It should be noted that, aside from the inherent uncertainties in the free field thermal radiation data, there are additional uncertainties in determining what fraction of the incident thermal radiation is actually absorbed by the ablative surface during the fireball fly through. This is due to a lack of knowledge of the spectral absorptivity of the vehicle surface under these conditions and of the possible attenuation of radiation as a result of an opaque layer of vaporized heat shield material in the flow field surrounding the vehicle.

[REDACTED] Two basic methods of structural analysis were employed for this sample calculation. The first method involves the application of a finite length, elastic cylinder response solution to determine the dynamic shell stresses resulting from head on intercept loadings. The second method, which was applied to the side on intercept, involved the evaluation of the dynamic response of a lumped parameter, free free beam model subjected to transient blast loadings. In actual practice, the analysis of the structural response of *RV* configurations should employ much more sophisticated and complex methods. The description of these relatively simple methods is included to indicate to the user the general analytical methods that could be used.

[REDACTED] The results of these two methods of structural analysis depend on assumptions made concerning the blast and thermal environment that the *RV* encounters. In this calculation, the transient aerodynamic loading was developed by using Newtonian theory for pressure magnitudes and distributions (see paragraphs 16-21 and 16-22) combined with a curve-fit exponential time decay obtained by flying an unperturbed trajectory through the blast model. To simplify the calculation, instantaneous engulfment was assumed and shock-on-shock interaction effects

were ignored. In addition, the structural response was only examined for blast entrance and for normal reentry conditions. Blast traversal and exit of the vehicle from the blast region were not examined. Thermal loading from normal reentry and nuclear burst thermal radiation were considered for structural response through the bulk skin temperature rise. No attempt was made to evaluate resulting thermal stresses from this high temperature environment; however, the bulk temperature effect was accounted for when choosing material elastic properties and allowables.

[REDACTED] Three separate bays or ring-stiffened sections of the *RV* were investigated for the head on intercepts. After a few dynamic response calculations were made, it became apparent that Bay L-I (Station 37.5 to Station 49) was the most vulnerable to head on blast loadings; therefore, the results presented are for Bay L-I. The cylinder solution used is a closed form, elastic response code that computes all stresses at both the inside and outside shell fibers at any desired point on the shell.

[REDACTED] The side on intercept conditions were examined with a lump-parameter, free-free, "Timoshenko" beam model. The bending rigidity was supplied completely by the ablator shell, whereas the mass distribution was made up of both the main shell structure and all internal components. As in the head on studies, the thermal effects were included only in the evaluations of material elastic properties and allowables. Using this lumped-parameter mode, a normal mode solution was employed to determine the complete time history of bending stresses that developed at a number of stations along the missile length from the transient pressure loading that resulted from blast intercept. In all cases, the peak beam bending stresses occurred in a region bounded by Stations 20 and 25.

[REDACTED] In addition to these two basic tools of structural analysis, i.e., cylinder solution and

[REDACTED]

beam model, a check of shell buckling was made by using the semi-empirical results from the HARTS Program. This check calculation revealed that, if buckling did occur during blast intercept, it probably would be elastic; however, since rather thick walled shells were involved, the calculated critical buckling pressures are very high compared to pressures necessary to cause conditions leading to plastic deformation and rupture.

16-27 Results of the RV Vulnerability Determination [REDACTED]

[REDACTED] The results of the structural response study are shown in Figure 16-47 for head on intercept and Figure 16-48 for side on intercept. Figures 16-47 and 16-48 show the allowable stresses and the peak stresses developed from blast entrance loads (characterized by the plotted loads) as a function of initial slant range from a 350 kt burst at an altitude of 40 kilofeet. For the side on intercept cases (i.e., interception by the blast wave normal to the longitudinal axis of the vehicle), the loads are the total g's obtained by vectorially combining the axial and lateral values. For the head on intercept cases, the total loads are the same as the axial loads.

[REDACTED] The incipient structural damage is indicated in the figures by the intersection of the curve showing peak stress developed with the allowable stress curve. The curve labeled "Developed Stress" indicates the variation with slant range of the peak dynamic stresses developed in the vehicle during blast wave intercept. These curves are shown for both the nominal RV and the 1.2 nominal vehicle, which is the same vehicle with the skin thickness increased by 20 percent. The slant range, stress, and loads are tabulated for each of the points of incipient structural damage.

[REDACTED] It is apparent that the addition of 20 percent to the skin thickness reduces the vulnerability of the RV by decreasing the slant range

for incipient structural damage markedly. It should be recognized that these values of slant range probably are minimum values for the onset of incipient structural damage as a result of the assumptions used in the stress calculations.

[REDACTED] The thermal response data are shown in Figure 16-49 in terms of the temperature at the aft end of the cone ($X/R_N = 19.4$) after burst exit as a function of the initial slant range of the vehicle from the burst. These data are the temperatures developed during normal reentry (including ascent heating) to the burst altitude plus the temperature rise caused by the fireball thermal radiation. Beyond initial slant ranges of 16 to 18 kilofeet, the temperatures shown are the normal reentry temperatures at the burst altitude, since the thermal radiation heat load is quite small at these large ranges. The 40-kilofeet burst altitude induces higher temperatures than the 60-kilofeet altitude because of increases in both reentry heating and thermal radiation heating.

[REDACTED] Two specific temperatures, 2,340°F and 1,750°F, are shown in Figure 16-49. The former is the ablator melt temperature, while the latter is the temperature at which the ablator has low structural strength. Since the bulk temperature generally lies somewhere in between the surface and backface temperatures, surface melting will commence before the bulk temperature reaches 2,340°F, but probably only in small amounts. Of more importance is the fact that if the vehicle emerges from the burst with a bulk temperature greater than 1,750°F at critical structural locations, it probably will not be able to survive the exit blast loads and/or the subsequent reentry loads as it descends through maximum dynamic pressure to impact, i.e., if the thermal radiation heat loads are sufficiently great to result in temperatures of 1,750°F at burst exit, "delayed" structural damage may occur subsequent to the blast entrance, even if the entrance loads are not sufficient to cause damage.

Pages 16-78 and 16-79
Deleted.
DNA (A)(3)

[REDACTED]

DAF
(-)(=)

Deleted

Figure 16-49 [REDACTED] Cone Bulk Temperature after Fly Through
as a Function of Initial Slant Range from Burst
(Head On Intercept [REDACTED])

[REDACTED]

[REDACTED]

[REDACTED]

16-28 Summary and Conclusions Concerning RV Vulnerability Calculations

[REDACTED] There are many different ways to summarize the blast/thermal vulnerability of an RV; this subsection employs a bar graph method, whereas the damage envelope method is used in the succeeding subsection to portray ABM Blast/Thermal Vulnerability. The minimum initial slant ranges for structural and thermal damage are summarized in Figure 16-50 for the 17,000 ft/sec/-35° trajectory and 40 kilofeet burst altitude. These data show that the RV is more vulnerable to the side on intercept/structural damage condition than any other condition. The 20 percent increase in ablator thickness reduces the initial slant ranges for damage considerably. The total "g" loading at the slant range for structural damage and the total free field radiation heat load at the slant range for thermal damage also are shown in the figure. It can be seen that there is *no unique* mechanical "g" load or thermal "Q" load that determines when damage occurs. This points out the requirement for more definitive information concerning damage criteria associated with actual RV designs.

[REDACTED] The separation distance at the burst altitude between two vehicles that were originally at the 130 and 200 cal/cm² X-ray separation distances apart in the exoatmospheric [REDACTED]

[REDACTED] also are shown in Figure 16-50. It can be seen that if two vehicles were spaced for these X-ray loadings from a 350 kt weapon in the exoatmosphere, and the lead vehicle encountered a direct hit from 350 kt at 40 kilofeet, the trailing vehicle definitely would incur damage if it encountered the blast wave.

(S) The foregoing description of the method and results of an RV blast/thermal vulnerability sample calculation was presented to give the user an indication of the important technical aspects that must be included in this type of analysis. Based upon the results, a few rather general conclusions can be drawn:

- It is apparent that the blast/thermal vulnerability of an RV cannot be uniquely expressed in terms of either rigid body "g" load levels or thermal radiation heat loads, but rather is a function of the particular reentry trajectory, intercept geometry, yield of the attacking weapon, and the specific damage mechanism considered.
- Vulnerability loads or damage criteria assigned to a particular RV corresponding to blast or thermal effects may not be compatible with the loads or criteria assigned for other nuclear weapon effects (e.g., X-rays).
- Thermal loads on the RV, resulting from a combination of reentry heating and radiation from the nuclear weapon, can have an important deleterious effect on the material properties (and in turn upon the structural response) of the RV ablator/structure combination.
- The accurate assessment of RV vulnerability to nuclear weapon effects requires detailed analyses using advanced analytical tools and high-speed electronic computer facilities.

ANTIMISSILE (ABM) SYSTEMS

[REDACTED] The assessment of blast and thermal vulnerability of an antimissile (ABM) system presents many of the same problems that were discussed for reentry vehicles; however, ABM systems have some important characteristics that are unique, and these will form the basis for a large portion of the following discussion.

[REDACTED] There are fundamental differences between the views of the designers of RV's and ABM concerning blast and thermal vulnerability. The designer of an RV may be willing to have his vehicle sustain limited damage if the damage would not degrade the probability of mission success significantly. This willingness to sustain



DNA
(b)(3)

Deleted

Figure 16-50. Minimum Initial Slant Range for Structural/Thermal
Damage at 40 kft Burst Altitude, $V_E/\gamma_E = 17,000$ ft/sec/35°



[REDACTED]

some level of damage results from the fact that the RV designer usually deals with large numbers of vehicles directed against an array of targets with the objective of insuring that a fraction of the RV's penetrate the defense and reach the targets. The defense, on the other hand, attempts to deny all "leakage" of enemy RV's. Therefore, when considering blast and thermal fratricide damage, the ABM designer usually will not tolerate any degree of damage to the vehicle (i.e., it is designed to be "sure safe"). When assessing the ability of an ABM to defend a target and to kill an enemy RV, however, the objective dictates that the ABM designer achieve a "sure kill" miss distance relative to the incoming RV.

[REDACTED] Most of the following discussion results from a study to determine the probable damage modes and damage envelopes for the AIRS I and II vehicles (paragraph 16-12) when exposed to blast waves and thermal radiation from nuclear explosions.

[REDACTED] The scope of the discussion can be summarized as follows:

- Two vehicles are considered, AIRS I and AIRS II. These vehicles nominally represent interceptor vehicles of the SPRINT and SPARTAN class, respectively. Inboard profiles of these vehicles are shown in Figures 16-51 and 16-52.
- Four response modes are considered:
 - (1) Shell breathing response to the blast wave.
 - (2) Vehicle bending response to the blast wave.
 - (3) Internal component damage due to rigid body acceleration produced by the blast wave.
 - (4) Material damage produced by the thermal radiation.
- Coupling effects among the damage modes are neglected, except for the inclusion of degradation of material properties that results from heating the material.

- Control surface damage is not considered.
- Each vehicle is assumed to be in a steady state "n"-g maneuver (where n can be zero).

[REDACTED] The aerodynamic loads initiated by the blast wave must be defined to perform a blast vulnerability analysis. In the definition of the aerodynamic loads imposed on a vehicle traveling at hypersonic speeds when subjected to a strong blast wave, the initial shock-on-shock interactions during the vehicle engulfment by the blast wave present the most difficulty. Recent studies of the response of missile structures to blast loads indicate that the response to the shock-on-shock loads does not contribute significantly to the total response experienced by the missile structure.

[REDACTED] The response of the structure to blast is separated into shell breathing, vehicle bending, and rigid body acceleration responses. The separation of the total response into uncoupled breathing and bending responses is required since current methods cannot perform the coupled problem; however, this separation is justified to some extent by consideration of the types of damage associated with each response. In shell breathing response, segments of the shell between bulkheads are excited, and the damage is associated with high frequency local shell deformation. In vehicle bending, the damage results from relatively low frequency excitations of the overall structure.

[REDACTED] Criteria for the yielding and buckling response have been generated primarily from data generated in tests of simple cylindrical and conical bodies subjected to air blast from HE detonations. Studies of damage to the vehicle by bending have neglected the short-duration diffractive loading, which is of little consequence in exciting the long period oscillations associated with bending deformations (except possibly for very low yield weapons). The damage criteria for bending deformations, and the response analysis

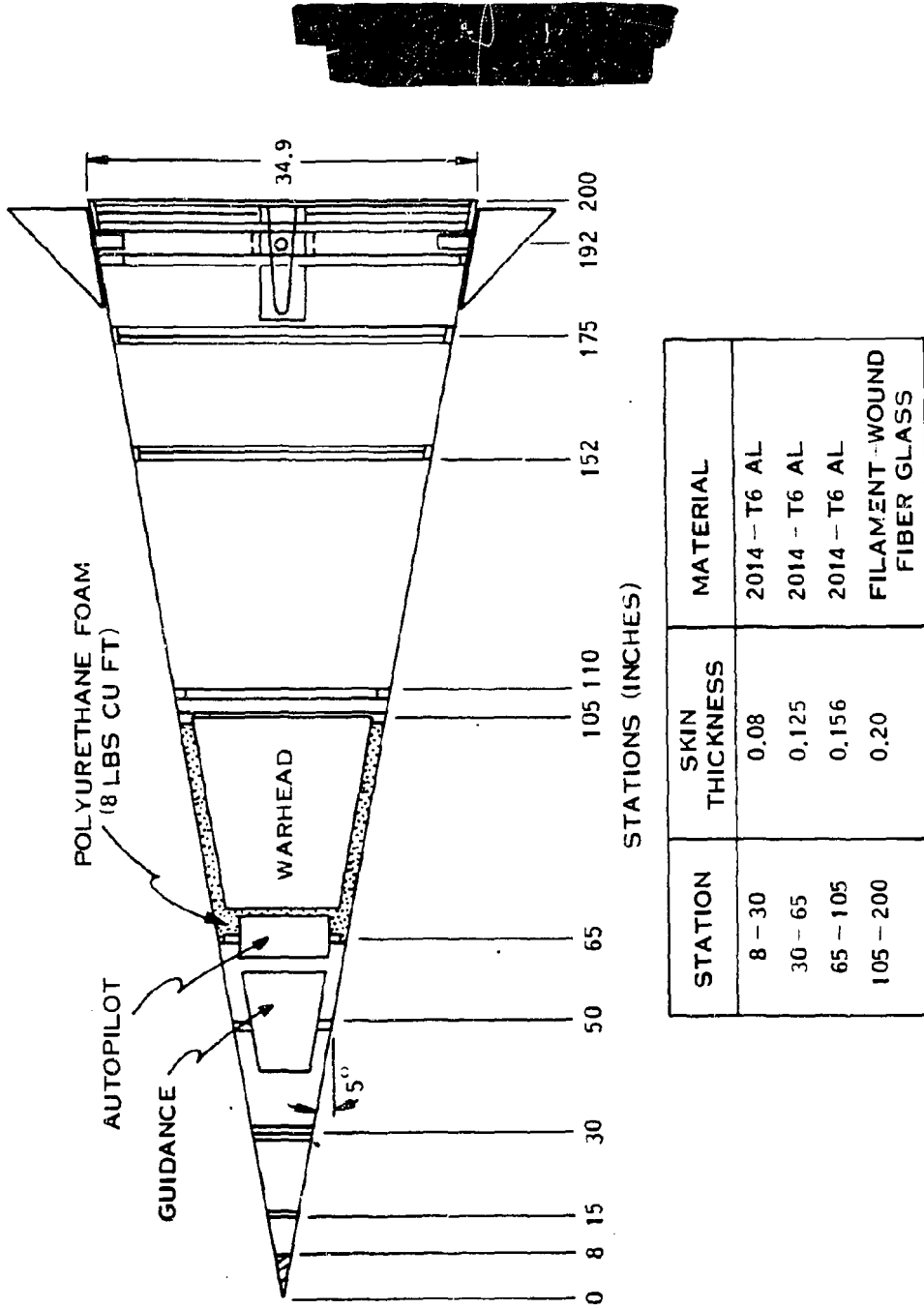


Figure 16-51. Inboard Profile of AIRS | Vehicle

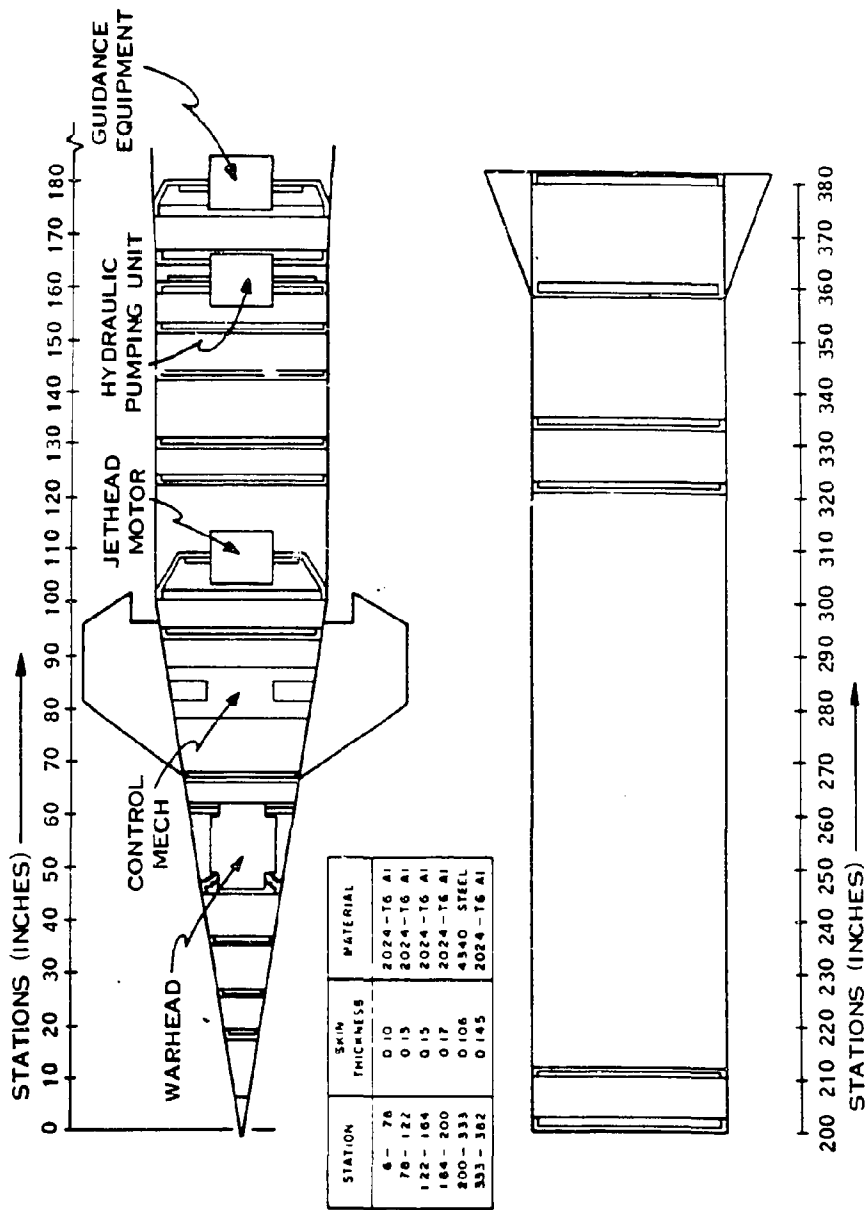


Figure 16.52. Inboard Profile of AIRS II Vehicle

[REDACTED]

techniques, rely on knowledge developed in similar studies performed for aircraft and launch vehicles in the boost phase.

Analysis of response to thermal radiation effects define the mechanisms by which heat is absorbed and distributed throughout the structure, both when the vehicle is outside and inside the fireball. Damage criteria from thermal radiation effects are selected on the basis of the loss of the insulative coverings over the substructure.

Blast and thermal radiation effects damage envelopes for both AIRS I and II are presented below. The relative sizes of these envelopes for the various effects on the two representative vehicles and for the encounter condition variations (in yield and altitude) are discussed briefly.

16-29 Shell Breathing Response [REDACTED]

Blast induced pressure loading causes the shell segments of the vehicle between the ring reinforcements to respond in what is usually termed the "breathing mode." Damage occurs in the form of permanent deformation of the skin through the formation of a dented area in the surface of the shell. The primary damage mechanism for the shells is an instability (buckling) of the shell that can occur either when the shell is all elastic or after portions of the shell have become plastic. This damage mechanism can be complicated by the presence of the ablator over the structural shell and by other states of stress and deformation imposed by bending of the vehicle as a result of blast and normal flight loads, or the thermal condition of the vehicle at blast intercept. These interaction problems are not considered.

A complete determination of the blast damage to a shell segment that would be required to prevent the AIRS vehicles from performing a specified maneuver requires two separate analyses. The first analysis predicts response

levels from threshold to severe post buckling damage, and a second analysis predicts the post damage response: the latter is the response of the "damaged" vehicle to the loads imposed by maneuver. Thus, it is not sufficient to calculate the shell response resulting from the blast loading. A sure-safe criterion also must be established for the actual in-flight conditions in the fratricide mode. The amount of damage that constitutes an "unsafe" level under a known set of environmental conditions must be determined eventually if vulnerability studies are to be considered useful to the military planner.

The analyses of the response of critical shell segments of the AIRS I and II vehicles to blast that were selected for this example can only predict the threshold damage level caused by elastic buckling or initial material yielding. Analyses that calculate elastic-plastic response in the post buckling region have only been developed recently for shell response to blast, but experimental data are not sufficiently comprehensive to apply the results to various loading conditions and to different materials. Thus, rather arbitrary criteria must be postulated to relate computed damage levels to "unsafe" conditions for the ABM.

The analyses discussed thus far primarily calculate the response of the shell up to threshold damage, i.e., sure-safe levels. These analyses are elastic in nature and cannot be used directly to determine response that includes severe damage. There are three additional elements required before lethality predictions can be made:

- Selection of the applicable analysis; that is, inelastic buckling or yielding (or possibly fracture).
- Definition of damage criteria, i.e., definition of the amount of damage that must occur in the selected damage mode to negate the intended mission of the vehicle.
- Selection of a means to apply the inelastic analysis to the determination of the load

[REDACTED]

[REDACTED] level required to produce the amount of damage specified.

16-30 Vehicle Bending Response (U)

[REDACTED] Discussions of prediction techniques for the response of the AIRS I and AIRS II vehicles to blast in their rigid body and bending degrees of freedom are separated into two parts. First, a formulation of *damage criteria* for these vehicles in bending is discussed for damage to the primary structure and to the internal components. In the second part, analysis that predicts the *structural response* is discussed. The inclusion of critical damage criteria in a computer program for the response analysis results in the capability to determine sure safe envelopes for bending response to blast.

[REDACTED] A most difficult, but necessary, part of defining damage contours for interceptor missiles in a blast environment is the definition of the amount of damage that must be produced in the primary structure in bending or to internal components to constitute a positive failure of the mission. The approach adopted is to use a simple damage criterion available for interceptor vehicles.

[REDACTED] Selection of simple damage criteria for an interceptor vehicle undergoing bending deformations requires an understanding of the damage modes involved. The primary bending damage modes possible to the primary structure of a vehicle may be:

- Damage to the joints resulting from tensile stresses in excess of the stresses allowable for the joints.
- Buckling damage to the overall shell structure resulting from combined axial and bending induced normal stresses in the shell.

For this discussion, a damage condition in which the vehicle damage cannot support the loads associated with a specific "n"-g maneuver after buckling was selected tentatively as sufficient.

[REDACTED] Damage criteria for internal components should involve detailed investigations of the acceleration-time history environment that a component can withstand. In addition, the supports of internal components and the load-carrying ability of the supports must be considered in a comprehensive vulnerability analysis. It is the usual practice to consider an acceleration time-history and to assign a certain peak acceleration value to be critical.

[REDACTED] In view of a lack of fragility data for the internal components of the AIRS I and II, representative allowable peak acceleration values were selected from information available for design requirements for SPRINT and SPARTAN. These acceleration values are used to demonstrate the procedures involved in determining damage envelopes for internal component damage, but they are not necessarily representative of what the internal equipment mounted inside the vehicles can actually withstand.

[REDACTED] It is necessary to perform a comprehensive analysis of the blast loading and response of the entire missile structure (including primary and secondary structures) to determine the details of the blast loads imposed upon (and the response of) specific internal components when a missile body is exposed to a nuclear weapon environment. This analysis includes development of a detailed mathematical lumped-mass/spring model of the missile to determine the proper "transfer functions" between the primary structure and the internal component of interest. Calculations that use the mathematical model and the definition of the blast loads imposed on the missile structure during a real encounter lead to the determination of the loads imposed on the internal structures.

16-31 Thermal Radiation Effects [REDACTED]

[REDACTED] The establishment of thermal radiation damage criteria for AIRS I and AIRS II required an examination of the individual structures involved.

[REDACTED]

[REDACTED] In general, data concerning thermal radiation effects consists of a description of the temperature distribution through the ablator (and substructure material) and the mass ablation rate, both as a function of time and position on the missile. This fundamental information provides the thermal portion of the inputs for a realistic assessment of the overall vehicle performance during and after an encounter with a nuclear burst. The temperature distribution data can be used in a structural analysis to determine the magnitude of the allowable stresses (or strains), thermal stresses, etc. Furthermore, there are usually internal components in the guidance section, fuzing, arming and firing section (FAF), or warhead section that have a fairly low temperature tolerance. The ablation rates also affect the mass distribution and can affect the aerodynamic characteristics of the missile, which can affect its flight characteristics; however, the following discussion is limited to an examination of thermal effects in the ablator and substructure. No concurrent structural and/or trajectory analyses were performed.

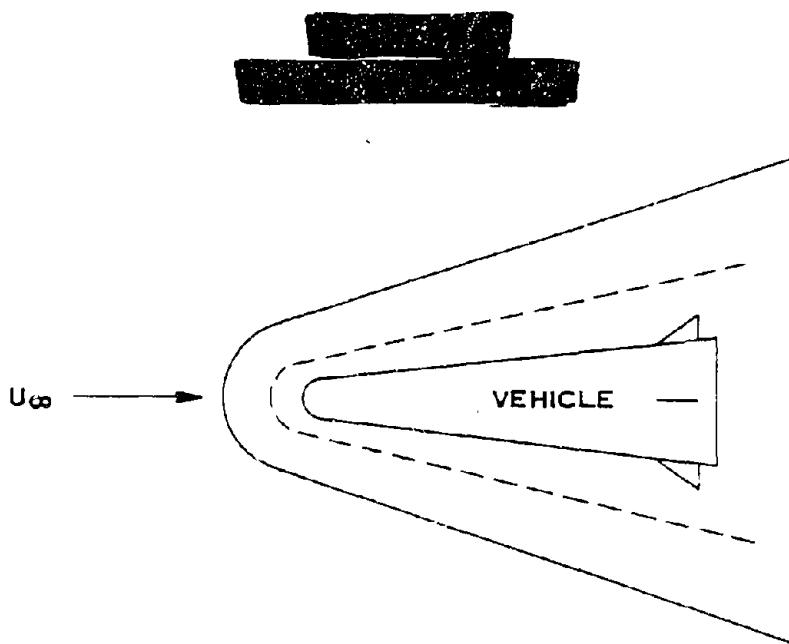
[REDACTED] The principal type of ablation material used on the AIRS I missile is tape-wrapped silica phenolic, which is a silica cloth impregnated with phenolic resin. A detailed theoretical prediction of the thermal response of a charring, melting and vaporizing ablator such as silica phenolic on a high-speed missile that flies through (or near) a nuclear fireball during some portion of its mission involves simultaneous consideration of complex physical and chemical phenomena. The general situation is illustrated in a simplified fashion in Figure 16-53. During normal flight (i.e., preburst or post traversal), the vehicle is heated by forced convection (\dot{q}_c) caused by friction forces in the boundary layer on the vehicle (aerodynamic heating). During the fireball traversal phase, the predominant mode of heating is thermal radiation (\dot{q}_R) from the high temperature fireball air. In this case, the

ablation rates generally are so high that the boundary layer is blown off, and the local flow field (which may be subsonic) is dominated by the ablation vapors. In either case, the heat transfer to the surface causes the ablator to heat, pyrolyze internally, and melt and vaporize at the surface.

[REDACTED] A realistic thermal analysis for a silica phenolic coated vehicle should consider the following effects:

- Internal heat conduction in the ablator and substructure.
- Pyrolysis of the phenolic resin in the ablator, with the attendant endothermic chemical reactions and pyrolysis gas flow through the char.
- Convective and radiative heat transfer at the ablator outer surface, and the accompanying surface recession that results from melting and vaporization of the silica cloth.
- The interaction of the injected ablation vapors with the local vehicle flow field, especially the absorption of thermal radiation by the vapors (radiation blocking).
- The time dependent nature of the fireball environment, as well as the transient nature of the temperature response of the ablator.
- Variation of all of the effects listed above with location on the body that result in differences in environment, type and/or thickness of ablator, etc.
- Variation of all of the effects with burst encounter conditions.

[REDACTED] It is convenient to separate the thermal analysis into several basic parts, each of which uses somewhat different techniques of analysis according to the most important physical processes that are treated. This concept can be visualized with the aid of Figure 16-53 and an energy balance at the outer surface of the ablator (denoted by a subscript w).



DEFINITION OF TERMS

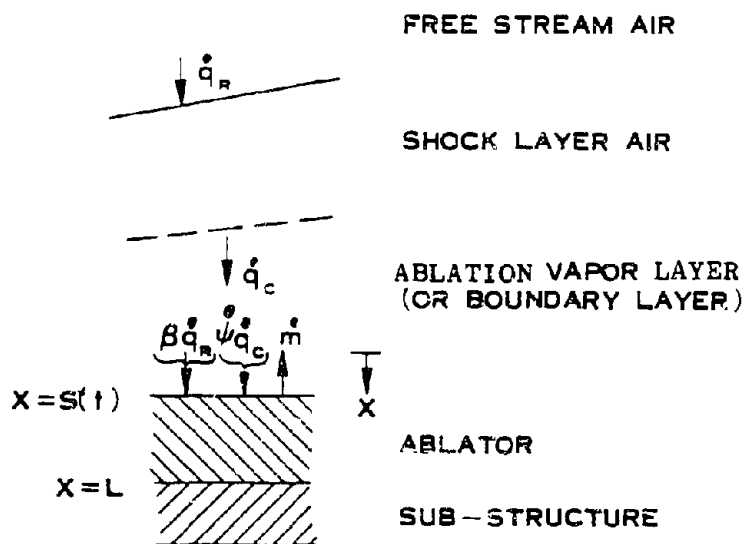


Figure 16-53. illustration of Ablation Phenomena

$$\psi \dot{q}_c + \beta \dot{q}_R - \epsilon \sigma T_w^4 - \dot{m} \Delta H = \left(-K \frac{\partial T}{\partial x} \right)_w$$

where \dot{q}_c and \dot{q}_R are the free field convective and radiant heating rates, respectively. The term "free field" heating rate denotes that the quantity is computed without regard to ablation effects. Thus, the free field convective heating is computed on the basis of nonblowing boundary layer solutions, while the free field radiative heating is computed on the basis of the fireball flow field being unperturbed by the presence of the vehicle. Therefore, by definition, the free field thermal environment depends only on time and body position for a particular trajectory and encounter condition, and not on the type of ablation material used.

The quantities ψ and β are the convective and radiative blocking functions, respectively. They denote the fraction of the free field heating rate that exists at the ablator surface during the actual ablation process. The blocking functions must be obtained from a solution for the local vehicle flow field that accounts for the effects of the injected ablation vapors on the flow field. In general, their values will depend on the level of the free field environment and on the particular ablation material. The quantity $\epsilon \sigma T_w^4$ represents the energy reradiated from the surface, while the term $\dot{m} \Delta H$ represents the energy absorbed in surface melting and vaporization. Finally,

$$\left(-K \frac{\partial T}{\partial x} \right)_w$$

is the heat conducted into the surface of the solid ablator, which in general must be obtained from a solution of the temperature profile in the ablator.

The equation simply states that the net convective and radiative heating at the surface,

less the energy reradiated and absorbed in melting and vaporization, equals the energy conducted into the ablator. When the net heating rate is sufficiently high to produce surface melting and vaporization, the equation relates the mass ablation rate (\dot{m}) to the free field environment and the temperature distribution in the ablator.

For the purpose of the present discussion, which is primarily concerned with the thermal effects of a nuclear environment, the overall analysis is separated into two basic parts: fireball radiation and ablation, and the internal temperature and ablation response. The former is essentially multidimensional (around the body) and quasi-steady in nature, since it deals with high temperature flow about a high speed missile, whereas the latter is primarily one dimensional (through-the-thickness) and transient in nature since it deals with heat conduction. The coupling condition (boundary condition) that relates the free field environment and local flow field to the internal response is the energy balance at the surface, i.e., the equation given above.

When the results of various theoretical methods are compared there is about a ± 50 percent uncertainty in the predictions of the total silica phenolic mass ablated during a nuclear fireball traversal, even among theoretical models that assume full vaporization. If only melting is assumed, the results are at least a factor of five higher, and typically a factor of ten.

The condition for thermal damage to the AIRS vehicles was taken to be the time at which 50 percent of the ablator mass was gone; this condition is probably on the conservative side, leading to an upper limit in the size of the vulnerability envelopes.

16-32 ABM Blast/Thermal Vulnerability Envelopes

The previous paragraphs described techniques of analysis that can be employed to de-

[REDACTED]

[REDACTED]

fine vulnerability envelopes for the AIRS I and AIRS II vehicles exposed to blast and thermal radiation from nuclear explosions. The vulnerability envelopes for the AIRS vehicles and for two typical encounter conditions are shown in Figures 16-54 through 16-57. In each figure, the vehicle under attack is at the origin (0, 0) flying from left to right. If the attacking weapon is burst inside the envelope, the load on the vehicle will exceed the critical level. Thus, the largest envelope on the graph identifies the "most" critical damage mechanism for the vehicle and the burst condition considered.

[REDACTED] Figures 16-54 and 16-55 correspond to the AIRS I vehicle in a typical fratricide situation; it is obvious that the size of the critical damage envelopes are very sensitive to the maneuver (or nonmaneuver) condition of the AIRS I. The AIRS II curves in Figures 16-56 and 16-57, indicate envelopes of somewhat different shapes, but the general behavior is similar to AIRS I.

16-33 Conclusions [REDACTED]

[REDACTED] The AIRS I and AIRS II vulnerability study produced the following main conclusions:

- The internal component acceleration envelopes are the largest for both AIRS I and AIRS II, but this predominance must be regarded cautiously as a result of the arbitrary nature by which acceleration damage

levels were selected for the AIRS internal components.

- Thermal radiation effects appear to be more important for AIRS I than for AIRS II; however, blast effects produce the larger envelopes for both vehicles.
- Thermal radiation effects tend to increase in relative importance for the larger yields and lower intercept altitudes.
- Shell response and bending response damage are of comparable importance for the nonmaneuver condition for both vehicles. For the maneuver condition, however, the shell damage mode is more important than the bending damage mode in defining vulnerability envelopes for both vehicles.
- The maneuver condition modifies the acceleration, bending and shell damage vulnerability envelopes appreciably. In general, the overall areas (or volumes) of these envelopes increase significantly for the maneuver condition.

[REDACTED] It should be emphasized that the conclusions only apply to the AIRS I and AIRS II vehicles. The foregoing discussion was presented to indicate the types of analyses that must be performed to assess the vulnerability of ABM vehicles to blast and thermal effects. The conclusions could well be significantly different for vehicles of different design.

Pages 16-92 through 16-95
DELETED. DNA (b)(3)

[REDACTED]

BLAST AND THERMAL LETHALITY [REDACTED]

[REDACTED] Previous subsections of this section have concentrated on concerns relative to the blast and thermal vulnerability of friendly RV's and ABM's. This subsection will discuss the concern of the defense in the effectiveness of ABM in "killing" an RV. The emphasis shifts from "sure safe" criteria to "sure kill" criteria.

[REDACTED] The definition of the threat RV vehicles and the details of the free field blast and thermal environments of the ABM are the two primary factors that influence the determination of the kill effectiveness of an ABM system. Calculations of blast kill radii have been performed by various groups for the SPRINT ABM against some representative RV threats. The results of these calculations are described in the following paragraphs.

16-34 Blast and Thermal Free Field Environments



DNA
(L-3)

16-86

[REDACTED]

Some of the results of these calculations are shown in Figures 16-58 through 16-61 in the form of blast wave parameters at one altitude, e.g., temperature and flow field profile data, at one typical time. These data are essentially self explanatory. They are useful to provide an overview of the environments; however, for detailed vehicle response studies, the principal output of a radiation-hydrodynamics code calculation consists of the radiation-hydrodynamic and field data as a function of radius at a large number of times after burst. These basic data are stored on magnetic tapes (called Usertapes), which allows dissemination of the principal results for use in many studies. This is necessary since blast/thermal effects studies often require that the vehicle be flown through the environment as a function of time, and it is impossible to present environmental data at the vehicle position as a function of time graphically for all possible combinations of vehicles, trajectories, and intercept conditions.

DNA
(L-3)

16-35 ABM Blast Loads on Threat Vehicles (Point Mass)

[REDACTED] The study of ABM blast loads on threat vehicles consisted of computer analyses using a generalized trajectory code, with capabilities of including the free field blast environment provided by the radiation-hydrodynamics Usertapes. A nonrotating spherical earth model with a 1962 atmosphere was used for this calculation. The aerodynamics were computed by Newtonian mechanics, based on the input size and shape data defining a sphere-cone for each vehicle. The reentry conditions for the RV nominal trajectories were defined in terms of altitude, flight path angle, and reentry velocity. Having computed a flight profile with the specified reentry conditions, the blast fly through runs included trajectory computations that started

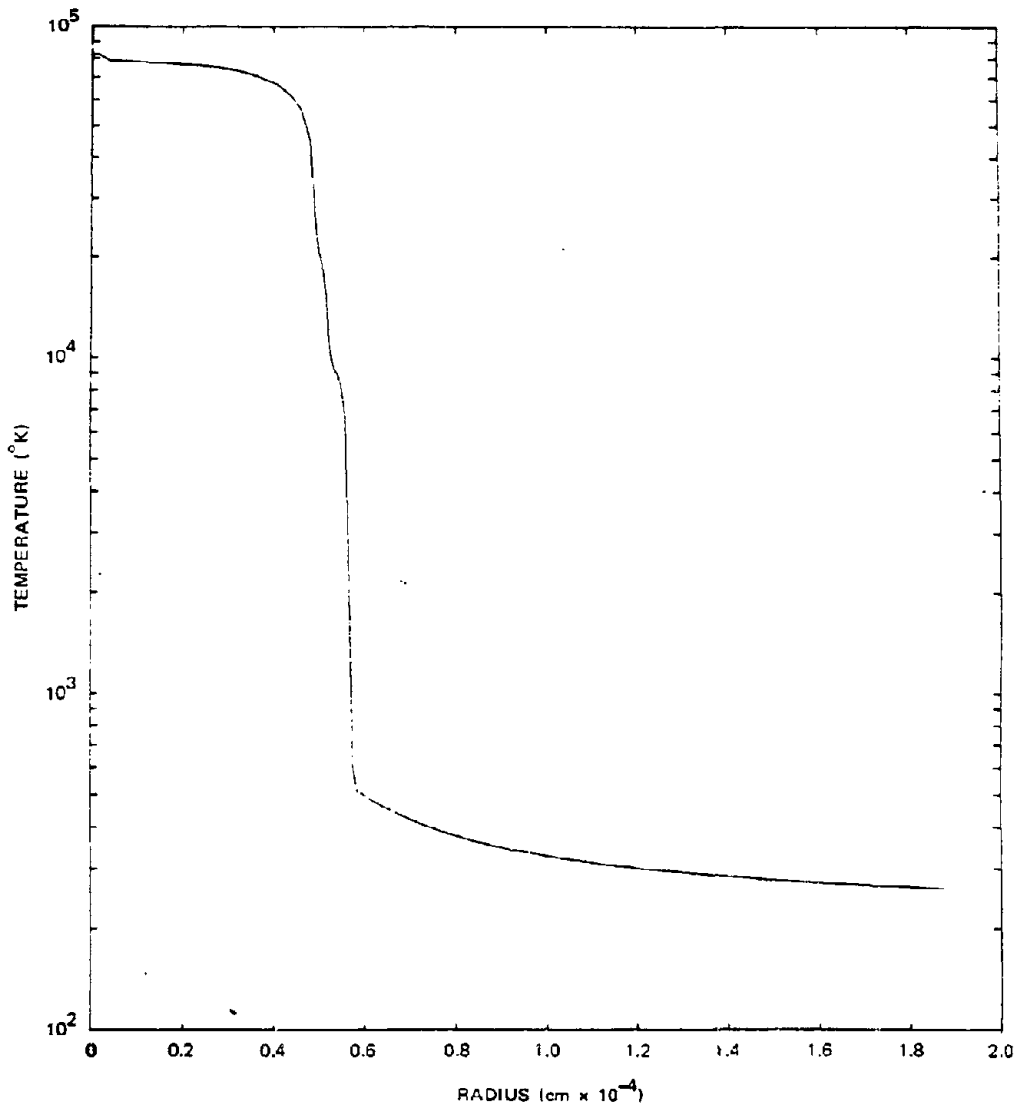


Figure 16-58. Computed Temperature Profile,
 $\tau = 4.64$ msec, 30 kilofeet Altitude

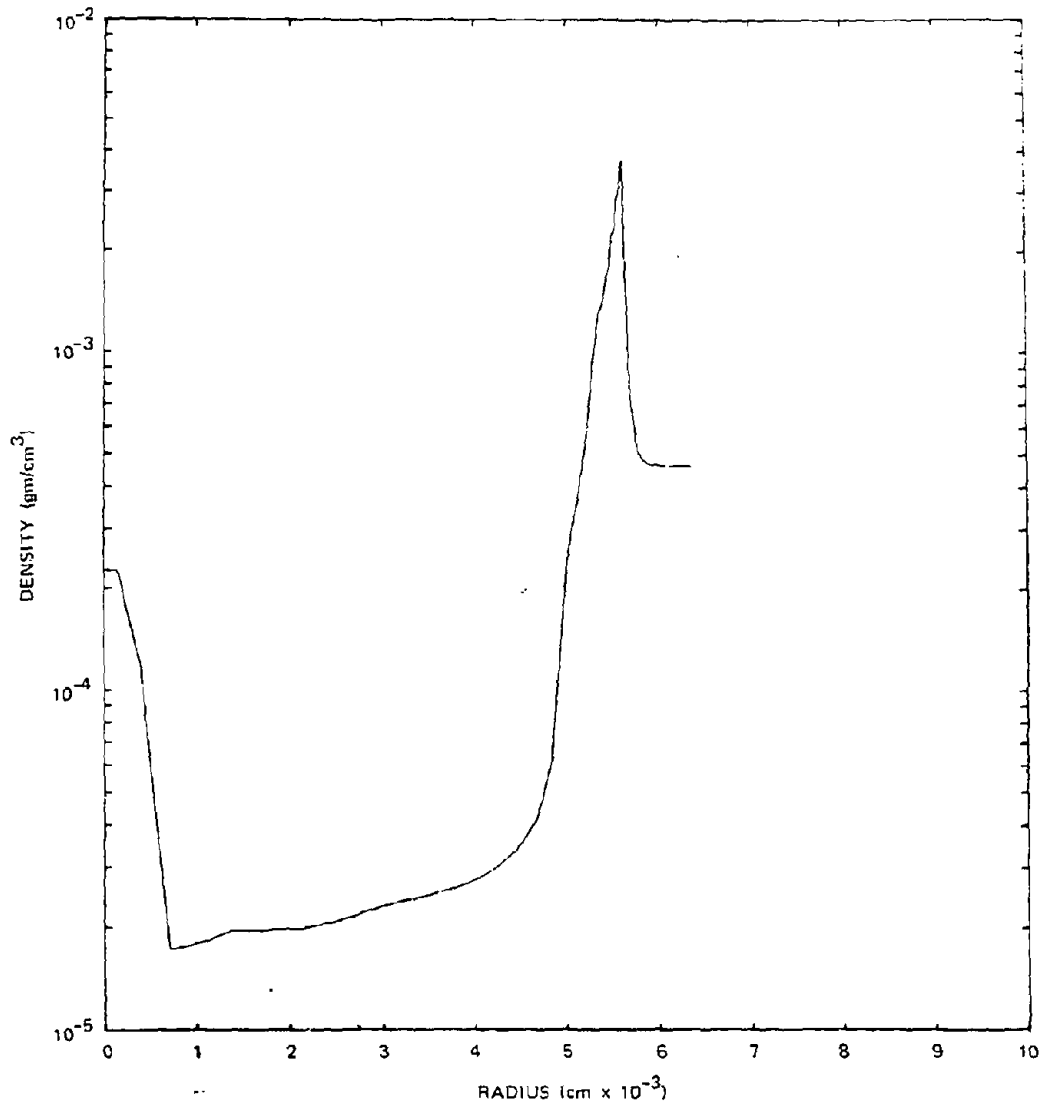


Figure 16-59. Computed Density Profile,
t = 4.64 msec, 30 kilofeet Altitude

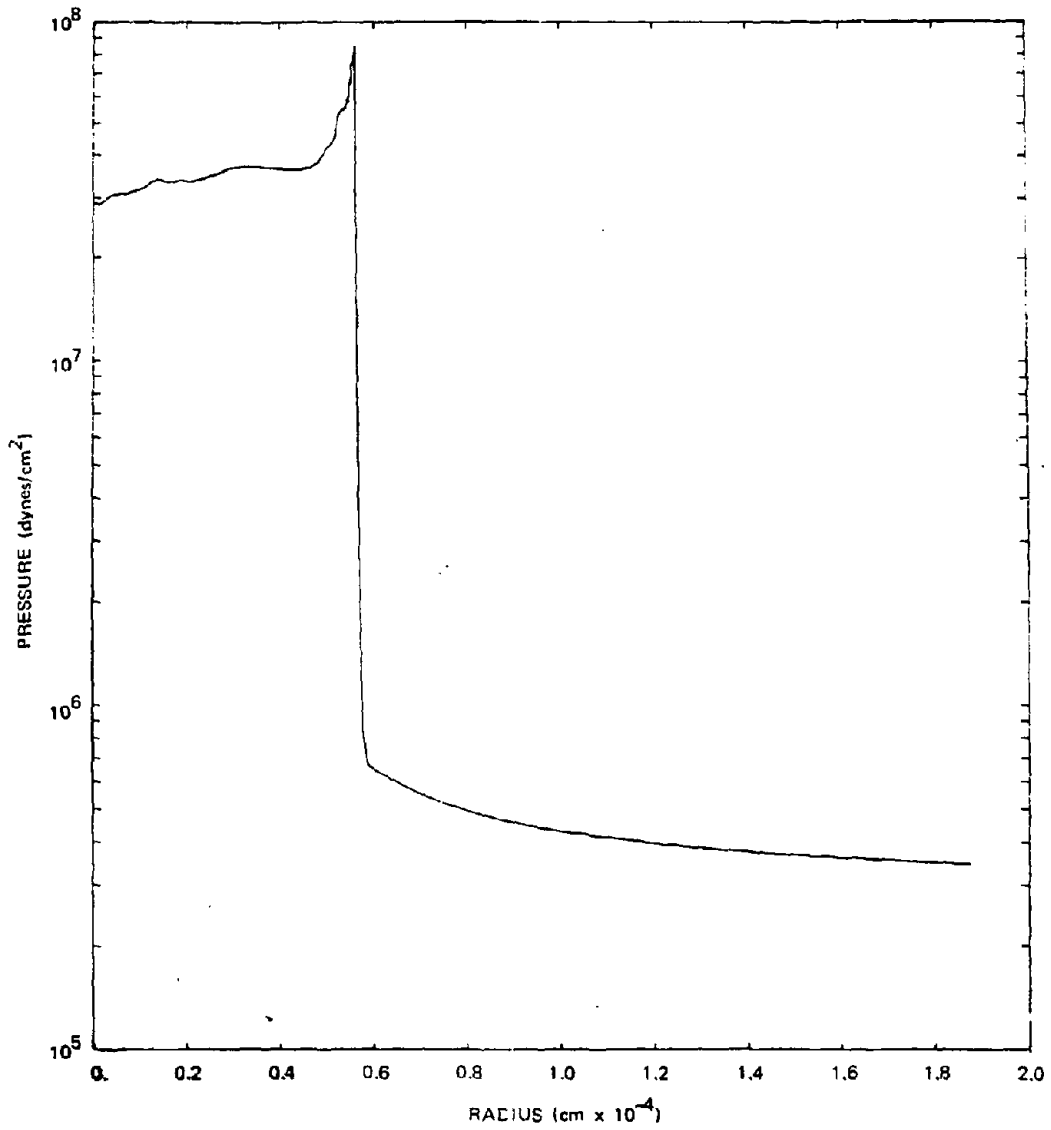


Figure 16-60. Computed Static Pressure Profile,
 $t = 4.64$ msec, 30 kilofeet Altitude

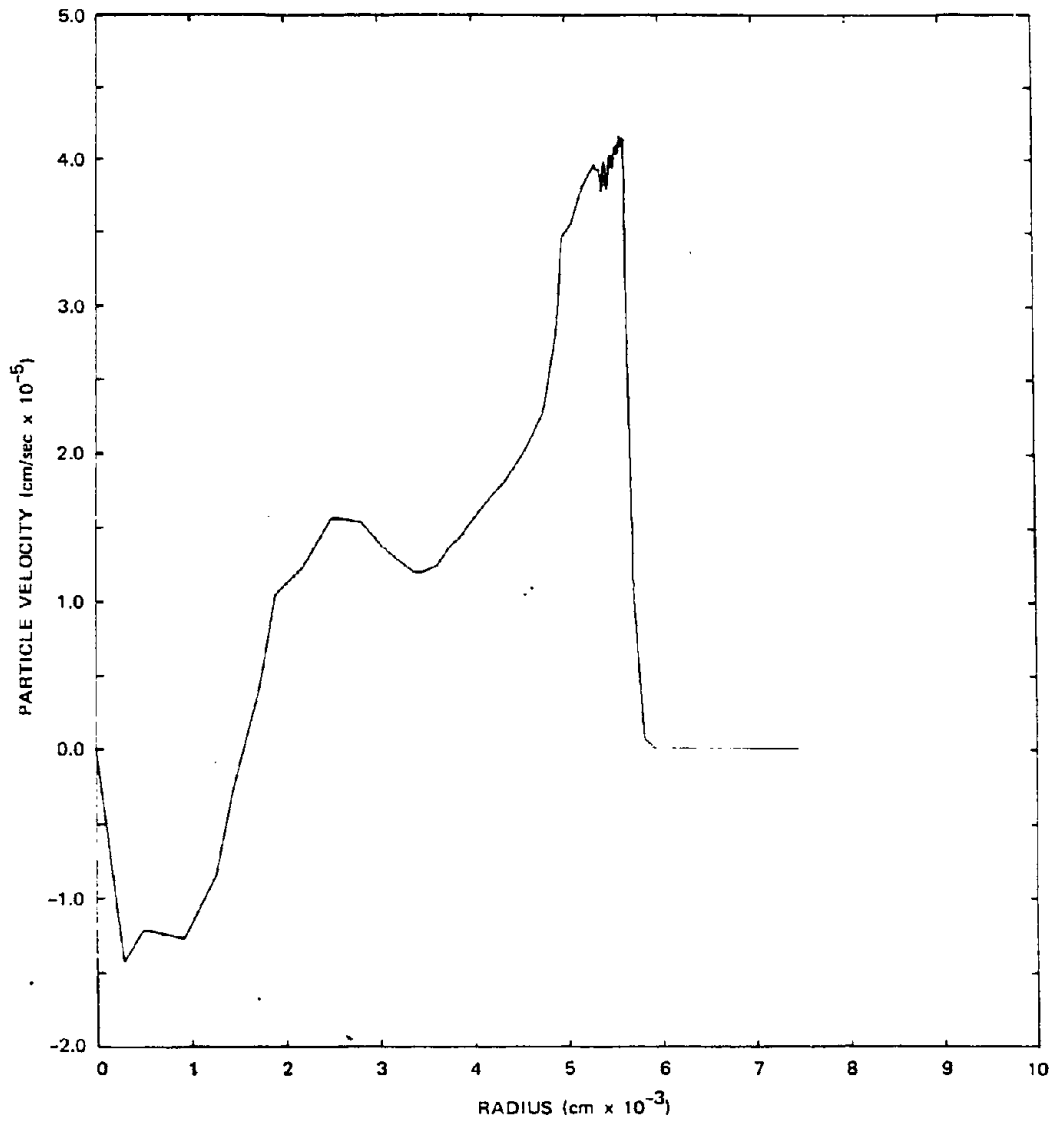


Figure 16-61. [REDACTED] Computed Particle Velocity Profile,
t = 4.64 msec, 30 kilofeet Altitude [REDACTED]

[REDACTED]

just prior to shock front intercept and terminated within one second. In the dynamic simulation involving interaction between the rapidly changing blast environment and the vehicle trajectory, the environment changes rapidly; changes are measured in microseconds and in inches. The computed dynamic response, nevertheless, is considered to be a valid model.

Figures 16-62 through 16-65 provide a graphic portrayal of a sample blast intercept condition. For this one intercept case, four curves are shown: static overpressure, dynamic pressure, static overpressure impulse, and dynamic pressure impulse. All times indicated are measured from the time of blast wave intercept. Twenty-five milliseconds of data are shown in Figure 16-62 while only the first millisecond is shown in Figures 16-63 through 16-65. The values of dynamic pressure impulse are the results of continuous summation from prior trajectory restart conditions, and the measurements must be read relative to a baseline value at time of intercept.

The two impulse curves (Figures 16-64 and 16-65) show the relative importance of the dynamic pressure impulse compared to overpressure impulse at early times. The former builds up and levels off extremely quickly while the latter continues to increase. This characteristic is due to the rapid drop in dynamic pressure, whereas the overpressure, plotted for 25 msec, illustrates a considerably slower decay rate.

16-36 Blast Loads on the RV Threat Vehicle

The time history of surface loading on a threat reentry vehicles were computed from knowledge of the fly through environments (overpressure, dynamic pressure, relative wind angle of attack) and local vehicle aerodynamics.

The time history of loading on any part of the RV is found to be the sum of a very short

duration dynamic pressure or drag loading, superimposed on a longer duration overpressure loading. (See Figures 16-62 through 16-65 for typical pressure-time histories.)

The spatial distributions of these two types of loads on the vehicle surface generally will differ considerably. Blast overpressure results in uniform pressure being applied over the complete vehicle surface, whereas dynamic pressure loadings vary over the vehicle surface, depending on the structural configuration and intercept geometry. These various relationships can be expressed in the following functional form.

$$P(t) = q(r, \alpha, \theta, \psi, \beta) + \Delta p(t)$$

where

q = dynamic pressure

Δp = static overpressure

α = relative wind intercept angle

ψ, θ = local angles defining structural geometry

β = circumferential angle on structure measured from windward ray of intercept.

Newtonian aerodynamics were used to determine the peak values of surface pressure resulting from the dynamic pressure environment for all the reentry vehicles that were studied. The structural configurations all were made up of some combination of a sphere nose cap and a conical body. Most of the early structural lethality studies were concentrated on the aft (or weakest) conical shell bay. Shock-on-shock loads were neglected in the analysis.

The surface pressure loading on the conical shell elements is computed from the equation on page 16-106.

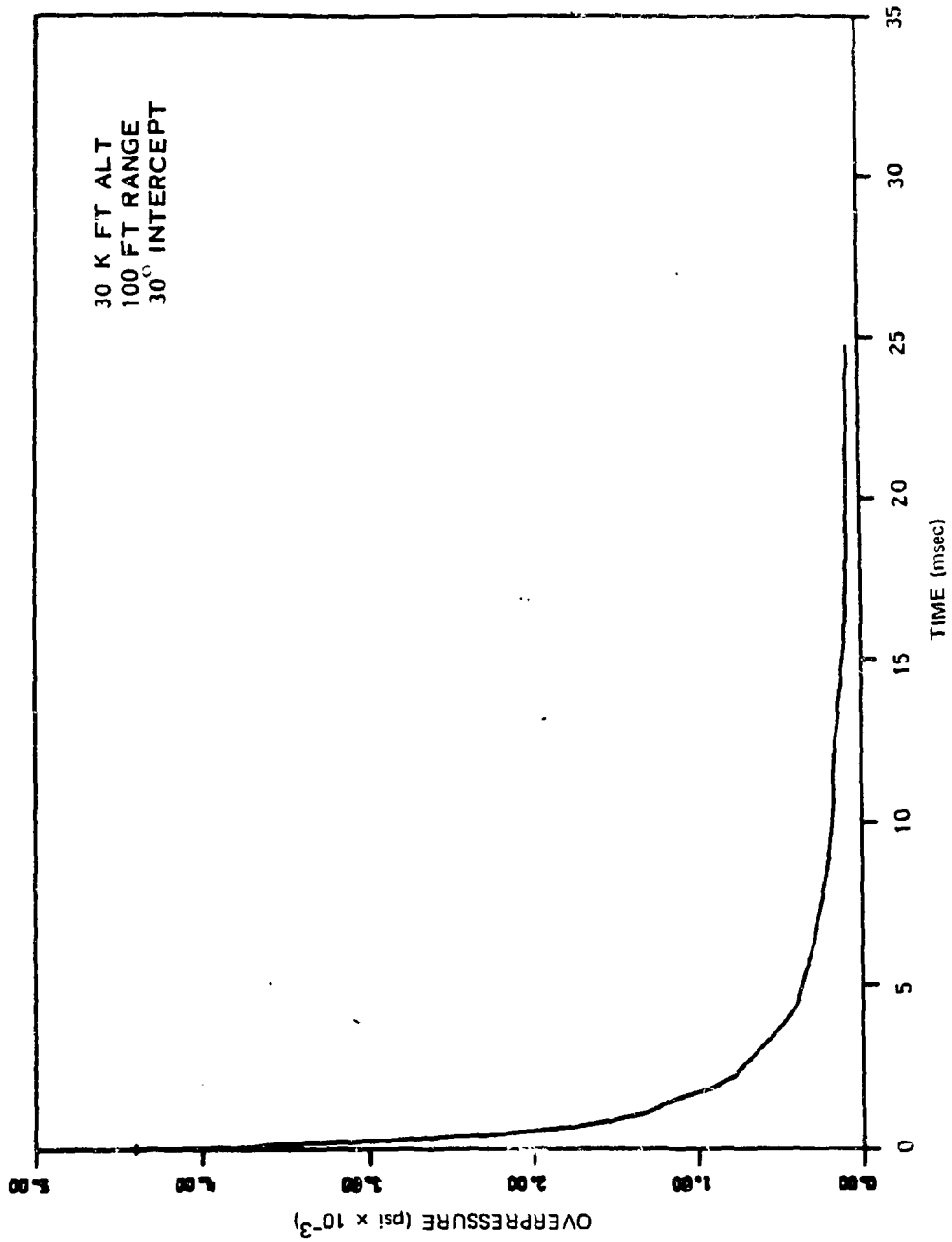


Figure 16-62. RV Target A, Static Overpressure as a Function of Time, 30° Intercept

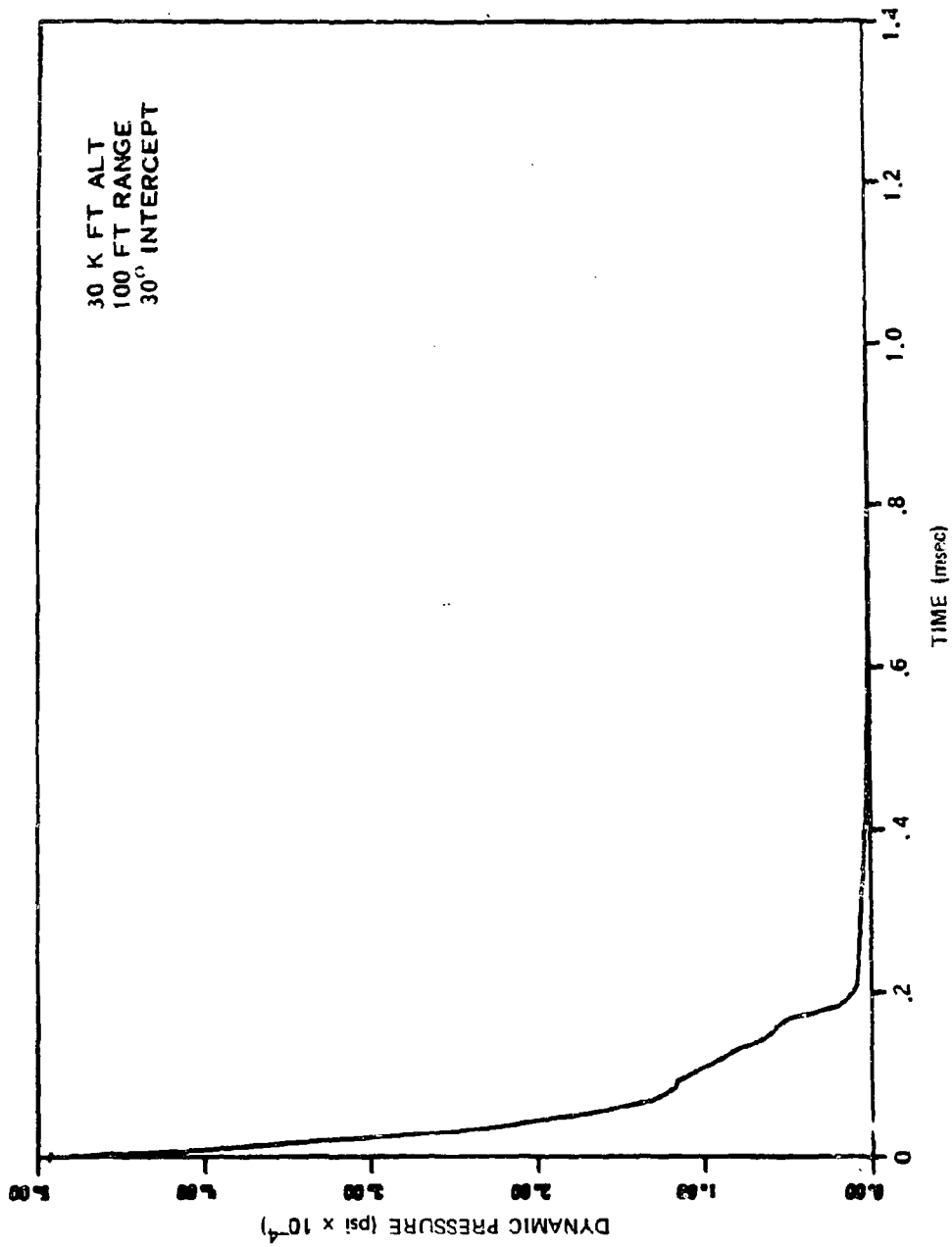


Figure 16-63. RV Target A, Dynamic Pressure as a Function of Time, 30° Intercept

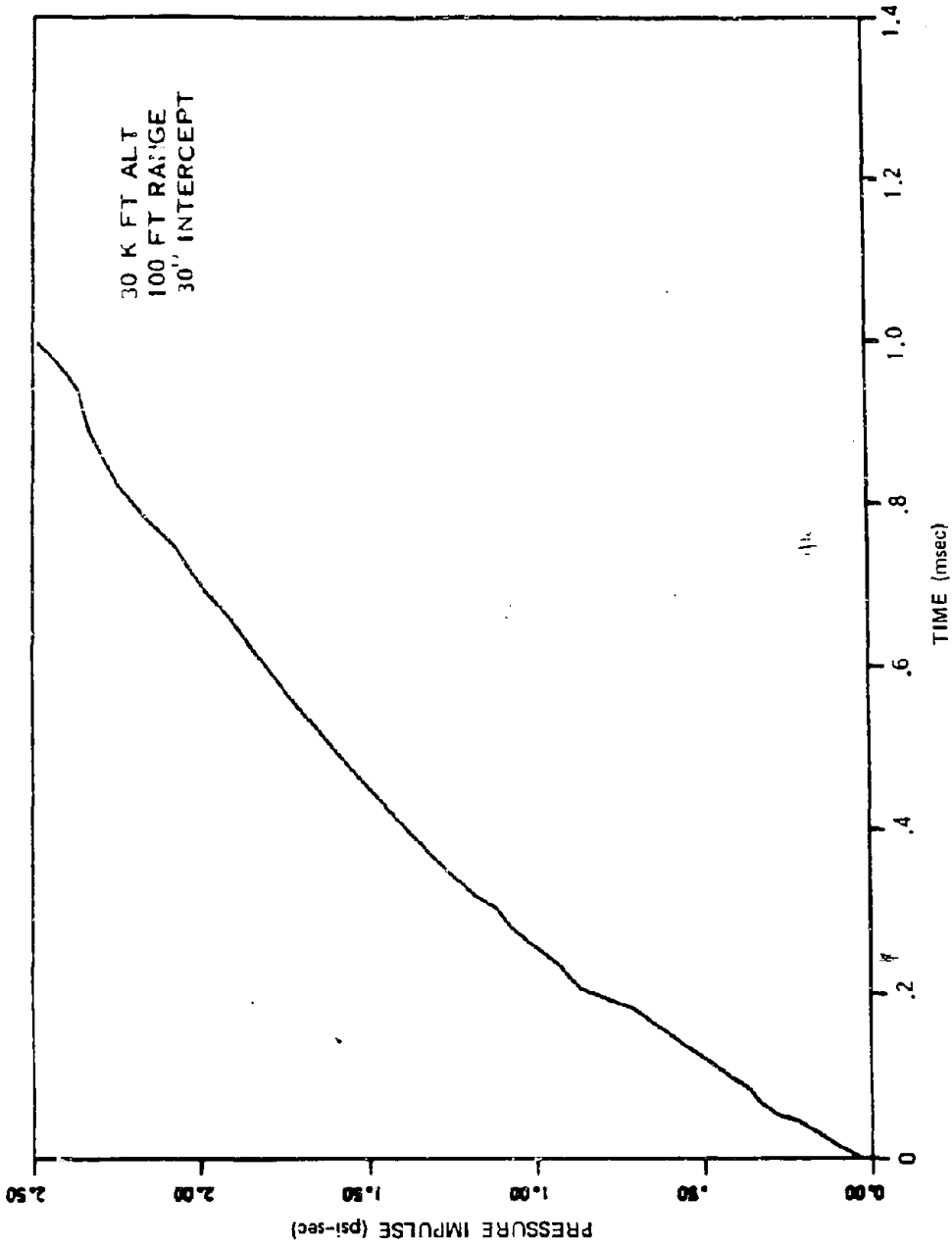


Figure 16-64. RV Target Static Overpressure Impulse as a Function of Time, 30° Intercept

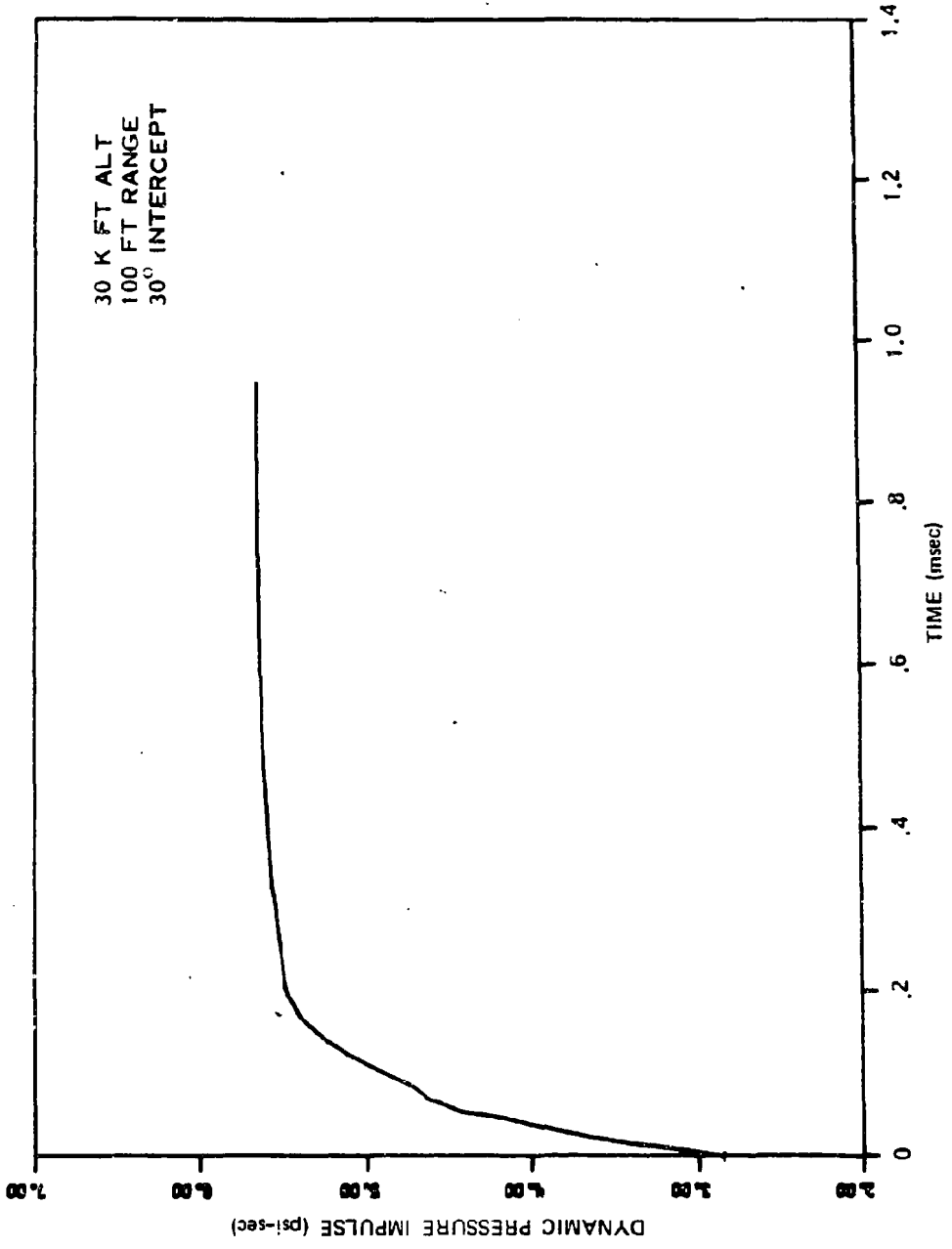


Figure 16-65. RV Target \ Dynamic Pressure Impulse as a Function of Time, 30° Intercept

$$P(t) = 2q(t) (\cos \alpha \sin \theta + \sin \alpha \cos \theta \cos \beta)^2 + \Delta p(t);$$

$$-\beta_{\max} \leq \beta \leq \beta_{\max}$$

$$P(t) = \Delta p(t) \quad \beta_{\max} \leq \beta \leq -\beta_{\max}$$

where

$$\beta_{\max} = \cos^{-1} \left\{ 1 - \left(\frac{\tan \theta}{\tan \alpha} \right)^2 \right\}^{1/2}$$

θ = cone half angle

at the windward ray $\beta = 0$, therefore maximum surface pressure is

$$P(t) = 2q(t) \sin^2 (\theta + \alpha) + \Delta p(t),$$

and the impulse at any time, T , at $\beta = 0$ on the cone is

$$I(t) = \int_0^T \left\{ 2q(t) \sin^2 (\theta + \alpha) + \Delta p(t) \right\} dt,$$

where it is noted that $q(t)$ and $\Delta p(t)$ will not, in general, have the same time dependency.

16-37 ABM Blast Kill Radii

Structural lethality levels of the threat reentry vehicles are evaluated in terms of the blast loadings on the primary structure of the vehicle. In the calculations described here, two categories of lethal loadings were evaluated: (1) Immediate kill, Category 6* and (2) Delayed kill, Category 4. Immediate kill corresponds to load levels sufficient to cause some degree of structural breakup of the metallic subshell. This

usually will be accompanied by removal of the ablative covering and severe structural deformation of the remaining subshell. Delayed kill refers to removal of the ablative covering over large portions of the loaded side of the vehicle. In general, this load level also will be sufficient to cause considerable plastic deformation in the vehicle subshell. These definitions of damage are consistent with those recommended by Stanford Research Institute following participation in the HARTS and SPINE experimental programs.

One approach used to relate these damage levels to the computed applied loading involves the establishment of a given damage level in terms of the pressure and impulse of the applied surface loading. The equation for a given damage level in the P - I plane is then defined by the following hyperbolic form:

$$\left(\frac{I}{I_0} - 1 \right) \left(\frac{P}{P_0} - 1 \right) = 1.0.$$

In this equation I_0 and P_0 are asymptotes corresponding to values of impulsive loading and static pressure loading necessary to induce the specified damage level. Thus, I_0 and P_0 must be determined for each structure to be studied and for both damage categories, i.e., immediate kill and delayed kill. Although much of the data are consistent with the value 1.0 on the right-hand side of the equation, some data indicate that a value near 3.0 would be more appropriate.

For a given structural element, the I_0 and P_0 asymptotes for a given damage level can be related to computed values of impulse and pressure based on some very simplistic structural analysis techniques. For example, modeling the two layered aft bay shell element as a rigid, perfectly plastic cylinder, the uniform externally applied impulse necessary to cause a permanent

* Sometimes referred to as "catastrophic damage."

strain, ϵ , in the shell wall is found to be:

$$I = \left[2\epsilon(\rho_s h_s + \rho_c h_c)(\sigma_{ys} h_s + \sigma_{yc} h_c) \right]^{1/2},$$

where

ρ_s, ρ_c = mass densities of shell and ablative cover materials.

σ_{ys}, σ_{yc} = yield stress values of shell and ablative cover materials.

h_s = shell thickness.

h_c = ablator thickness.

Under similar assumptions, the value of uniform static pressure necessary to cause material yielding in the shell wall is

$$P_y = \frac{1}{a} \left\{ \sigma_{ys} h_s + \sigma_{yc} h_c \right\}$$

where a = average radius of cylinder. The well-known $I_{0.5}$ parameter for impulsively loaded shells can be obtained by setting $\epsilon = 0.05$.

$$I_{0.5} = \left\{ 0.1(\rho_s h_s + \rho_c h_c)(\sigma_{ys} h_s + \sigma_{yc} h_c) \right\}^{1/2}.$$

The next step in lethality evaluation is to relate the $I_{0.5}$ and P_y load levels to load levels corresponding to the Category 6 and Category 4 damage. For the cylindrical or slightly conical shells representative of the aft bay of most threat RV's, these relationships are empirically established based on results obtained from a large number of experimental tests performed during the HARTS, SPINE, and DRIS Programs. Based on the results of these correlations, the following relations were selected to establish the impulsive and quasistatic load level asymptotes for damage Categories 6 and 4.

IMPULSE ASYMPTOTE

$$\text{Category 4: } I_4 = I_{0.5}$$

$$\text{Category 6: } I_6 = 2.5 I_{0.5}$$

QUASISTATIC PRESSURE ASYMPTOTE

$$\text{Category 4: } P_4 = 0.7 \frac{a}{L} P_{0.5}$$

$$\text{Category 6: } P_6 = 1.56 \frac{a}{L} P_{0.5}$$

It should be noted that, in the definition of the quasistatic pressure asymptote, the effect of shell length has been included empirically by including the radius-to-length ratio (a/L).

Based on the structural lethality estimates described above and the blast environment loading for the various encounter geometries, lethality estimates of the unreat RV's can be made. A sample plot is shown in Figure 16-66; the $I_{0.5}$ and $P_{0.5}$ (P_y) asymptotes have been determined, and the curves corresponding to the damage asymptotes I_6 , P_6 (immediate kill) and I_4 , P_4 (delayed kill) are shown. The dashed line shows the damage curve for immediate kill corresponding to the constant in the pressure-impulse equation being equal to 3.0 instead of 1.0.

By combining the loads calculated for the various encounters, in terms of pressure and impulse of peak surface loading, with the damage level plot (Figure 16-66), estimates of loads (in terms of slant range and intercept angle) necessary to incur lethal damage can be made for each vehicle. An example of the superposition of the structure load pressures and impulses on the damage definition curves is shown in Figure 16-67. In the figure, different symbols correspond to loads for various intercept angles, and the number adjacent to each symbol defines the value of slant range at burst time to which that particular load calculation corresponds.

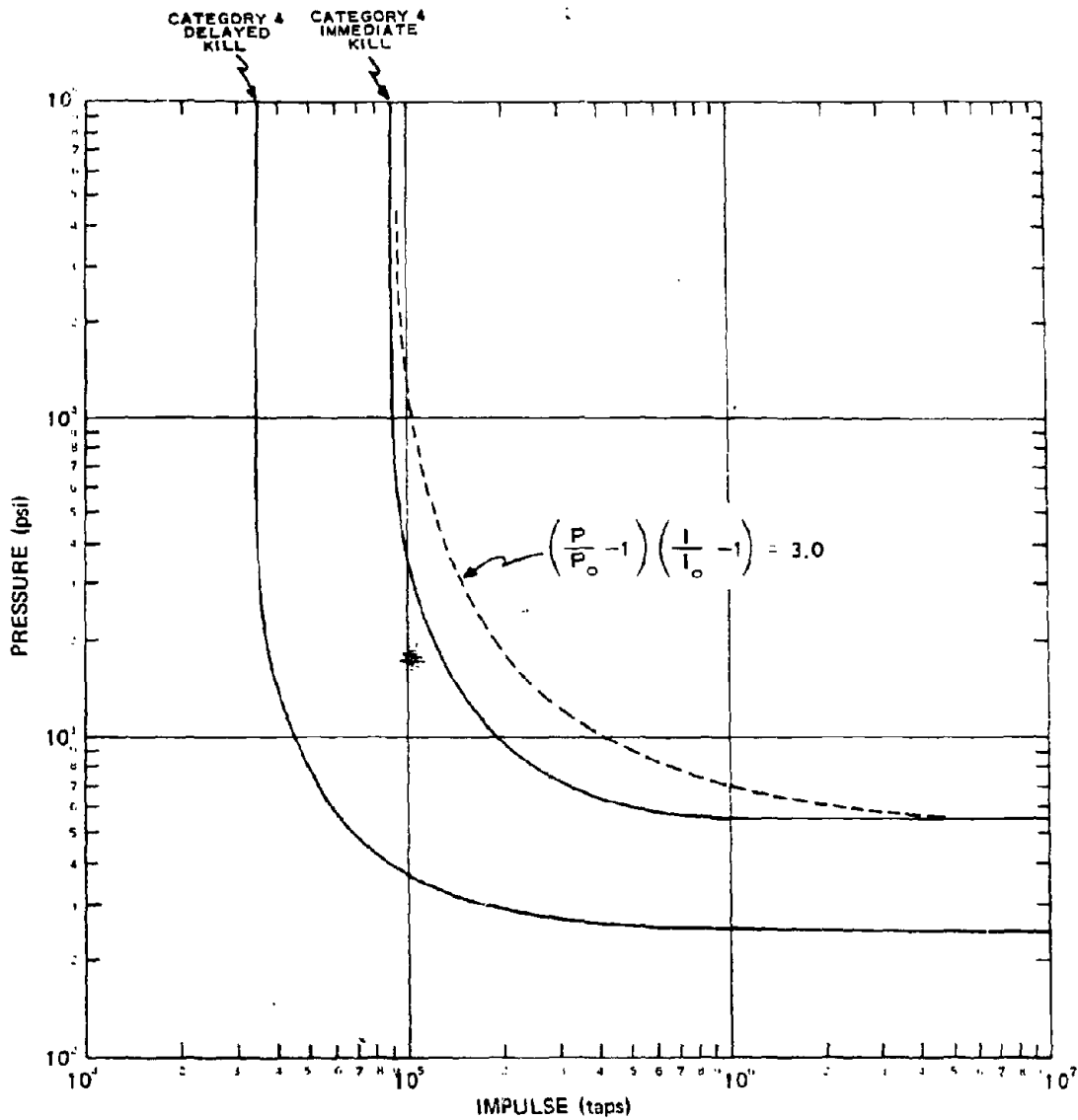
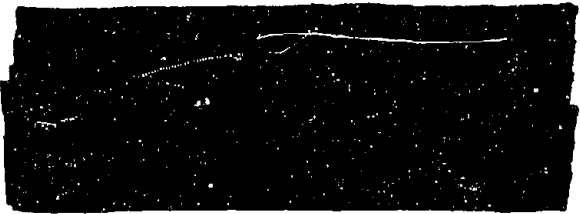


Figure 16-86. Pressure-Impulse Damage Levels, RV Target A Configuration, Aft Bay

[REDACTED]

[REDACTED] By noting where the blast loading points cross the damage level lines in the *P-I* plane, estimates of burst time slant range can be made, for a given intercept angle, that will result in Category 6 immediate kill and Category 4 delayed kill. The following RV kill slant ranges (at burst time) are obtained from the example (Figure 16-67).

DNA
(E)(3)



[REDACTED] It should not be inferred that the *P-I* plot method described above is the only method of analysis that is used to determine blast lethality radii. Some investigators have been successful in computing the structural response of RV's to the derived blast load inputs; however, here experimental data must be used to relate the computed response to damage level, e.g., immediate kill.

16-38 Fireball Thermal Effects on Threat RV's

[REDACTED] Whenever a vehicle intercepts an early time blast wave, it subsequently traverses through (or very near) a high temperature nuclear fireball. Therefore, as one part of a lethality investigation, the thermal effects that would be expected on a threat RV flying through an ABM nuclear fireball would be examined. The calculations for the following example employed the RAD ABLE code. This code uses the free field fireball thermal environment data as read off of a rad-hydro Usertape. The RAD ABLE code formalism assumes that the vehicle flies a constant velocity-straight line trajectory in the vicinity of the burst point. A simplified method is used that accounts for radiation blocking

effects in an approximate manner based on detailed stagnation point (rad-hydro) flow field solutions.

[REDACTED] Figure 16-68 shows a typical history of the ablation rate (\dot{m}) and the amount of material ablated

$$m = \int_0^t \dot{m} dt$$

for a head on traversal of an ABM explosion at 30 kilofeet altitude. The burst time standoff distance (X_0) of the vehicle was 100 feet in this case.



DNA
(E)(3)

Figure 16-69 summarizes the results of a number of fireball traversal calculations (similar to those illustrated in Figure 16-67) in the form of total mass ablated at fireball exit as a function of initial standoff distance (X_0) and burst altitude. All of these results are for head on ($X_0 > 0$) or tail on ($X_0 < 0$) intercepts with

[REDACTED]

[REDACTED]

[REDACTED]

DWA
(b)(3)

Deleted

Figure 16-67. [REDACTED] SPRINT Blast Loads, RV Target A,
30 kilofeet Altitude, Aft Bay [REDACTED]

16-110

[REDACTED]

[REDACTED]

[REDACTED]

DJSP
(R)E

Deleted

Figure 16-68. [REDACTED] Ablation Rate and Mass Ablated as a Function of Time for Target A Threat RV [REDACTED]

[REDACTED]

[REDACTED]

[REDACTED]

DD-1
H-12

Deleted

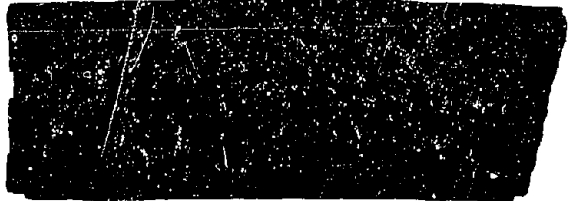
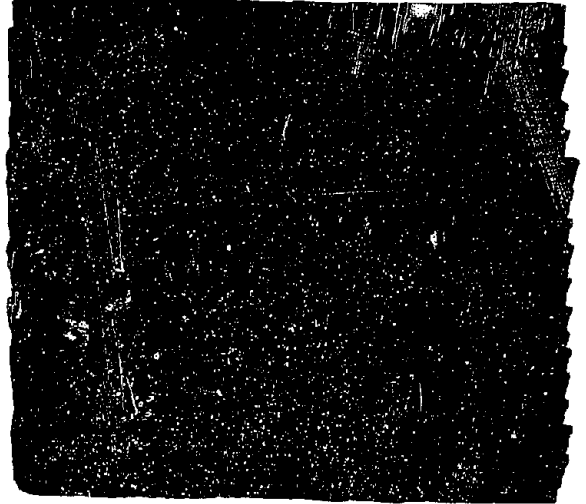
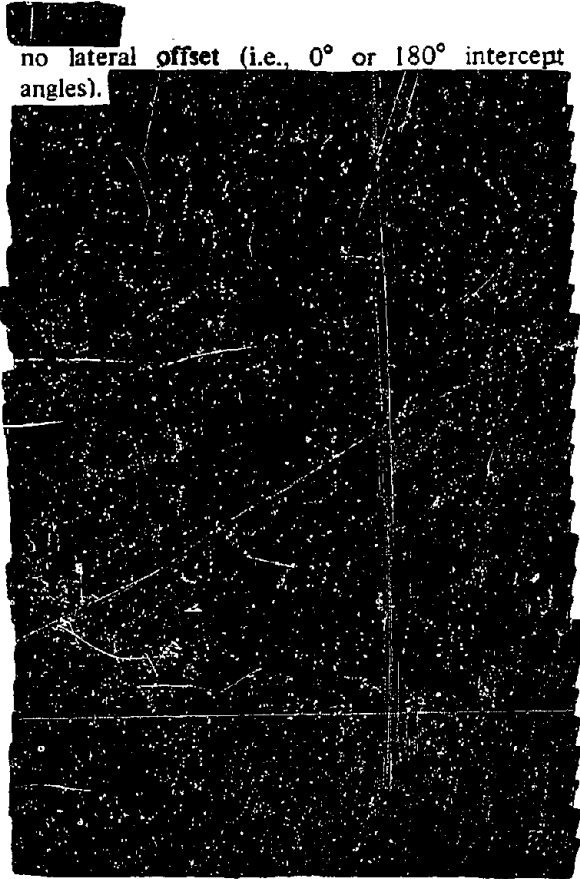
Figure 16-69. [REDACTED] Mass Ablated as a Function of Burst Time
Standoff Distance for Target A Threat RV [REDACTED]

[REDACTED]

[REDACTED]

[REDACTED]
no lateral offset (i.e., 0° or 180° intercept angles).

DNA
(8)(3)



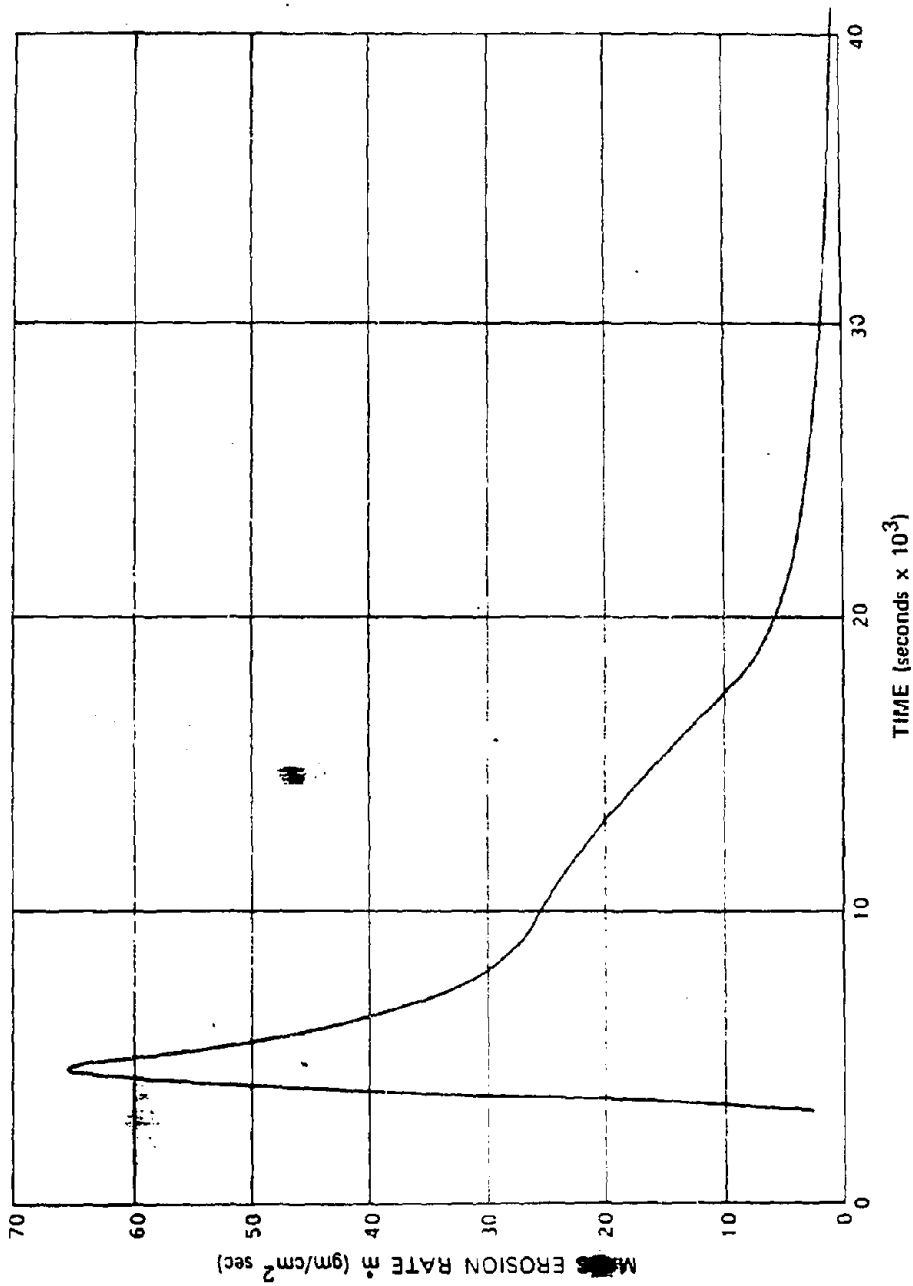


Figure 16-70. Typical Traverse-Mass Erosion Rate History

16-114

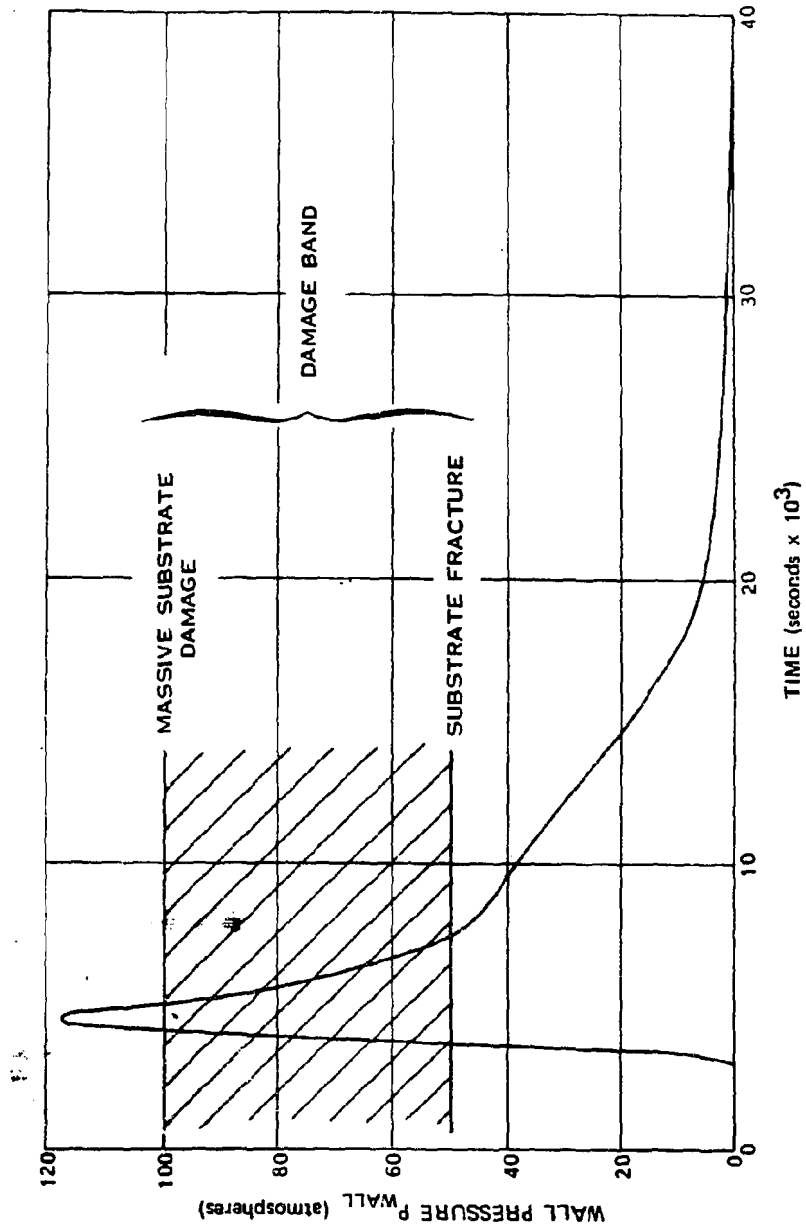


Figure 16-71. Typical Traverse-TML History

[REDACTED]

Hardening Technology Studies - II [REDACTED] LMSC-B130391, Volumes I-IV, Lockheed Missiles and Space Company, Sunnyvale, California, 30 September 1966 [REDACTED]

Hillendahl, R. W., *Theoretical Models for Nuclear Fireballs* [REDACTED] DASA 1589-1 through 1589-39, Lockheed Missiles and Space Company, Sunnyvale, California, 1965-1966 [REDACTED]

Joint Engineer/Service Test SERGEANT Guided Missile System [REDACTED] Volume I, U.S. Army Test and Evaluation Command Technical Report 143, November 1963 [REDACTED]

Johnson, O. T., R. D. Mayerhofer, and W. J. Schuman, Jr., *Effect of Blast Upon Simulated and Actual Missiles (Project 1.4 Operation Snow Ball)* [REDACTED] Memorandum Report No. 1655, U.S. Army Ballistic Research Laboratories, Aberdeen Proving Ground, Maryland, May 1965 [REDACTED]

Johnson, O. T., and R. D. Mayerhofer, *Susceptibility and Vulnerability of the Lance Missile System to Nuclear Effects (Blast)* [REDACTED] BRL-MR-1862, U.S. Army Materiel Command, Ballistic Research Laboratories, Aberdeen Proving Ground, Maryland, August 1967 [REDACTED]

Johnson, O. T., R. D. Mayerhofer, *Susceptibility and Vulnerability of the SERGEANT Weapon System to Nuclear Effects (Blast)* [REDACTED] BRL-R-1324, U.S. Army Materiel Command, Ballistic Research Laboratories, Aberdeen Proving Ground, Maryland, June 1966 [REDACTED]

Kelley, B. E., *LANCE Automet Control System* [REDACTED] RG-TR-64-3, U.S. Army Missile Command, Redstone Arsenal, Alabama, 25 June 1964 [REDACTED]

Lindberg, H. E., et al., *Response of Reentry Vehicle-Type Shells to Blast Loads*, LMSC-B130200, Volume IV-C, Stanford Research Institute, Menlo Park, California, for Lockheed Missiles and Space Company, Sunnyvale, California, 30 September 1965 [REDACTED]

Lindberg, H. E., and G. E. Sliter, *Response of Reentry Vehicle-Type Shells to Transient Surface Pressures*, AFWL-TR-68-56, Stanford Research Institute, Menlo Park, California, June 1969 [REDACTED]

Logistic Support Plan for the LANCE Missile System [REDACTED] (Second Revision), U.S. Army Missile Command, Redstone Arsenal, Alabama [REDACTED]

Mente, K. J., *Standard Research Systems for Army Interceptors* [REDACTED] TR-35, Kaman Avidyne, Burlington, Massachusetts, July 1965 [REDACTED]

Mente, K. J., *Supplementary Data for the AIRS-I Vehicle* [REDACTED] TM-24, Kaman Avidyne, Burlington, Massachusetts, June 1966 [REDACTED]

[REDACTED]

Mikami, K., R. D'Amato, *Criteria for the Effect of Damage on the Operational Capabilities of U.S. Army Missile Systems Volume 2, Lance Missile System* [REDACTED] TR-38, Kaman AviDyne, Burlington, Massachusetts, February 1966 [REDACTED]

Mikami, K., L. J. Mente, R. D'Amato, *Criteria for the Effect of Damage on the Operational Capabilities of U.S. Army Missile Systems Volume 5, Hawk Missile System* [REDACTED] TR-38, Kaman AviDyne, Burlington, Massachusetts, July 1966 [REDACTED]

Muller, J. and D. L. Blank, *SLEDGE Program: Phase I, Feasibility Study* [REDACTED] DASA-1988, Martin Marietta Corporation (Orlando Division), Orlando, Florida, September 1967 [REDACTED]

Nicholson, J. E., and J. J. Rossi, *Pressure-Time Histories of Blast Wave Interactions with a Re-Entry Body*, MC-65-163-R1, Mithras, Inc., February 1966 [REDACTED]

Nicholson, J. E., E. F. Kent, N. Zessoules, and P. H. McIngvale, *A Ballistic Wind Tunnel Test Technique for Measuring Shock-on-Shock Interactions*, MC-66-142-R31, Mithras, Inc., 4 October 1966 [REDACTED]

Nuclear Radiation Effects Study on LANCE Directional Control Electronics [REDACTED] RG-TR-64-14, U.S. Army Missile Command, Redstone Arsenal, Alabama, September 1964 [REDACTED]

Nuclear Weapons Blast Phenomena, Volume I, Source and Development of Blast Waves in Air [REDACTED] DASA 1200-I, DASIAC, Santa Barbara, California, 1 March 1971 [REDACTED]

Nuclear Weapons Blast Phenomena, Volume II, Blast Wave Interaction [REDACTED] DASA 1200-II, DASIAC, Santa Barbara, California, 1 December 1970 [REDACTED]

Nuclear Weapons Blast Phenomena, Volume III, Air and Subsurface Explosions [REDACTED] DASA 1200-III, DASIAC, Santa Barbara, California, 1 March 1970 [REDACTED]

Organizational Maintenance Manual: SERGEANT Artillery Missile XM 15 (SERGEANT Artillery Guided Missile System) [REDACTED] Notes on Material NOM 9-1410-302-20, May 1962.

Operation and Field Maintenance Manual: General Support Shop Set (GSSS) (SERGEANT Field Artillery Guided Missile System) [REDACTED] Technical Manual TM 9-4935-305-40/1, July 1963.

Operator and Organizational Maintenance Manual: Guided Missile System, Components Organizational Maintenance Test Station AN/MSM-35 (SERGEANT Artillery Guided Missile System) [REDACTED] Notes on Material NOM 9-4935-303-12, October 1961.

[REDACTED]

Operator's Manual: Guided Missile System Components Field Maintenance Test Station AN/MSM-36 (SERGEANT Artillery Guided Missile System) [REDACTED]. Notes on Material NOM 9-4935-304-10, October 1963.

Operator's Manual, SERGEANT Artillery Guided Missile System [REDACTED]. Notes on Material NOM 9-1400-300-10, December 1960 [REDACTED]

Operator and Organizational Maintenance Manual: Air Defense Guided Missile XM3E1 [REDACTED]. TM 9-1410-500-12, July 1962 [REDACTED]

Operator and Organizational Maintenance Manual: Emplacement of Hawk Air Defense Guided Missile System [REDACTED]. TM 9-1400-500-12/1, August 1961 [REDACTED]

Operator's Manual: Description for Hawk Air Defense Guided Missile System [REDACTED]. TM 9-1400-500-10, June 1960 [REDACTED]

Operator and Organizational Maintenance Manual: SERGEANT Missile Trainer, Device 3G52 (SERGEANT Artillery Guided Missile System) [REDACTED]. Technical Manual TM 9-5920-130-12, January 1963.

Operator and Organizational Maintenance Manual: Four-Wheel Semitrailer-Mounted Guided Missile Launching Station XM 504 (SERGEANT Artillery Guided Missile System) [REDACTED]. Notes on Material NOM 9-1440-301-12, October 1961.

Parechianian, H. S., et al., *Dynamic Response Investigation of Simulated R/V Structure - Volume II Impulse and Blast Tests* [REDACTED]. SAMSO TR-69-144, Volume II, McDonnell Douglas Astronautics Company, Santa Monica, California, September 1969 [REDACTED]

Proceedings: DASA/RAND Hydrodynamic Code Conference [REDACTED]. DASA-1553, DASA Data Center, General Electric Company, Tempo, Santa Barbara, California, September 1964 [REDACTED]

Proceedings: DASA Conference on Nuclear Weapons Effects on Re-Entry Vehicles and Interceptor Missiles [REDACTED]. DASA-1651, DASA Data Center, General Electric Company, Tempo, Santa Barbara, California, September 1965 [REDACTED]

Proceedings: DASA/AFFDL Shock-on-Shock Interaction Conference [REDACTED]. DASA-1674, DASA Data Center, General Electric Company, Tempo, Santa Barbara, California, May 1966 [REDACTED]

Proceedings: DASA Anti-Ballistic Missile Blast Vulnerability Conference [REDACTED]. DASA-1744, DASA Data Center, General Electric Company, Tempo, Santa Barbara, California, April 1966 [REDACTED]

[REDACTED]

Reck, R. J., and H. E. Lindberg, *Structural Response of the SPINE Reentry Vehicle Models to Blast and Impulsive Loads* [REDACTED]. AFWL-TR-67-118, Stanford Research Institute, Menlo Park, California and Douglas Aircraft Company, Santa Monica, California, January 1968

Sachs, D. C. and R. E. Keefe, *An Investigation of Static Blast/Vehicle Intercept Simulation Methods* [REDACTED]. AMC-67-30, Kaman Nuclear, Colorado Springs, Colorado, November 1967

Sachs, D. C., et al., *An Investigation of Dynamic Blast/Vehicle Intercept Simulation Methods* [REDACTED]. AMC-67-28, Kaman Nuclear, Colorado Springs, Colorado, August 1967

Schuman, W. J., Jr., *The Response of Cylindrical Shells to External Blast Loading*, BRL Memorandum Report No. 1461, U.S. Army Ballistic Research Laboratories, Aberdeen Proving Ground, Maryland, March 1963 [REDACTED]

Schuman, W. J., Jr., *The Response of Cylindrical Shells to External Blast Loading, Part II*, BRL Memorandum Report No. 1560, U.S. Army Ballistic Research Laboratories, Aberdeen Proving Ground, Maryland, May 1964 [REDACTED]

SERGEANT Missile System Operation and Environment Test Program [REDACTED]. White Sands Missile Range Technical Memorandum 874, White Sands, New Mexico, June 1961

Sieck, D. W., *Stress Analysis of the Hawk I Missile* [REDACTED]. NA 1-55-10, Volumes I & II, Northrop Aircraft, Inc., [REDACTED]

Sliter, G. E., et al., *Warhead Optimization for Structural Kill of Re-Entry Vehicles, Lethality Tests of SPINE Vehicles* [REDACTED]. DASA-2215, Stanford Research Institute, Menlo Park, California, July 1969 [REDACTED]

Sliter, G. E., et al., *Warhead Optimization for Structural Kill of Re-Entry Vehicles* [REDACTED]. DASA-2281, Stanford Research Institute, Menlo Park, California, July 1969 [REDACTED]

SPRINT Blast Survivability Program-Interim Report [REDACTED]. AMC-4-69(T), Kaman Sciences Corporation, Colorado Springs, Colorado, June 1969 [REDACTED]

Studies of Blast Simulation Techniques on Re-Entry Vehicles [REDACTED]. AFSWC TDR 62-129, Sandia Corp., Albuquerque, New Mexico, November 1962 [REDACTED]

Transportation Data for the U.S. Army Hawk Missile System [REDACTED]. AR-150, Raytheon Company Aero/Weapons Division, Andover Plant, Andover, Massachusetts, June 1961.

[REDACTED]

Wells, P. B. and E. A. Bathke, *Theoretical Methods and Computer Codes for Fireball Ablation Effects* [REDACTED] KN-70-220(R), Kaman Nuclear, Colorado Springs, Colorado, 14 April 1970 [REDACTED]

Wells, P. B., E. A. Bathke, and D. C. Sachs, *SPRINT Blast and Thermal Environment Calculations* [REDACTED] KN-70-754(R), Kaman Nuclear, Colorado Springs, Colorado, 2 October 1970 [REDACTED]

Whitaker, W. A., et al., *Theoretical Calculations of Early Phenomenology - 200 kt at 32 kilometers* [REDACTED] AFWL-TR-67-68, Air Force Weapons Laboratory, Kirtland Air Force Base, Albuquerque, New Mexico, October 1967 [REDACTED]

Zvara, J., R. D'Amato, *Criteria for the Effect of Damage on the Operational Capabilities of U.S. Army Missile Systems, Volume I. SERGEANT Guided Missile System* [REDACTED] TR-38, Kaman Avidyne, Burlington, Massachusetts, February 1966 [REDACTED]



(This page intentionally left blank)

